THE REGULATION OF CONFORMATION AND BINDING KINETICS OF INTEGRIN $\alpha_L\beta_2$

A Thesis
Presented to
The Academic Faculty

by

Fang Zhang

In Partial Fulfillment
of the Requirements for the Degree
Doctor of Philosophy in Bioengineering

Georgia Institute of Technology
August 2007

THE REGULATION OF CONFORMATION AND BINDING KINETICS OF INTEGRIN $\alpha_L\beta_2$

Approved by:

Dr. Cheng Zhu, Advisor
Department of Biomedical Engineering
Georgia Institute of Technology

Dr. Julia E. Babensee
Department of Biomedical Engineering
Georgia Institute of Technology

Dr. Andres J. Garcia
School of Mechanical Engineering
Georgia Institute of Technology

Dr. Larry V. McIntire
Department of Biomedical Engineering
Georgia Institute of Technology

Dr. Periasamy Selvaraj
Department of Pathology and Laboratory Medicine
Emory University

Dr. Timothy A. Springer
CBR Institute for Biomedical Research, Department of Pathology
Harvard Medical School

Date Approved: July 5, 2007

I dedicate this thesis
to

My Parents

I am forever indebted to my parents, 张铁威 and 甘立起.
I would not have been able to get to this point if not for their unconditional love, endless patience, and understanding.

My Husband

I am grateful to my husband, **Tiejun Zhao**, who was always there for me and encouraged me to continue on. I am deeply thankful for him to put up with me, comfort me and lift my spirit especially over the past two years.

My Daughter

My deep gratitude goes to my beautiful daughter, **Nicole Yiran**, for being such a lovely baby and rewarding me with her big magic smile even though I have not been able to spend enough time with her because of this thesis work. Thank her for bringing so much joy into my life and making it all worthwhile.

ACKNOWLEDGEMENTS

This thesis is the result of years of work whereby I have been supported and accompanied by so many people. I would therefore like to express my greatest gratitude to all those who helped to make this thesis possible.

Firstly, I would like to thank my advisor, Dr. Cheng Zhu, for the opportunity of completing my thesis work under his guidance. He provided a motivating, enthusiastic, and critical atmosphere which has been essential to our success in the world of science. I also wish to thank him for his patience and constant encouragement during all these years.

I would like to thank the members of my thesis committee, Dr. Julia Babensee, Dr. Andres Garcia, Dr. Larry McIntire, Dr. Periasamy Selvaraj, and Dr. Timothy Springer. Thank them for monitoring the process of my work and taking efforts in reading and providing me with valuable comments and suggestions.

Special thanks to our collaborators, Dr. Springer and Dr. Selva. Dr. Springer provided me with most of the reagents for this work. Without these reagents, this thesis could not be possible. I would also like to thank him for taking time to discuss with us and for his invaluable advises. I went over to Dr. Selva's lab at the Emory University to do experiments from time to time during these years. Thank Dr. Selva for spending a lot of time in helping me and always being available for answering my questions.

I am thankful for all members of the Zhu lab for their help and sharing in research and beyond. Thank Warren Marcus for the training in micropipette and the preliminary data. Thank Jenny Ning Jiang, who is more like a sister to me as well as a closest friend. I have learnt a lot from her. I own lots of gratitude to Fang Kong, who kindly donated his

blood every once in a while for 5 years and assisted in the data analysis. Thank Jizhong Lou for his insights into research and life. Thank Jack Wei Chen, Tao Wu, Jun Huang, and Wei Chen, I felt fortunate to have you to travel this journey with me. My acknowledgements also go to Yan Zhang, Jun Yang, Veronika Zarnistyna, Timothy Tolentino, Krishna Sarangapani, Annica Wayman, and Brandy Rogers.

I would like to extend my appreciation for the staff of the Institute of Bioengineering and Bioscience [1]. Particularly, I would like to thank Johnafel Crowe in the IBB Core Facility and Chris Ruffin, our academic advisor, of the Bioengineering Degree Program.

Finally, I thank all other individuals who have supported me on the journey of my life. Special thanks to Dr. Jianhua Wu and his family. They treated me as a family member and provided me enormous help ever since my freshman year. Thank all of my friends in China, who were rooting for me all the way, for the precious friendship.

TABLE OF CONTENTS

LIST OF TABLES

LIST OF FIGURES

LIST OF SYMBOLS AND ABBREVIATIONS

ICAM-1	Intercellular Adhesion Molecule-1
I domain	Inserted domain
PSGL-1	P-selectin Glycoprotein Ligand-1
MIDAS	Metal Ion Dependent Adhesion Site
RBC	Red Blood Cell
mAb	Monoclonal antibody
WT	Wild Type
HBSS	Hank's Balanced Salt Solution
EDTA	Ethylenediamine Tetraacetic Acid
EGTA	Ethylene Glycol Tetraacetic Acid
HSA	Human Serum Albumin
BSA	Bovine Serum Albumin
SPR	Surface Plasmon Resonance
2D	Two dimensional
3D	Three dimensional
k_{off}	Off-rate (reverse rate)
k_{on}	On-rate (forward rate)
K_a	Affinity
P_a	Adhesion probability (frequency)
P_{NS}	Nonspecific adhesion probability
A_c	Contact area

m_l	Site density of ligand
m_r	Site density of receptor
K_D	Dissociation constant
s.e.m.	Standard error of the mean

SUMMARY

The interaction between $\alpha_L\beta_2$ and its ligand, Intercellular Adhesion Molecule (ICAM)-1, plays a major role in inflammatory and other immune responses by regulating leukocyte adhesion and trafficking. In order to bind ICAM-1 and to mediate subsequent functions, $\alpha_L\beta_2$ needs to be converted from inactive to active state. The activity of $\alpha_L\beta_2$ integrin is regulated by multiple mechanisms, including avidity change and conformational change. Crystal structures and other lines of experimental evidence suggest that $\alpha_L\beta_2$ has multiple conformational states which strongly correlate with its functions. This study focuses on the conformational regulation of $\alpha_L\beta_2$ and the effects of conformational change on the binding affinity and kinetics of $\alpha_L\beta_2$.

The inserted (I) domain contains the ligand binding site of $\alpha_L\beta_2$. To examine the effects of the I domain conformational changes on ligand binding, micropipette adhesion frequency assay was used to measure the two-dimensional (2D) binding affinity and kinetics of ICAM-1 interacting with $\alpha_L\beta_2$ on K562 cells, including wild type (WT) $\alpha_L\beta_2$ and mutant $\alpha_L\beta_2$ containing an I domain locked in open, intermediate, or closed conformation. Locking the I domain into open and intermediate conformations increased the ligand binding affinities of $\alpha_L\beta_2$ by ~3000 and ~30 fold, respectively, from locked closed $\alpha_L\beta_2$, which has similar affinity as the WT $\alpha_L\beta_2$. Surprisingly, the 2D affinity increases were mostly due to the 2D on-rate increases, as the 2D off-rates only decreased by several fold. The WT $\alpha_L\beta_2$ could be activated by Mn^{2+} and Mg^{2+} to have high ligand binding affinity; while locking the I domain in any of the three conformations abolished the ability for regulation by divalent cations. These results indicate that a downward

displacement of the I domain C-terminal helix, induced by the conformational changes of other domains of the $\alpha_L\beta_2$, is required for affinity upregulation.

The crystal structure of integrin $\alpha_V\beta_3$ ectodomain revealed a surprising bent conformation. Upon activation, some integrins convert from bent to extended conformation, which propagates the conformational change of the cytoplasmic domain to the ligand binding site. Using activating antibodies and small molecule antagonists combining with the locking of I domain, the effects of extension of $\alpha_L\beta_2$ on its binding affinity and kinetics were studied. The results indicate that with the I domain locked, the extension of $\alpha_L\beta_2$ itself only lengthens the molecule to provide a more accessible ligand binding site and therefore increases the on-rate. The results also indicate that the off-rate change of $\alpha_L\beta_2$ is mainly due to conformational change of I domain instead of the extension of $\alpha_L\beta_2$.

Divalent cations are very important for integrin-ligand interactions, but the mechanism of integrin regulation by divalent cations are still not very clear. ICAM-1 binding was used as a probe to investigate the binding affinity and kinetics of divalent cations for I domain and for $\alpha_L\beta_2$. The results suggested the binding properties are determined by the nature of divalent cations and the conformation of I domain. Compare to Mg^{2+}, Mn^{2+} has higher binding affinities for both I domain Metal Ion-Dependent Adhesion Site (MIDAS) and other metal ion binding sites that are critical for ligand binding of $\alpha_L\beta_2$. Ca^{2+} binding showed two different affinities, which might be due to two different conformations that I domain could adapt after Ca^{2+} binding. Open and intermediate I domains have higher binding affinity for Mn^{2+} and Mg^{2+} than WT and closed I domains. Divalent cations dissociate very slowly from I domain MIDAS but

rapidly from those metal ion binding sites that important for ligand binding of $\alpha_L\beta_2$. This difference may reflect the different roles of I domain MIDAS and other metal ion binding sites in the regulation of conformational change and ligand binding of $\alpha_L\beta_2$.

One of the most important biological processes mediated by $\alpha_L\beta_2$ and other β_2 integrins is the recruitment and migration of neutrophils during inflammation. It is suggested that E-selectin binding to neutrophils could activate β_2 integrins and this event might have physiologically significance *in vivo*. The activation of neutrophil β_2 integrins by E-selectin binding was studied here by a micropipette technique. Binding of E-selectin Ig chimera was found to activate β_2 integrins on neutrophils and increase their binding affinity for ICAM-1 coated together with E-selectin on RBCs. A contact of 5 seconds or longer with rapid binding and dissociation of E-selectin bonds induces binding of β_2 integrins and to ICAM-1 with intermediate binding affinity. The activation might require the crosslink of E-selectin ligands. P- and L-selectin were not able to induce upregulation binding to ICAM-1 observed with the current experimental setting.

In summary, this study investigated the conformational regulation of $\alpha_L\beta_2$ and the effects of conformational changes on its 2D ligand binding affinity and kinetics. The conformations of $\alpha_L\beta_2$ were altered by mutations, antibodies, small molecule antagonists, as well as divalent cations. The activation of $\alpha_L\beta_2$ by a signaling induced by E-selectin binding was also studied. This study determined the 2D binding affinities and kinetics of $\alpha_L\beta_2$ at different conformational states, which provided new evidence that the conformational change could regulate the ligand binding of $\alpha_L\beta_2$ when it is bound to cell surface and conformational changes in different part of $\alpha_L\beta_2$ have distinct effects. The binding affinities and kinetics of divalent cations for I domain MIDAS and other metal

ion binding sites of $\alpha_L\beta_2$ shed light onto the mechanism of integrin regulation by divalent cations. Besides the stimulation from outside of the cell, β_2 integrins could also be activated by the intracellular signaling induced by E-selectin binding on a timescale of seconds. These results provide insights into the relationship between conformational change and function of $\alpha_L\beta_2$ and most importantly contribute to the understanding of integrin regulation mechanisms.

CHAPTER 1

INTRODUCTION

Integrins are heterodimeric adhesion molecules consisting of α and β subunits. They transmit signals bi-directionally across cell membrane and undergo conformational change upon activation. $\alpha_L\beta_2$, a member of the β_2 integrin family, participate in various important biological processes, including leukocyte trafficking, lymphocyte homing, and immunological synapse formation. The functions of $\alpha_L\beta_2$ are precisely regulated and any dysregulation of $\alpha_L\beta_2$ could result in diseases. The overall objective of this study is to characterize the regulation of $\alpha_L\beta_2$ function, specifically ligand binding, by its conformational change. Micropipette adhesion frequency assay is used as the major method to measure the 2D binding affinity and kinetics.

Previous studies showed that a 10 Å downward movement of the C-terminal α7 helix allosterically induced the conformational change in ligand binding site of the I domain and increased ligand binding 3D affinity of isolated I domain by 10,000 fold. Although cell adhesion experiment showed difference in binding affinity of $\alpha_L\beta_2$ containing I domain locked at different conformations, the 2D binding affinity and kinetics of these $\alpha_L\beta_2$ have never been measured. The measurement of the binding affinity and kinetics of WT $\alpha_L\beta_2$ and $\alpha_L\beta_2$ containing a locked I domain could further our understanding of the effect of I domain conformational change in intact $\alpha_L\beta_2$. Using activating agents, such as divalent cations Mn^{2+} and Mg^{2+}, the relationship between the I domain and other domains of $\alpha_L\beta_2$ in conformational change is further revealed.

I domain conformational change might be the most effective and direct pathway to regulate the binding activity of $\alpha_L\beta_2$, because it contains the ligand binding site. However, for the whole $\alpha_L\beta_2$, other conformational changes are also necessary for the regulation. Indeed, it is the extension of $\alpha_L\beta_2$ that propagates the conformational change of the cytoplasmic domain to the outmost I domain. The conformational change of I domain and the extension of $\alpha_L\beta_2$ could be independent of each other, i.e. $\alpha_L\beta_2$ could be extended but has a closed I domain, or has an open I domain but still be bent. It is not known whether the conformational change of I domain and the extension of $\alpha_L\beta_2$ each have distinct influence on ligand binding. The binding affinities and kinetics of the multiple conformational states of $\alpha_L\beta_2$ has not been systematically studied and compared either. The complexity of the nature of integrin conformational change makes it difficult to address these questions. Using I domain locking, activating antibodies, small molecule antagonists, and reporting antibodies, the conformation of $\alpha_L\beta_2$ could be better controlled and accessed, which allows the effects of $\alpha_L\beta_2$ extension to be studied. Moreover, the binding affinities and kinetics of $\alpha_L\beta_2$ at various conformations are measured, categorized, and compared, which allows the characterization of the multiple conformational states of $\alpha_L\beta_2$.

It has been shown that a divalent cation directly coordinates into the MIDAS of the α_L I domain and is part of the receptor-ligand complex. Some of other divalent cation coordination sites play critical roles in conformational regulation of $\alpha_L\beta_2$. However, the characteristics of divalent cation binding to I domain MIDAS and other coordination sites are presently unclear. Different divalent cations may have different binding affinities and kinetics for the same divalent cation coordination site of $\alpha_L\beta_2$. The conformation of I

domain or may $\alpha_L\beta_2$ would influence the divalent cation binding characteristics by altering the position and orientation of those amino acids that form coordination with divalent cations. In order to test these hypotheses, part of this study is to measure the binding affinity and kinetics of divalent cations, Mn^{2+}, Mg^{2+}, and Ca^{2+}, to α_L I domain and other metal ion binding sites that are important for ICAM-1 binding of $\alpha_L\beta_2$. These measurements could provide evidence to support (or against) the hypotheses and provide insights into the divalent cation regulation of $\alpha_L\beta_2$.

In physiological environment, perhaps the most important regulation of $\alpha_L\beta_2$ is by intracellular signaling. The binding of other molecules on cell surface could trigger a signal, which is transmitted to $\alpha_L\beta_2$ from inside of the cell and activates $\alpha_L\beta_2$. For neutrophil recruitment and transmigration during inflammation, $\alpha_L\beta_2$ and other β_2 integrin are suggested to be activated by chemokine binding. Recent studies brought out another activation pathway of $\alpha_L\beta_2$, that is, activated by E-selectin binding to neutrophils. This newly proposed signaling pathway involves tyrosine kinase and is independent of the chemokine induced signaling pathway. The activation of β_2 integrins is suggested to be rapid, but there is no accurate estimation of the time scale so far. Using micropipette assay, the activation of β_2 integrins by E-selectin binding on neutrophils is detected in a real time fashion and the timescale is estimated. Furthermore, binding affinity of β_2 integrins activation by E-selectin binding is also accessed.

CHAPTER 2

BACKGROUND

2.1 $a_L\beta_2$ Mediated Cell Adhesion

2.1.1 Cell Adhesion and Cell Adhesion Molecules

Cell adhesion plays important roles in normal functions of cells, including cell proliferation, metabolism, and gene expression. Cell adhesion is necessary for many physiological processes and is involved in many diseases, such as inflammation, thrombosis, and cancer.

Cells adhere to each other or to the extracellular matrix through specific molecular interactions of proteins or carbohydrates referred to as receptors and ligands, or cell adhesion molecules. The known families of cell adhesion molecules include integrins, cadherins, selectins, and members of the immunoglobin (Ig) superfamily. Receptor-ligand mediated cell adhesions usually involve concurrent binding of multiple species of receptors and ligands and take place as a dynamic process. Adhesion receptors not only simply sticking cells down in the correct locations, although that in itself is important, they also form physical linkages between the extracellular environment and the internal structures of cells.

2.1.2 β_2 integrins

Integrins are a family of cell surface receptors that integrate the cytoskeleton with points of attachment in the extracellular environment to mediate cell adhesion, polarization, and migration. Integrins are heterodimeric molecules composed of two transmembrane subunits, an α subunit (~120–180 KDa) and a β subunit (~90–120 KDa).

So far, at least 18 different α subunits and 8 β subunits have been described in vertebrates, forming at least 24 heterodimers [2, 3] (Figure 2-1).

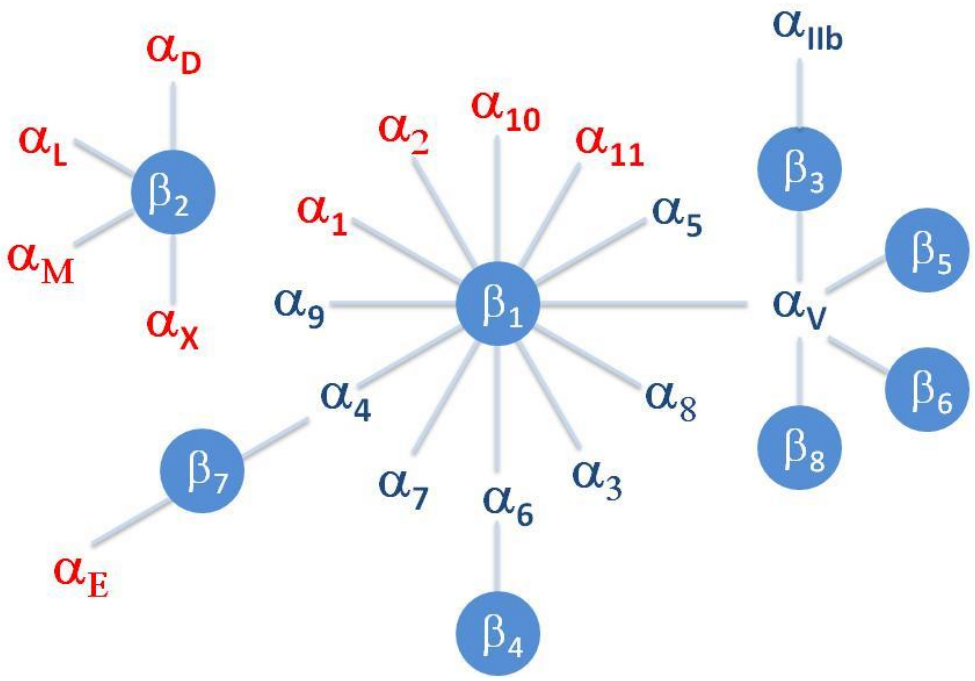

Figure 2-1. The family of 24 integrin heterodimers. The α subunits that contain an I domain are shown in red.

$\alpha_L\beta_2$ (CD11a/CD18) is also known as lymphocyte function-associated antigen-1 or LFA-1 [4]. $\alpha_L\beta_2$, together with $\alpha_M\beta_2$ (CD11b/CD18, Mac-1), $\alpha_X\beta_2$ (CD11c/CD18, P150,95), and $\alpha_D\beta_2$ (CD11d/CD18) constitute β_2 integrin family, also called leukocyte integrins (Figure 2-1) [3]. Cell-cell adhesions mediated by these integrins contribute to many physiological processes of leukocytes, such as antigen presentation, cytotoxicity and phagocytosis. The discovery of the genetic basis of an inherited disease called leukocyte adhesion deficiency (LAD) syndrome, which manifests as defect in leukocyte adhesion and is caused by the lack of expression of β_2 integrins on the cell surface,

underscored the important biological role of these receptors in the inflammatory and immune responses [5].

2.1.3 Ligands of $\alpha_L\beta_2$

Physiological ligands of $\alpha_L\beta_2$ include Intercellular Adhesion Molecule (ICAM)-1,-2, and -3 [6, 7]. Two additional ligands, ICAM-4 and -5 have also been shown to bind specifically to $\alpha_L\beta_{2,}$ but their physiological function is currently unknown [6, 8]. ICAM-1, -2, and -3 are structurally related glycoproteins that belong to the immunoglobulin superfamily (IgSF). Among them, ICAM-1 (CD54) is the major ligand for $\alpha_L\beta_2$ in mediating most biological functions of leukocytes.

ICAM-1 is a Type-I transmembrane glycoprotein of 85–110 KDa composed of five IgSF domains (D1-5), a transmembrane domain, and a short cytoplasmic tail that binds α-actin (Figure 2-2A) [9]. It is expressed at relatively low basal levels on leukocytes and several other cell types, but the expression is induced or greatly increased by various pro-inflammatory cytokines and phorbol esters [10, 11] ICAM-1 is important for granulocyte extravasation, lymphocyte mediated cytotoxicity, and the development of specific immunological responses involving cell-cell interactions. Among the five Ig-like domains of ICAM-1, only the structure of domains 1-2 has been solved in X-ray crystallography (Figure 2-2B). The most important residue in ICAM-1 for binding to $\alpha_L\beta_2$ is Glu-34, which has been shown to ligate the Mg^{2+} in the MIDAS of the I domain [12] (Figure 2-2B). Although there are differences between ICAM-1s in different species, Johnston *et al.* (1990) showed that human $\alpha_L\beta_2$ also binds specifically to murine ICAM-1

and the cross-species binding is unidirectional, that is, mouse $\alpha_L\beta_2$ could not bind to human ICAM-1 [1].

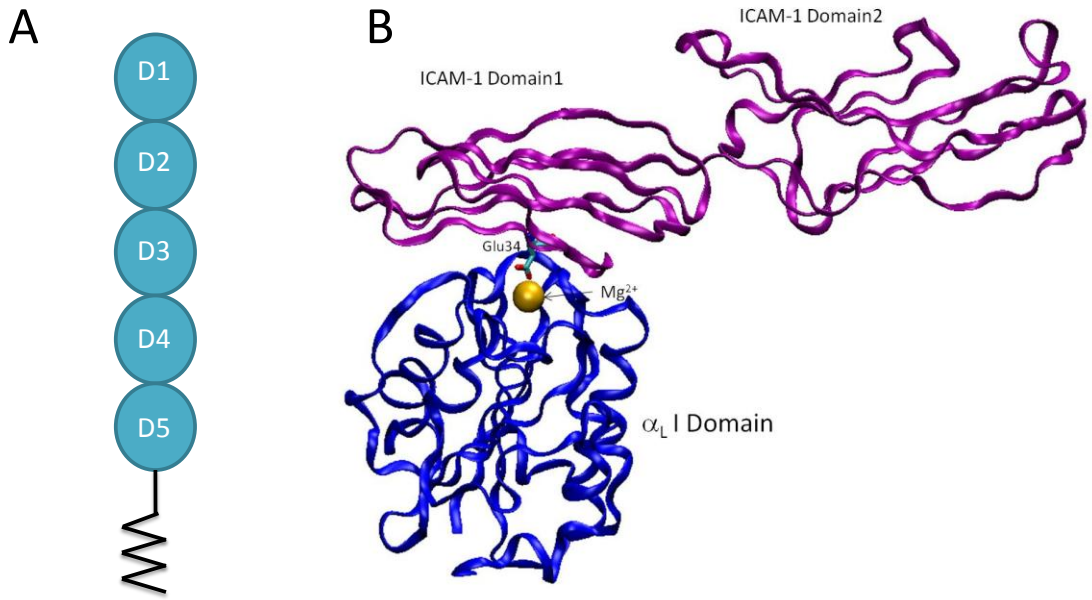

Figure 2-2. (A) Domain arrangement of ICAM-1. (B) Diagram of the intermediate affinity α_L I domain (blue) complex with the first two domains of ICAM-1 (purple) [12]. Mg^{2+} (gold sphere) in I domain MIDAS and ICAM-1 Glu-34 (shown as ball-and-stick) are indicated. The structure is drawn by Visual Molecular Dynamics using PDB codes 1MQ8.

2.1.3 $\alpha_L\beta_2$ Mediated Cell Adhesions in Immune Responses

$\alpha_L\beta_2$ is present on nearly all leukocytes and mediates a variety of leukocyte adhesion and signaling processes, such as firm adhesion to the vascular surface during the initiation of inflammatory reaction or during lymphocyte trafficking, transendothelial migration into inflamed tissues or lymphoid tissues [13] and adhesion to antigen presenting cells to form the immunological synapse [14].

Leukocyte Adhesion during Inflammation

Inflammation is a defense reaction of vascular tissues to harmful stimuli, such as pathogens, damaged tissue and cells, or irritants. It is a protective attempt by the organism to remove the harmful stimuli as well as initiate the healing process for the tissue. In order to eliminate the pathogen and to repair the injured tissue, leukocyte need to be recruited and transmigrate through endothelia to the site of infection or injury. Selectins and integrins are the two most important cell surface adhesion molecules in the recruitment of leukocytes.

Selectins are another family of cell adhesion molecules. All selectins contain an N-terminal C-type lectin domain, with structural homology to calcium-dependent lectins, followed by an epidermal growth factor (EGF)-like domain, a series of consensus repeats, a transmembrane domain, and a cytoplasmic tail (Figure 2-3). L-selectin, the smallest of the vascular selectins, is expressed on leukocytes and binds to constitutively or inducibly expressed ligands on endothelial cells and to ligands on other leukocytes. E-selectin is expressed on activated endothelial cells with chemically or cytokine-induced inflammation, and binds to ligands on leukocytes. P-selectin is the largest selectin and is stored in secretory granules of platelets and endothelial cells. All known selectin ligands are transmembrane glycoproteins which present oligosaccharide structures to the selectins. Selectins bind to these ligands with low affinity and thus form transient bond. P-selectin glycoprotein ligand-1 (PSGL-1) is originally identified as a high affinity ligand for P-selectin [15], but recent studies showed it also binds to L-selectin and supports the initial tethering of flowing leukocytes to E-selectin [16-18]. E-selectin ligands on

leukocytes are not yet fully identified, but potential candidates are PSGL-1, L-selectin, and other fucosylated, sialyated oligosaccharides.

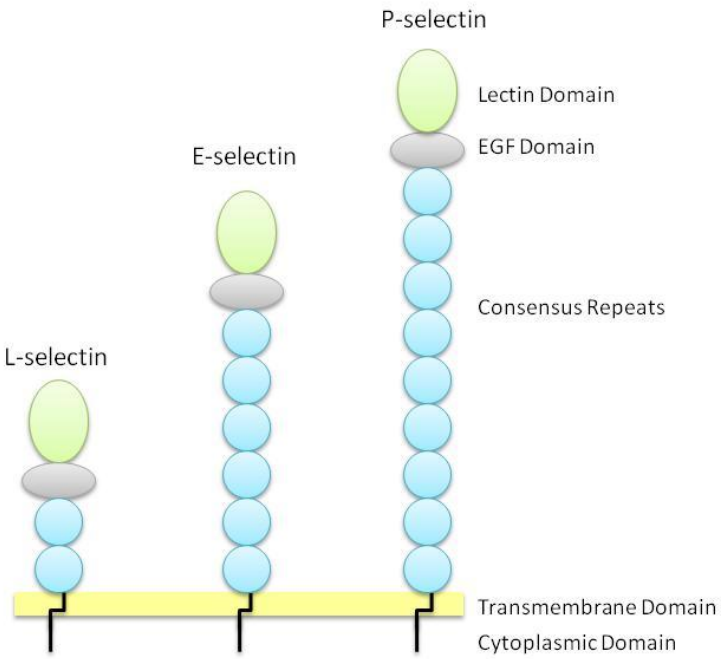

Figure 2-3. Molecular structure of three selectins. They all contain an N-terminal lectin domain, an EGF domain, consensus repeats, a transmemberane domain, and a cytoplasmic domain.

Leukocyte recruitment during inflammation is a sequence of adhesion and activation events [19]. There are several steps of the adhesion cascade of leukocyte recruitment, including tethering, rolling, firm adhesion, and transmigration (also called diapedesis) (Figure 2-4). Interaction of selectins with cell-surface expressed ligands initiates rolling of leukocytes to activated endothelial cells. Selectin-mediated cell rolling is thought to promote ligation of endothelial-bound chemotatic molecules and lead activation of $\alpha_L\beta_2$ and $\alpha_M\beta_2$ integrins [13]. The activated β_2 integrins on leukocyte bind with high affinity to their ligand, mainly ICAM-1, to convert rolling to firm adhesion. It

has been suggested that the G protein-coupled receptor engagement of inflammatory mediators (such as IL-8, platelet-activating factor) presented on the endothelium is the primary recognition event inducing firm adhesion of leukocytes via activation of β_2 integrins [20] (Figure 2-4). Emerging evidence implicated there might be other means of leukocyte activation, one of them involves binding of selectins triggering activation of β_2 integrins [21-23].

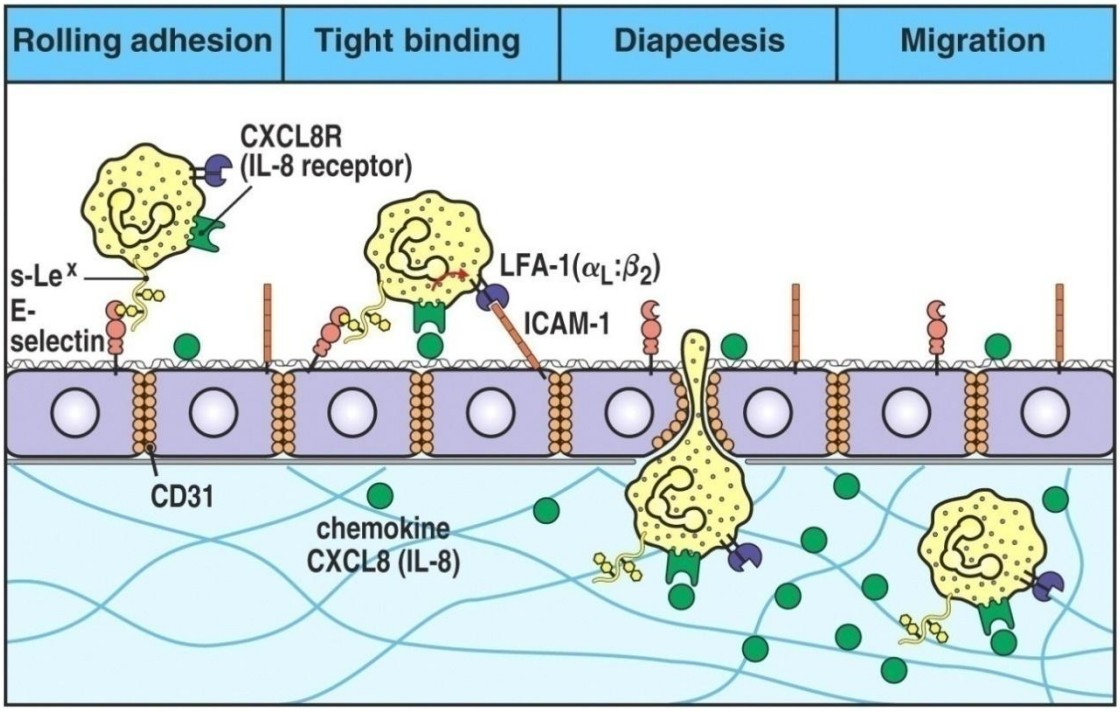

Figure 2-4. The recruitment of leukocytes to the site of infection is a multistep process. (Reproduced from Immunology, © 2001 by Garland Science)

T Cell and Antigen-Presenting Cell Adhesion

T cells play a central role in cell-mediated immunity. The key steps of effective T cell activation and mounting an immune response include the ability to firmly adhere to

blood vessel wall, the scanning by T cells of other cells within tissue, and the formation of the immunological synapse between T cells and APCs. Every step requires regulated adhesion of T cell to other cells. $\alpha_L\beta_2$ is particularly important in promoting the interaction of T cells in each step. It is essential for the arrest of rolling lymphocytes in many vascular beds to facilitate transmigration [24], for the crawling of activated T cell [25], and for the formation of the immunological synapse, a specialized structure that forms between T cells and APCs during T cell activation [14, 26]. $\alpha_L\beta_2$ mediated adhesion facilitates antigen presentation to T cells, especially in situations of low affinity T cell receptor (TCR)-Major Histocompatibility Complex (MHC):peptide interaction, and by enabling adequate duration of antigenic stimulation [27, 28].

Evidences have shown that $\alpha_L\beta_2$ may have more roles than simply an adhesion molecule. $\alpha_L\beta_2$ is also capable of transducing signals to influence T cell activation, particularly in the context of the immunological synapse, probably also during transmigration and migration [29, 30].

2.2 The Regulation of $\alpha_L\beta_2$ Activity

The term “integrin” was coined to reflect the unique capacity of members of this adhesion molecule family to integrate the extracellular and intracellular environments [31]. Integrin mediated interactions are vital to the maintenance of normal cell functions because of their ability to mediate signaling bi-directionally, i.e., from extracellular to intracellular and from intracellular to extracellular [3]. The most unusual feature that distinguish integrin from other adhesion molecules is that their ligand binding ability can be activated very rapidly through signaling. This feature is particularly important for the integrins to mediate normal function of platelets and leukocytes in bloodstream.

2.2.1 The Biological Significance of $\alpha_L\beta_2$ Regulation

The adhesive capacity of $\alpha_L\beta_2$ is not constitutively active; it is expressed on cell surfaces in an inactive or "off" state, in which it does not bind ligands and does not signal. Its activity is subjected to fine spatial and temporal regulation and this is very important for its biological functions.

One of the most important roles of $\alpha_L\beta_2$ is to mediate the leukocyte recruitment during inflammation, in which it binds to ICAM-1 on endothelial cells upon leukocytes become activated, for example by cytokines. It is critical that $\alpha_L\beta_2$ remain inactive and remain low binding affinity for ICAM-1 on the surfaces of resting leukocytes to avoid inflammation, and it can be rapidly activated to allow proper immune function. Defects in either have pathological consequences. Therefore, the regulation of $\alpha_L\beta_2$ activity has become therapeutic targets for inflammatory diseases, autoimmune diseases, and certain types of cancer [32].

2.2.2 The Mechanisms of $\alpha_L\beta_2$ Regulation

The mechanism of the regulation of $\alpha_L\beta_2$ activity is unclear, but a change in the molecular conformation or redistribution of the molecule in cell membrane seems most likely. The conformation change in a single molecule that alters the ligand binding affinity is also referred as affinity change; while the changes in molecule diffusivity on cell surface or changes in molecule local density that affect the number of adhesive bonds that can form is termed avidity change.

Dynamic regulation of $\alpha_L\beta_2$-mediated adhesion and functions requires integration of signals initiated by a wide range of stimuli. On resting circulating leukocytes, $\alpha_L\beta_2$ are

in the constitutive inactive state. However, upon activation of leukocytes by different stimulations, such as chemokine exposure or upon antigen-dependent interaction of a T cell with an APC, a variety of intracellular signals are generated that ultimately lead to the conversion of $\alpha_L\beta_2$ to active state. Major signal transduction pathways often act in concert with G protein-coupled or kinase receptors for soluble factors. This so called "inside-out" signaling is initiated from inside of the cell and eventually induces high ligand binding affinity of the ligand binding site of $\alpha_L\beta_2$. Although the molecular mechanism of this regulation is not clear, more and more evidences suggested that the inside-out signaling involves the separation of the transmembrane and intracellular regions of $\alpha_L\beta_2$ and long-range conformational rearrangement of the extracellular domains [33-35].

By comparison, outside-in signaling is induced by the binding of $\alpha_L\beta_2$ to its ligands. Due to the multivalent nature of ICAM-1, ligation may result in clustering of $\alpha_L\beta_2$ on cell surface, and thus enable the recruitment of signaling molecules to the cytoplasmic face of the adhesion complex to initiate downstream signaling events [36]. Another possibility is that the outside-in signaling pathway can be viewed as the reciprocal process of inside-out, that is, the ligation of $\alpha_L\beta_2$ could induce the same conformational rearrangement as in the inside-out activation but in a reverse direction, and finally lead to the separation of cytoplasmic tails to induce signaling. It is possible that the overall outside-in signaling is achieved as a sum of intermolecular clustering and conformational change of individual molecule, since integrin clustering alone is not sufficient to reproduce full outside-in events [37].

2.3 The Conformational Change of $\alpha_L\beta_2$

2.3.1 $\alpha_L\beta_2$ Domain Structure Arrangement

The N-terminal half of the α subunit's extracellular portion contains seven tandem repeats, which are predicted to adopt a β-propeller fold. In $\alpha_L\beta_2$ and other β_2 integrins as well as $\alpha_1\beta_1$, $\alpha_2\beta_1$, $\alpha_{10}\beta_1$, $\alpha_{11}\beta_1$, and $\alpha_E\beta_7$ integrins, an additional highly conserved I domain (or A domain, also designed as α–I/A domain), approximately 200 amino acids long, is found between the second and third repeats of the β-propeller domain [38]. The C-terminal half of the α_L subunit's extracellular portion is the stalk region. There are three β-sandwich domains in this region, including the thigh, Calf-1, and Calf-2 domains (Figure 2-5). The N-terminal region of β_2 subunit contains a PSI (Plexin, Seaphorins, and Integrin) domain. It also contains an evolutionarily conserved domain termed I-like domain (or β I/A domain)**.** This domain appears to directly bind ligand in integrins that lack I domain and to indirectly regulate ligand binding of the I domain in the I domain-containing integrins. The hybrid domain is folded from amino acid sequence segments on either side of the I-like domain. The C-terminal half of the extracellular portion of the β subunit contains four cysteine-rich repeats, called integrin-epidermal growth factor (I-EGF) 1-4 domains, which are characteristic of all integrin β subunits [39] and a β-tail domain (βTD) (Figure 2-5).

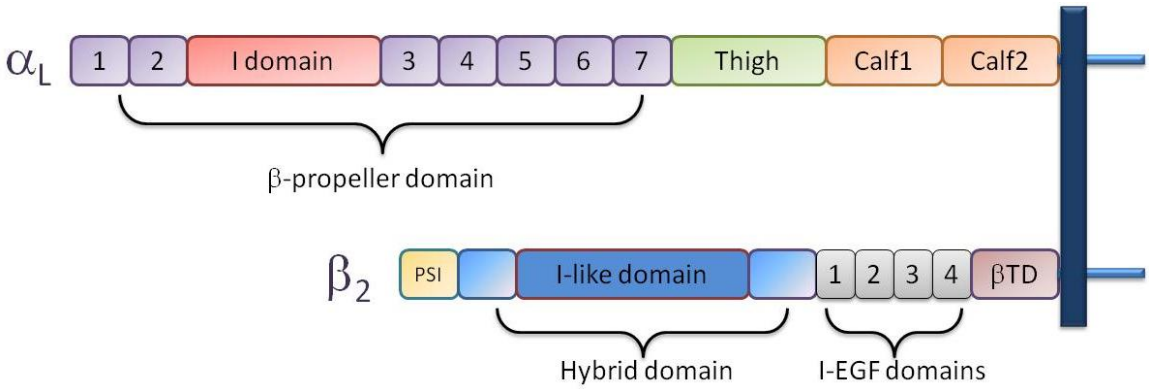

Figure 2-5. The arrangement of multiple domains in the primary structure of the extracellular portion of $\alpha_L\beta_2$.

2.3.2 Structure and Allosteric Regulation of the I Domain

I domain is the major ligand binding site for I domain-containing integrins. Recombinant I domain binds ligand with the same specificity as the parental integrin and the binding is also in the same cation-dependent manner [40]. The deletion of the I domain abolished ligand binding in the context of the intact integrin [41].

I domain assumes a dinucleotide-binding fold with α-helices surrounding a central β-sheet with a metal ion coordinating site on one end (defined as the top of the domain) and is connected through the adjacent N and C termini on the opposite end (bottom) to the body of the integrin [42] (Figure 2-6). The metal-coordinating residues and the residues surrounding the metal-binding site form the binding site for several physiologic ligands. Therefore, this site has been designated as the metal ion-dependent adhesion site (MIDAS) [42].

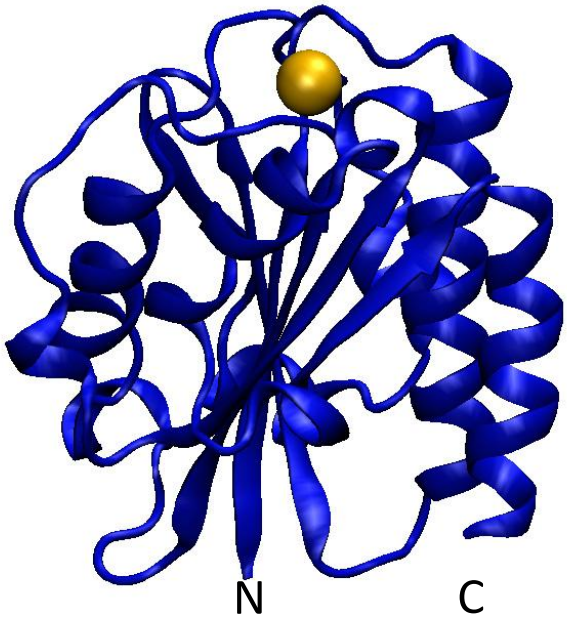

Figure 2-6. Structure of the α_L I domain [43]. The structure of intermediate α_L I domain is shown as ribbon diagram. Mg in MIDAS as a golden sphere and C- and N-terminus are indicated. The structure is drawn by Visual Molecular Dynamics using PDB codes 1ZOP.

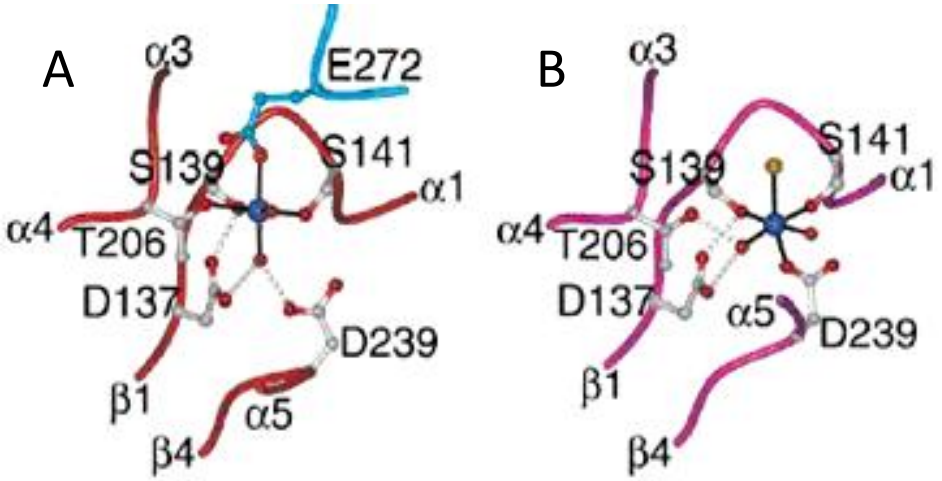

Figure 2-7. MIDAS structures of (A) the pseudo-liganded high-affinity I domain, and (B) the unliganded WT I domain. The ligand mimetic molecule is colored cyan. The metal ions are colored blue, water molecule and ligating side chain oxygen atoms are colored red, and the chloride ion from the wild-type I domain structure is colored orange. The MIDAS residues and Glu-272 from a lattice mate I domain in (A) are shown as ball-and-stick models. Metal coordination and hydrogen bonds are represented by solid black lines and gray dotted lines, respectively. (Figure and legend reproduced from reference [12])

The integrin WT α_M [42, 44], α_2 [45] and α_L [46-49] as well as mutant α_L I domains [12] were found to crystallize in two different conformations, which were termed open and closed conformers. In the open structure, an acidic residue donated either by a ligand or by a ligand mimetic lattice contact contributes to the metal ion coordination sphere in the MIDAS. The metal ion is central to the binding site and directly coordinates a Glu residue in the ligand [50] (Figure 2-2B). By comparison, no ligand-like contact in the closed structures has been determined (Figure 2-7). The structural rearrangement of the MIDAS is coupled to backbone movements of the loops that bear the coordinating residues. The open and closed conformations also differ in the position of the C-terminal α7 helix (Figure 2-8). The transition from the closed to the open structure is linked to a large 10 Å downward movement of the C-terminal α7 helix and a repacking of the hydrophobic face of the α helix [51].

Based on the crystal structures, it is hypothesized that the downward movement of the α7 helix allosterically change the conformation of MIDAS and thus change the ligand binding affinity. Mutations have been introduced to stabilize a particular conformation, and tested for effect on ligand binding. α_L I domain were locked in either open or closed conformation using the structure of the open α_M I domain as a template [52]. The candidate positions were chosen far away from the MIDAS and thus presumed not to disturb the structure and function of the binding site. The positions were found bracket the loop between the C-terminal α-helix and the preceding β-strand (Figure 2-9A). A pair of cysteines was introduced to lock this loop in two alternate conformations. The mutations were at residues 287 and 294 for the open conformation, and at residue 289

and 294 for the closed conformation (Figure 2-9B). Locked intermediate I domains have also been designed using similar mutations. Cysteine mutations were introduced at residue 161 and 299, 160 and 299, or 161 and 300 [12].

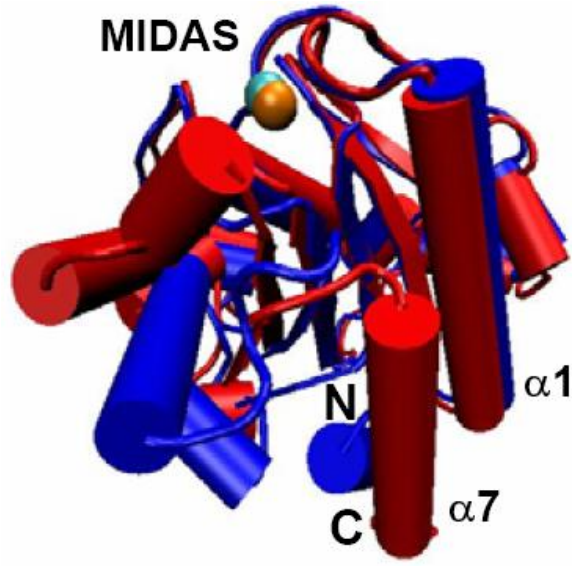

Figure 2-8. Structures of I domain at open and WT closed conformations. Overlay of the locked open (blue) and WT closed (red) I domain structures showing the conformational change of the I domain (drawn by Visual Molecular Dynamics using PDB codes 1MQ9 and 1ZOP, respectively). MIDAS is located on the top of the I domain with a coordinating Mn^{2+} ion, which is in cyan (closed) and orange (open). The N- and C-termini are located on the bottom (indicated).

The mutants were tested for ligand binding to investigate the effect of conformational change. Both 3D [50] and 2D [53] binding kinetics measurements showed that the open, intermediate, and closed conformers correspond to the high, intermediate, and low affinity states. These data also suggested that the conformation and position of the C-terminal α helix and the preceding loop allosterically regulate the affinity of ligand binding at the MIDAS.

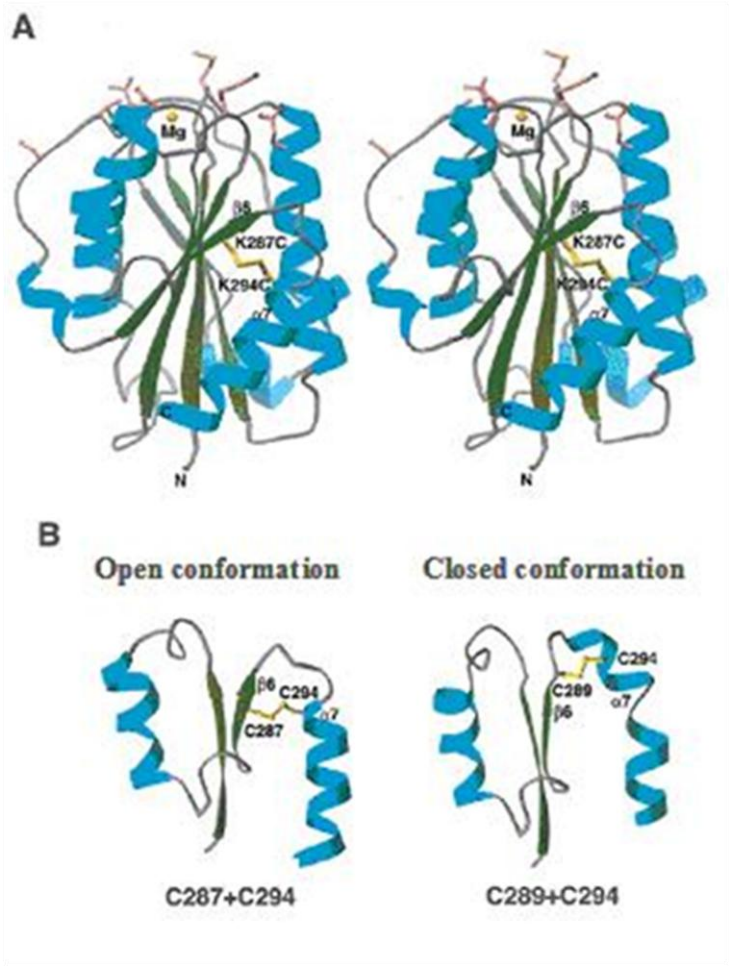

Figure 2-9. Mutant α_L I domains. (A) Stereodiagram of the open conformation model of the α_L I domain, with mutations to introduce a disulfide bond. The side chains and disulfide bond of C287 and C294 are shown in yellow. The Mg^{2+} ion of the MIDAS is shown as a gold sphere. Sidechains of residues important in binding to ICAM-1 are shown with rose-pink sidechains and yellow sulfur, red oxygen, and blue nitrogen atoms. Note that these residues surround the Mg^{2+} ion and are distant from the disulfide. (B) Predicted disulfide bonds that are selective for open (left) or closed (right) conformers of the αL I domain. Only residues 254–305 of the models are shown. The downward movement of the α7 helix in the left panel compared to the right panel is readily apparent. (Figure and legend reproduced from reference [50])

It is believed the conformational changes induced by the downward movement of the α7 helix appears to be first propagated to the hydrophobic core of the I domain and then to the MIDAS loop [51]. Crystal structures have shown that a hydrophobic pocket holds the β6-α7 loop in three different positions, and each movement displaces the α7 helix a distance downward corresponding to one turn of helix. In the close, intermediate, and open structures, this hydrophobic pocket is occupied by Leu-295, Phe-292, and Leu-289, respectively (Figure 2-10) [12]. This hypothesis is supported by the experimental evidences that mutation of key residues in the hydrophobic core disrupted the hydrophobic interactions and conformational restrain [54]. The single mutations of the hydrophobic core, F265S, F292A, and F292G, increased the 3D binding affinity to ICAM-1 by 20 to 10,000 fold. Double mutation F265S/F292G induced an increase of 200,000-fold in 3D binding affinity to ICAM-1. Further support for the allosteric regulation of I domain is provided by flow chamber cell rolling experiment. When mediating cell rolling, the force exerted on C-terminal α7 helix, but not N-terminus, appears to convert WT isolated I domain to open conformation and stabilize it [55, 56].

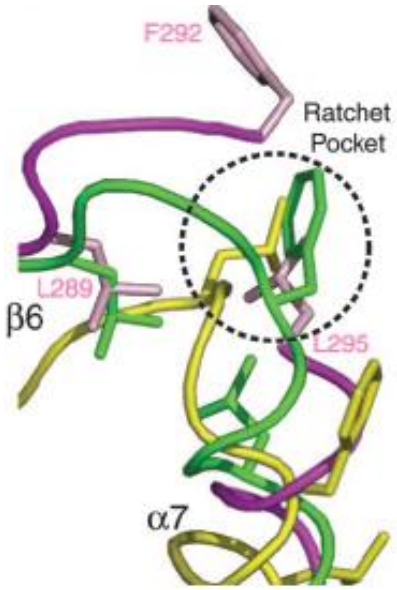

Figure 2-10. The hydrophobic pocket that acts as a detent for the rachet-like movement of the β6-α7 loop. The C_α trace and ratchet side chain (Leu-289, Phe-292, Leu-295) for the closed (magenta), intermediate (green), and open (yellow) conformations of the α7-helix are depicted. (Figure and legends reproduced from reference [54])

2.3.3 Global Conformational Change and Rearrangement of $\alpha_L\beta_2$

It has been suggested that the activation of integrins on cell surface is accomplished by conformational changes of the extracellular domains. Electronic microscopy (EM) studies showed that the extracellular portion of integrin contains a globular headpiece, and two long stalk regions containing C-terminal segments from the α and β subunits that connect the headpiece to the transmembrane and the cytoplasmic domains [57, 58]. In 2001, the first X-ray crystal structure of the extracellular domain of integrin $\alpha_V\beta_3$ was published [59]. Surprisingly, $\alpha_V\beta_3$ assumed a bent conformation, in which the ligand-binding headpiece is folded back onto the tailpiece of the molecule (Figure 2-11). There is no crystal structure for the ectodomain of $\alpha_L\beta_2$ to present.

Recently, an EM study showed that $\alpha_L\beta_2$ could also adapt the same V-shape bent conformation when α and β subunits are clasped together [60].

The bent conformation appears unfavorable for binding to extracellular matrix or cell-surface ligands. Nuclear Magnetic Resonance (NMR), EM, mapping on the structures of epitopes of conformation-sensitive and activating antibodies, and engineering of disulfide bonds across the head-tail interface, have together established that the bent or closed integrin conformation represents the physiological low affinity state [35, 61, 62]. Activation and ligand binding are associated with a separation of the α and β tails that is coupled to a long-range global conformational change in which the integrin extends with a switchblade-like motion [35, 58, 61].

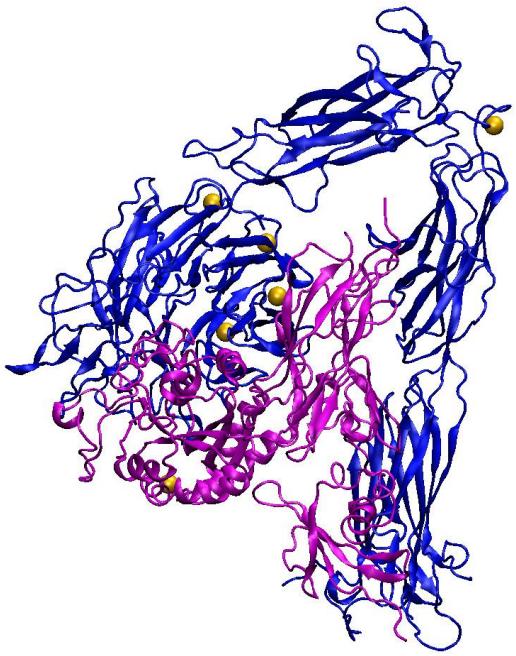

Figure 2-11. Crystal structure of the ectodomain of $\alpha_V\beta_3$ [59]. The two subunits are shown in different colors (α_V subunit in blue and β_3 subunit in purple) and the Ca^{2+} is shown as golden sphere. The structure is drawn by Visual Molecular Dynamics using PDB codes 1JV2.

The cytoplasmic domain regulates the integrin activation by initiating the separation of the α and β subunit cytoplasmic and transmembrane domains. As a consequence, the extracellular interface between the two subunits in the tailpiece becomes destabilized, which facilitates the switchblade-like opening. The disruption of this interface enables the hybrid domain to swing out from the I-like domain in the β subunit, facilitating the downward movement of the I-like domain C-terminal α helix that is coupled to I-like domain MIDAS rearrangement (Figure 2-12). For $\alpha_L\beta_2$, an "intrinsic ligand" α subunit residue Glu-310 binds to the activated I-like domain MIDAS. This binding pulls the C-terminal α helix of the I domain downward and converts it to the activated conformer for high affinity ligand binding [63, 64] (Figure 2-12).

Both EM studies [35] and kinetic measurements of I domains [50] indicated that multiple conformational states of integrin coexist. It has been suggested that the regulation of integrin conformation should be viewed as a shifting of the dynamic equilibrium among three conformers, a bent conformation, an extended conformation with a closed headpiece, and an extended conformation with an open headpiece, rather than the flipping of a switch [12, 65, 66] (Figure 2-13).

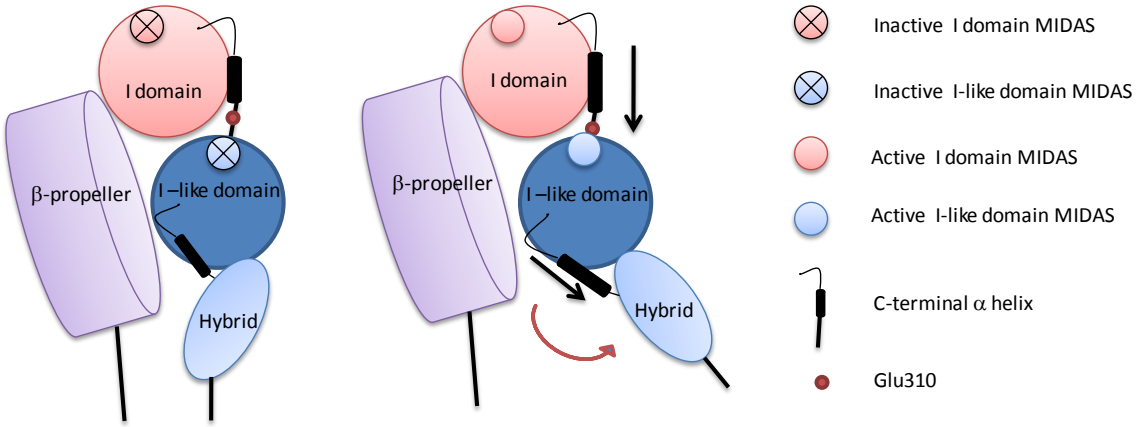

Figure 2-12. Conformational change model for the activation of headpiece of I domain containing integrin [64]. The out-swing of the hybrid domain from I-like domain changes the angle between these two domains and pulls the C-terminal α-helix of the I-like domain. This further converts the I-like domain MIDAS to open conformation with high affinity. The intrinsic ligand Glu-310 in turn binds to the activated I-like domain MIDAS and the binding pulls down the I domain C-terminal α7 helix. The I domain MIDAS is then converted to the open conformation and can bind to ligand with high affinity.

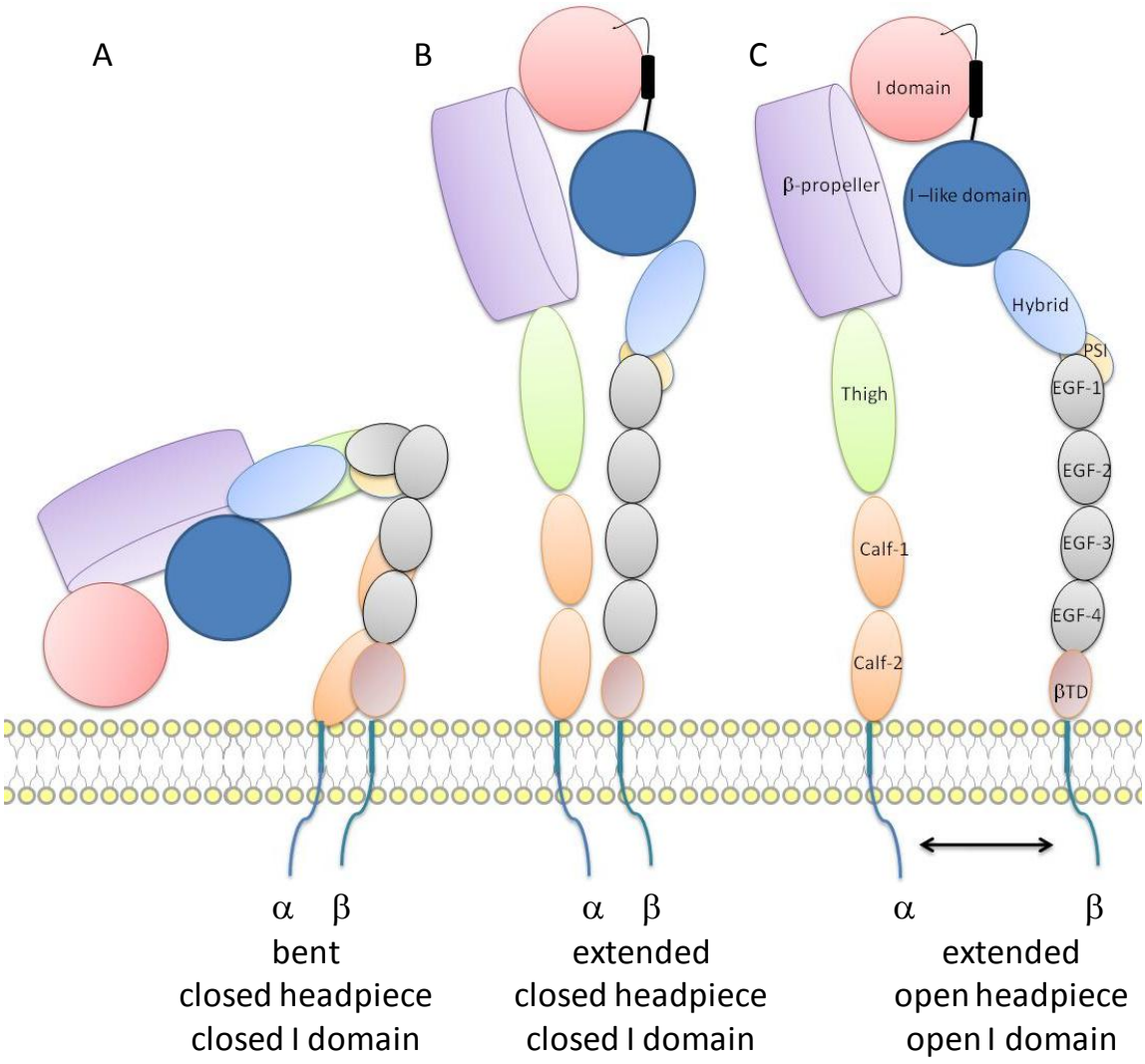

Figure 2-13. Models for multiple conformational states of $\alpha_L\beta_2$. (A) Bent conformation with closed headpiece and closed I domain with low ligand binding affinity. (B) Extended conformation with closed headpiece and closed I domain. (C) Extended conformation with open headpiece and open I domain. This conformation has high ligand binding affinity.

2.4 Receptor-Ligand Binding Kinetics and Micropipette Adhesion Frequency Assay

2.4.1 Receptor-Ligand Binding Kinetics

Receptor-ligand interactions are usually modeled by a chemical kinetics framework. For example, the following simple reversible reaction scheme models binding between a free receptor R and a free ligand L to form a bond B:

$$R + L \underset{k_r}{\overset{k_f}{\leftrightarrow}} B \qquad \text{Equation 2-1}$$

where k_f and k_r are the respective on-rate (forward rate) and off-rate (reverse rate) constants. These kinetic rate constants are essential determinants of cell adhesion, for these parameters describe how rapidly cells bind and how long they remain bound [67]. The time rate of change of the bond concentration [B] is related to the free receptor concentration [R] and the free ligand concentration [L] through these constants:

$$\frac{d[B]}{dt} = k_f[R][L] - k_r[B] \qquad \text{Equation 2-2}$$

At equilibrium, d[B]/dt = 0. The free receptor, free ligand, and bond concentration are related through the dissociation constant, $K_D = k_r/k_f$,

$$K_D = \frac{[R][L]}{[B]} \qquad \text{Equation 2-3}$$

The affinity constant is K_a, $K_a = 1/K_D$.

2.4.2 Micropipette Adhesion Frequency Assay

Much progress has been made in recent years to determine some of the relevant adhesion parameters experimentally. There are many methods for measuring 3D receptor-ligand interaction kinetics when at least one of the molecular species is in

solution. Examples are stop-flow experiments and SPR experiments [68]. However, few techniques allow quantification its 2D counterpart, when the two species are bound to two apposed surfaces, as in the case of cell-cell or cell-extracellular matrix adhesion. Recently, several techniques and models have been developed to characterize of bonds formed between two opposing surfaces. Using quantitative fluorescent microscopy, 2D affinity of CD2 to LFA-3 was determined by Dustin *et al*. using cells resting on a glass-supported lipid bilayer [69]. Chesla *et al*. developed a model with a micropipette binding frequency assay for measuring the force-free 2D affinity and kinetic rates for several forms of the Fcγ receptor CD16a and its ligand IgG [67]. This method is an extension of that of Evans [70, 71], which used an ultrasensitive red blood cell as a picoforce transducer to detect the adhesion mediated by a low number of receptor-ligand bonds (Figure 2-14). The measured adhesion frequency can be expressed as a function of the contact duration and kinetic rate constants,

$$P_a = 1 - \exp\{-m_r m_l A_c K_a [1 - \exp(-k_r t)]\} \qquad \text{Equation 2-4}$$

where m_r and m_l are respective densities for receptor and ligand. The effective binding affinity ($A_c K_a$) and the reverse-rate (k_r) were extracted from the binding frequency data by iteratively reweighted nonlinear regression to this model. Since the exact contact area A_c could not be measured but controlled by the experimenter to remain a constant, the affinity is called effective binding affinity because A_c and K_a are lumped together.

The micropipette adhesion frequency assay is an effective and reliable technique to measure the 2D binding kinetics of receptor-ligand interactions. Using this system, the binding kinetics of Fcγ receptor [67], selectin [72], T cell receptor, integrin [53], and cadherin for their respective ligands have been characterized. It is also an useful tool for

investigating biophysical and biological problems, such as the influence of anchoring form, molecule length, and glycosylation on 2D binding kinetics of receptors.

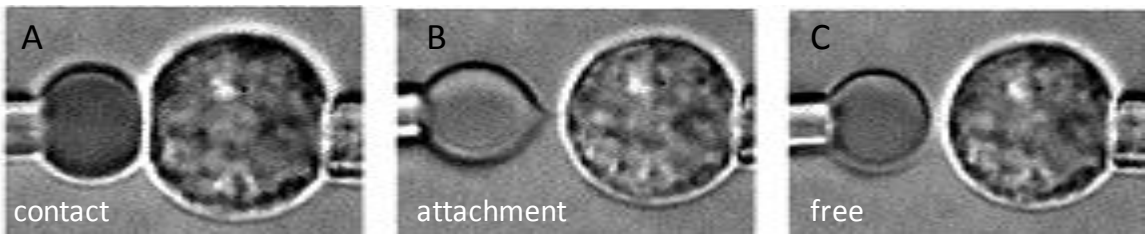

Figure 2-14. Photomicrographs of a typical adhesion test. (A) Two cells were brought into contact. (B) The elongation of the bound RBC indicates an adhesion event. (C) The spherical shape of the unspirated portion of the RBC indicates there is no adhesion.

CHAPTER 3
MATERIALS AND METHODS

3.1 Cells, Proteins, Antibodies, and Small Molecule Antagonists

3.1.1 Cell Culture and Isolation

K562 Cell line

Human erythroleukemia cell line K562 stably transfected with WT, locked open (K287C/K294C), locked intermediate (L161C/F299C), or locked closed (L289C/K294C) α_L I domain fused with a platelet-derived growth factor receptor transmembrane domain and the first five amino acids of its cytoplasmic domain or with intact $\alpha_L\beta_2$ containing the WT or locked I domains are generous gifts of Dr. Timothy Springer (Harvard Medical School, Boston, MA) [12, 50]. The cells were cultured in RPMI with 10% fetal calf serum with glutamine (4 mM), penicillin/streptomycin (0.1 mg/ml). Hygromycin B (0.4 mg/ml) and Puromycin (4 μg/ml) were used as selection agents for I domain and $\alpha_L\beta_2$ cells, respectively. Maximum cell densities were ~$5x10^5$/ml.

Human RBCs Isolation and Storage - Human RBCs were isolated from whole peripheral blood of healthy donors. Approximately 7 ml whole blood was collected by venipuncture into sterile Vacutainers (Becton Dickinson, San Jose, CA) containing ethylenediamine-N,N,N',N'-tetraacetic acid (EDTA). This was carefully layered over 3 ml of Histopaque 1119 (Sigma Chemical Co., St. Louis, MO) and centrifuged (30 min, 2000 g, room temperature). The supernatant was removed and the pelleted RBCs were washed once in RBC storage solution (EAS45) [73]. RBCs were stored aseptically at 4°C in EAS45 at 20% hematocrit.

Human Neutrophil Isolation

Human neutrophils were isolated from a drop of whole blood via a finger prick. The RBCs were lysed by brief hypotonic shock with ddH_2O for 10 seconds. The blood cells were then spinned down and resuspended in Hank's Balanced Salt Solution (HBSS, Sigma-Aldrich, St. Louis, MO) with 1% human serum albumin (HSA, ZLB Plasma, Boca Raton, FL). Cells were put into micropipette chamber immediately for experiment.

3.1.2 Proteins and Antibodies

Purified Proteins

Mouse and human glycosyl phosphatidylinositol (GPI)-anchored ICAM-1 molecules were purified from Chinese hamster ovary (CHO) cell transfectants by affinity chromatography [74]. Recombinant human ICAM-1/Fc chimera and recombinant human ICAM-1 were from R&D Systems (Minneapolis, MN). Recombinant human E-selectin/Fc chimera was purchased from Glycotech (Gaithersburg, MD). Human soluble E-selectin, recombinant human P-selectin/Fc chimera, and L-selectin/Fc chimera were generous gift from Dr. Rodger McEver (University of Oklahoma Health Sciences Center, Oklahoma City, OK).

Antibodies

Fluorescein isothiocyanate (FITC)-conjugated mouse anti-human α_L I domain monoclonal antibody (mAb) MEM-25 (IgG_1) (Caltag Laboratories, Brulingame, CA) and a nonbinding FITC-conjugated mouse isotype-matched control antibody were used to determine surface expression of the α_L I domain and $\alpha_L\beta_2$ on K562 cells by immunofluorescence flow cytometry. FITC-conjugated mouse mAb MEM-111 (Caltag Laboratories, Carlsbad, CA) and FITC-conjugated rat mAb YN1/1.7.4 (eBioscience, San Diego, CA) were used to determine the site densities of the human and mouse ICAM-1, respectively. The mouse anti-human α_L mAb 38 (Ancell, Bayport, MN) was used for antibody-antigen adhesion kinetic measurement. FITC-conjugated rat anti-mouse IgG_{2a}

mAb (Fc specific) (BD Biosciences Pharmingen, San Jose, CA) was used to measure the site density of mAb 38 coated on RBCs. The anti-ICAM-1 capturing mouse mAb CA7 was a generous gift of Dr. Robert Rothlein (Boehringer-Ingelheim Pharmaceuticals, Ridgefield, CT).

The mAb MEM83 (Abcam, Inc., Cambridge, MA), and mAb CBR LFA1/2 [75] (a generous gift of Dr. Timothy Springer) were used to activate $\alpha_L\beta_2$. The mAb KIM127 [76], kindly provided by M. Robinson (Celltech, Slough, U.K.), was used as a conformation reporting antibody. β_2 integrin blocking mAb 7E4 was purchased from Beckman Coulter, Inc. (Fullerton, CA).

Mouse mAbs ES-1, PL-1, and DREG56 were kindly provided by Dr. Rodger McEver. ES-1 was used to determine E-selectin site density and to block E-selectin mediated adhesion. PL-1 and DREG56 were used to block PSGL-1 and L-selectin, respectively. A secondary FITC-conjugated goat anti-mouse IgG (Pierce Biotechnology, Inc., Rockford, IL) was used for site density determination. A biotinylated goat anti-human IgG Fc specific antibody (eBioscience, San Diego, CA) was used to capture recombinant human ICAM-1/FC, E-/P-/L-selectin/Fc chimeras.

Antibody Fragmentation

mAbs ES-1, PL-1, and DREG-56 Fab were prepared using the Fab preparation kit (Pierce Biotechnology, Inc., Rockford, IL) following the manufacture's instruction. Briefly, antibodies were incubated with immobilized papain with continuous rotation for overnight at 37^{o}C. The digested antibody mixture was then subjected to a Protein A column to separate Fab and Fc fragments. Fab fragments were collected at 1 ml fractions and concentrated using Amicon Ultra-15 Centrifugal Filter Units (Millipore, Billerical, MA). Fc fragments were eluted and collected as well. The Fab and Fc fragments were subjected to a SDS-PAGE gel to verify the purity.

3.1.3 Small Molecule Antagonists

Small molecule antagonists BIRT 377, and XVA 143 were generously provided by Dr. Timothy Springer.

3.2 Coupling of Proteins to RBCs

3.2.1 GPI-ICAM-1 Reconstitution in RBCs

Mouse or human GPI-ICAM-1 was reconstituted in RBC membrane by a 2.5-hour incubation with different concentrations to achieve the desired site densities [77]. Coated RBCs were washed and assayed for site density by flow cytometry and stored in EAS45 at 4^{o}C.

3.2.2 Coupling of Proteins to RBCs Using Chromium Chloride Method

Chromium Chloride ($CrCl_3$) method [67] was used to covalently couple capture antibody CA7, anti-human α_L I domain mAb 38, and recombinant human ICAM-1 to the membranes of RBCs. Coated RBCs were washed and assayed for site density by flow cytometry and stored in EAS45 at 4^{o}C. CA7-coated RBCs were incubated with human ICAM-1 prior to micropipette experiment.

For coupling, RBCs were washed with 0.85% NaCl for at least 5 times. 10^7 RBCs were suspended in 250 μl 0.85% NaCl and 1 mg protein/antibody was added. 1% $CrCl_3$ was diluted in 0.02M acetate buffer (PH 5.5) to achieve desired concentration. The RBCs and protein/antibody mixture was vortexed and at the same time, 250 μl of the diluted $CrCl_3$ was added drop by drop. After incubation at room temperature for 5 min, PBS/EDTA/1%BSA was added to quench the reaction. The coupled RBCs were washed 3 times with PBS/EDTA/1%BSA and stored in EAS45 at 4^{o}C.

3.2.3 Coupling of Proteins on RBC by Biotin-Streptavidin Reaction

Biotin-streptavidin binding was used to coat biotinylated goat anti-human IgG Fc antibody on RBC membrane. For RBC biotinylation, RBCs were washed 3 times with PBS, and incubated with titrated Biotin-X-NHS (Calbiochem, San Diego, CA) for 30 min at room temperature. The RBCs were then washed for 3 times with PBS/1%BSA. The biotinylated RBCs were incubated with 10 μg/ml streptavidin (Pierce Biotechnology, Inc., Rockford, IL) for 30 min at RT, and washed 3 times with EAS45 afterwards. The RBCs were then incubated with 10 μg/ml biotinylated goat anti-human IgG Fc specific antibody for 30 min at 4^{o}C and washed 3 times with EAS45. Recombinant human ICAM-1/Fc Chimera and human E-selectin/Fc (or P-selectin/Fc, L-selectin/Fc) chimera were captured onto RBCs by incubating the proteins with capture antibody coated RBCs. To adjust the site density, proteins were added at different concentrations. The RBCs with captured molecules were used immediately for micropipette experiments.

3.3 Cell Sorting and Site Density Measurements

3.3.1 Fluorescent Staining

Fluorescent staining cells for flow cytometry followed the standard protocol. Cells were washed in FACS buffer (RPMI with 1% FBS, 5mM EDTA, 0.02% Sodium Azide) and counted. $5x10^4$ cells were then resuspended in 100 μl FACS buffer and placed in a 1.5 ml Eppendorf tube.

To measure the site densities of cell surface molecules or to sort the cells, samples were incubated on a shaker for 30 min at 4°C, with saturating concentrations of primary antibodies (usually 10 μg/ml of purified mAb or follow the manufacturer's instruction).

For FITC-conjugated primary antibodies, cells were washed 3 times with FACS buffer and analyzed immediately. For non-conjugated primary antibodies, FITC-conjugated secondary antibody was added at saturating concentration and the cells were incubated for an additional 30 min at 4^{o}C in dark. Cells were then washed 3 times with FACS buffer and analyzed immediately.

To access the effect of activating antibodies and small molecule antagonists on the conformation of $\alpha_L\beta_2$, the cells were incubated with activating antibodies (10 μg/ml) or small molecule antagonists (1 μM XVA143, or 10 μM BIRT 377) for 30min at room temperature. The cells were then incubated with KIM127 (10 μg/ml) for 30min at 37^{o}C. FITC-conjugated goat anti-mouse IgG (Pierce Biotechnology, Inc., Rockford, IL) was used as secondary antibody for fluorescent staining for flow cytometry.

3.3.2 Data Acquisition

Samples were read on BD LSR flow cytometry (Becton-Dickinson Immunocytometry Systems, San Jose, CA) using FACS DiVa 3.1 software. Standard beads (Quantum™ 25 FITC High Level, Bangs Laboratory, Fisher, IN) were prepared for quantification of MESF (molecules of equivalent soluble fluorophore). 2D gates of FL1 (FITC) histogram were created to gate on the forward scatter vs. side scatter histogram and placed around the singlet population to isolate single cells from aggregates and debris. These gates were created with the guidance of experience regarding the characteristic scatter patterns for single cells and aggregates of a particular cell type. The forward scatter thresholds were raised to exclude debris. FL1 (FITC) voltage levels were adjusted to place the fluorescent histograms of reference blank near the origin of the log intensity scale. After having established the calibration plot, no further adjustments were

made to the instrument. The mean channels for each of the five calibrated microbeads were recorded. After completing the FI calibration procedure, the samples were run and the FL1 mean channels were recorded. Generally 10,000 events per sample were recorded.

3.3.3 Cell Sorting

Fluorescent staining for cell sorting followed the same procedure as that for site density determination. Samples were read on BD FACSVantage SE flow cytometry (Becton-Dickinson Immunocytometry Systems, San Jose, CA). One of two gates was set at desired level of the log fluorescence intensity scale. The sorted cells were collected and the site densities were determined immediately after the sorting following the same procedure in site density determination. To achieve a high site density, cells need to be sorted multiple times at regular basis. Cells were cultured for two weeks before the next sorting. As long as the desired site density was reached, the sorted cells were used for experiment after one or two day's culture.

3.3.4 Site Density Determination

The MESF (y-axis) vs. the RCN (relative channel number) (x-axis) for the five fluorescent microbeads were plotted on a graph to obtain a calibration curve. The MESF value (corrected from the negative control) corresponding to the mean channel of each sample was read on the calibration curve. The site density of the molecule on cell surface was determined by dividing the MESF value by cell surface area and fluorine/protein ratio.

3.4 Micropipette Adhesion Frequency Assay

3.4.1 Micropipette System Setup

The micropipette system was designed, built, and calibrated in house [67]. The system consists of video-enhanced optical microscopy, micromanipulation, and pressure regulation subsystems. The centerpiece of the microscopic system is a Zeiss inverted microscope (Axiovert 100; Oberkochan, Germany) with a 100x oil immersion, 1.25 N.A. objective. Additional magnification is obtained using a 5x relay lens, leading to a charge-coupled device (CCD) camera (model 72S; Dage-MTI, Michigan City, IN). A digital image processor (model DSP-2000; Dage-MTI) is used to enhance the image. The signal also passes through a digital voltage multiplexer (model 401; Vista Electronics, Ramona, CA), which allows video integration and display of a timer on screen. Recording is accomplished using a super VHS video cassette recorder (model AG-7355; Panasonic, Secaucus, NJ).

Micropipettes were made from borosilicate glass tubing (O.D. 1mm) (VWR). A two-step process was used with the first, utilizing a micropipette puller (Model PN-30, Narishige, Japan). Next, a microforge (built in house, similar to commercial models, except that a glass bead is added to the filament, adapted from the laboratory of Robert M. Hochmuth, Duke University, Durham, NC) was used to break the micropipette with a flush tip at the desired diameter. Depending on the cell types, the openings of micropipettes vary from 2 to 10 μm inner diameter. The pipettes were connected to the pressure regulation system through stainless steel injection holders. Each pipette could be coarsely manipulated by a mechanical drive mounted on the microscope and finely positioned with a three-axis hydraulic micromanipulator (Narishige, Tokyo, Japan). In

addition, one of the pipette holders was mounted on a piezo translator (Physik Instrumente, Waldbronne, Germany), the driver of which was controlled by a computer to achieve precise and repeatable movement of the pipette in an adhesion test cycle. To avoid vibration of the micropipettes during the experiment, the microscope, along with the micromanipulators, was placed on an air suspension table (Kinetics Systems, Boston, MA). A pressure regulation subsystem was used to control suction during the experiment and was critical for tuning the sensitivity of the RBC picoforce transducer. A hydraulic line connected the micropipette holder to a fluid reservoir. The centerpiece of the design was a fine jack that allowed the height of the reservoir to be precisely manipulated.

3.4.2 Micropipette Adhesion Frequency Assay

The micropipettes were filled with HBSS without calcium and magnesium just before experiment. For K562 cell experiments, chamber solution was HBSS without calcium and magnesium, sterile filtered just prior to use. For neutrophil experiments, chamber medium was HBSS, 1% HSA, mixed and filtered prior to use. For some experiments, desired concentration of Mg^{2+}, Ca^{2+}, Mn^{2+}, EGTA (ethylene glycol-bis(2-aminoethylether)-N, N, N', N'- tetraacetic acid), EDTA (ethylenediaminetetraacetic acid), and/or Dithiothreitol Dithiothreitol (DTT) was added to the chamber solution. For experiments with blocking or activating antibodies, cells were incubated with antibodies at 10 μg/ml for 30 min at room temperature prior to experiment. The mAb was also present in the chamber medium during experiments at 10 μg/ml. For experiments with small molecule antagonists, cells were pre-incubated with 1 μM XVA143, or 10 μM BIRT377 for 30min at room temperature. The small molecule antagonists were present in chamber medium at the indicated concentrations during experiments. For neutrophil

experiments, chamber was incubated with chamber medium for 30 minutes so that cells would not adhere to the bottom of chamber.

One pipette was used to hold K562 cell or neutrophil and the other to hold a RBC. The two cells were aspirated gently and aligned with a small axial gap between them. One pipette was connected to a computer-controlled piezoelectric actuator that was programmed to move a prescribed distance at a uniform rate of 1 μm/sec. Cells would remain in contact for a prescribed duration and then retract. Background-subtracted images were viewed in real time on a monitor and stored on videotape for future analysis [67]. This test cycle was repeated one hundred times with the same pair of cells, controlling the duration and area of the contact in these tests, and counting the numbers of adhesive events as adhesion frequency.

3.5 Data Analysis

3.5.1 $\alpha_L\beta_2$-ICAM-1 Binding Affinity and Kinetics

Before extracting kinetics data, the nonspecific binding data were fitted to the equation,

$$P_{NS} = 1 - \exp[-a(1 - e^{-bt})] \qquad \text{Equation 3-1}$$

The specific binding probability P_a was determined by removing the fitted nonspecific data from the total adhesion frequency observed.

The effective binding affinity ($A_c K_a$) and reverse-rate [47] were extracted from the binding frequency data by iteratively reweighted nonlinear regression to the single-species model [67] (Equation 2-4). The forward kinetic rate can be obtained from the relationship $K_a = k_f/k_r$. The adhesion frequency data (P_a) were fitted along with the known

predictor variables (receptor and ligand surface site densities m_r and m_l, contact time t) (Figure 2-4).

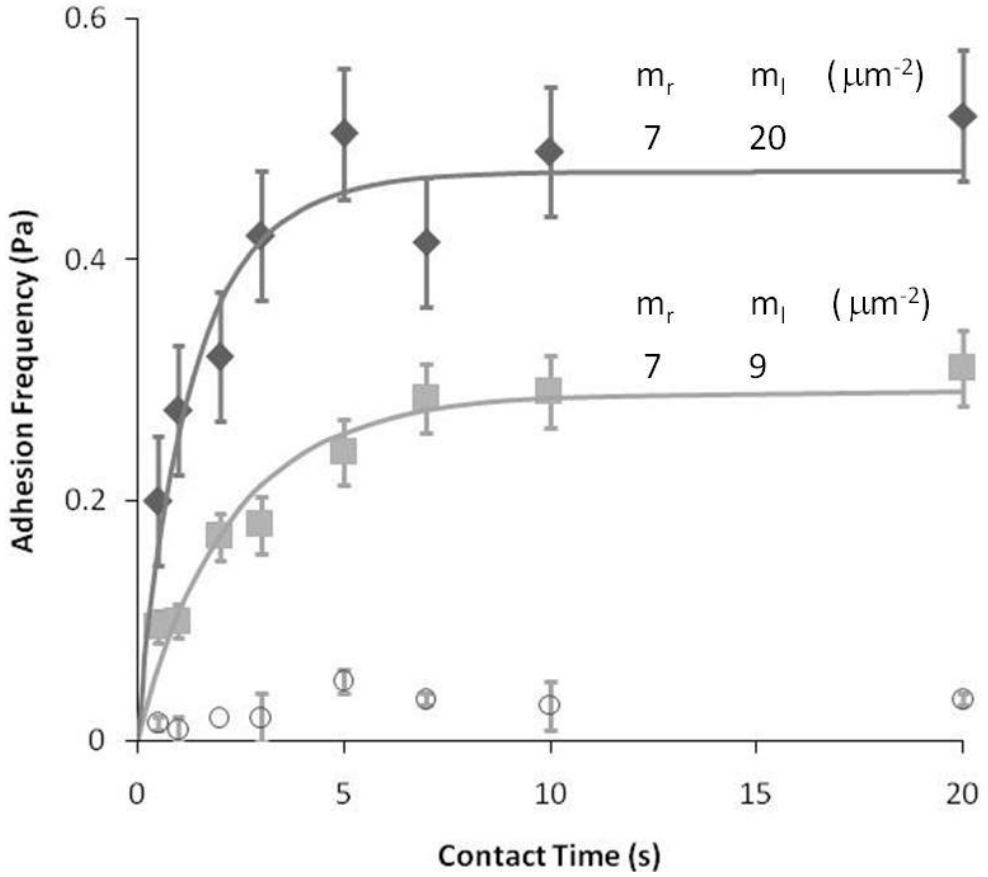

Figure 3-1. The dependence of adhesion frequency (*Pa*) on contact time (*t*) and site densities of receptors (m_r) and ligands (m_l). The adhesion frequency is plotted as a function of the contact duration for each set of receptor and ligand densities, and fitted with the theoretical solution (Equation 2-4) (curves).

For some experiments, the adhesion frequency was measured for a constant contact duration and the effective binding affinity (A_cK_a) was estimated. When adhesion reached equilibrium, the effective affinity was estimated from the following equation,

$$A_c K_a = \frac{1}{m_r m_l} \ln(1 - P_a)^{-1} \qquad \text{Equation 3-2}$$

which is derived from the steady state version (i.e. $t \rightarrow \infty$) of Equation 2-4.

3.5.2 Divalent Cation Binding Affinities and Kinetics to α_L I Domain and $\alpha_L\beta_2$

To measure the binding affinity of divalent cations to α_L I domain, the total receptor density m_r in Equation 2-4 was replaced by the density of I domain that is bound with a metal ion, $m_r/[1+(CK_c)^{-1}]$, where C is the divalent cation concentration and K_c is the affinity of divalent cation for I domain. The modified equation (Equation 3-3) allows to estimate K_c for divalent cations,

$$P_a(t) = 1 - \exp\left\{ - A_c K_a m_l m_r \left[\frac{(1 - e^{-k_r t})}{1 + (CK_c)^{-1}} \right] \right\} \qquad \text{Equation 3-3}$$

where k_r is the reverse-rate of α_L I domain and ICAM-1 binding.

If the dependence of adhesion frequency on divalent cation displays a double sigmoidal shape, as in the case of Ca^{2+}, another model is used. It was assumed the the I domain MIDAS can exchange between two stable conformations with probabilities p_1 and p_2 ($p_1 + p_2 = 1$) for being at conformations 1 and 2, respectively. Divalent cation binds the two conformers with different affinities, K_{Ca1} and K_{Ca2}. When bound with divalent cation, both conformers can bind ICAM-1 but with different affinities and kinetic rates, K_{ai}, k_{ri}, and $k_{fi} = K_{ai} \times k_{ri}$ (i = 1 and 2). This proposed mechanism results in an extension of Equation 2-4 that reads,

$$P_a(t) = 1 - \exp\left\{ - A_c m_l m_r \left[\frac{p_1 K_{a1}(1 - e^{-k_{r1} t})}{1 + (CK_{Ca1})^{-1}} + \frac{p_2 K_{a2}(1 - e^{-k_{r2} t})}{1 + (CK_{Ca2})^{-1}} \right] \right\} \qquad \text{Equation 3-4}$$

In the experiment, the contact time is chosen to be long enough for I domain or $\alpha_L\beta_2$-ICAM-1 binding to reach equilibrium, so that the $(1 - e^{k_r t})$ in Equations 3-3 and 3-4 becomes 1, which simplifies the equations. Equation 3-3 becomes,

$$P_a(t) = 1 - \exp\left\{ - A_c K_a m_l m_r \left[\frac{1}{1 + (\mathrm{C}K_c)^{-1}} \right] \right\}$$ Equation 3-5

and Equation 3-4 becomes,

$$P_a(t) = 1 - \exp\left\{ - A_c m_l m_r \left[\frac{p_1 K_{a1}}{1 + (\mathrm{C}K_{\mathrm{Ca1}})^{-1}} + \frac{p_2 K_{a2}}{1 + (\mathrm{C}K_{\mathrm{Ca2}})^{-1}} \right] \right\}$$ Equation 3-6

The binding affinity of Mg^{2+} and Mn^{2+} to I domain (K_c) was extracted from the binding frequency data by fitting to Equation 3-5. The binding affinities of Ca^{2+} to I domain (K_{Ca1} *and* K_{Ca2}) and the probability of I domain adapting the two conformations (p_1 *and* p_2) were extracted from the binding frequency data by fitting to Equation 3-6. The adhesion frequency data were fitted along with the known predictor variables (receptor and ligand surface site densities m_r and m_l, contact time t, and divalent cation concentration C) (Figure 3-2).

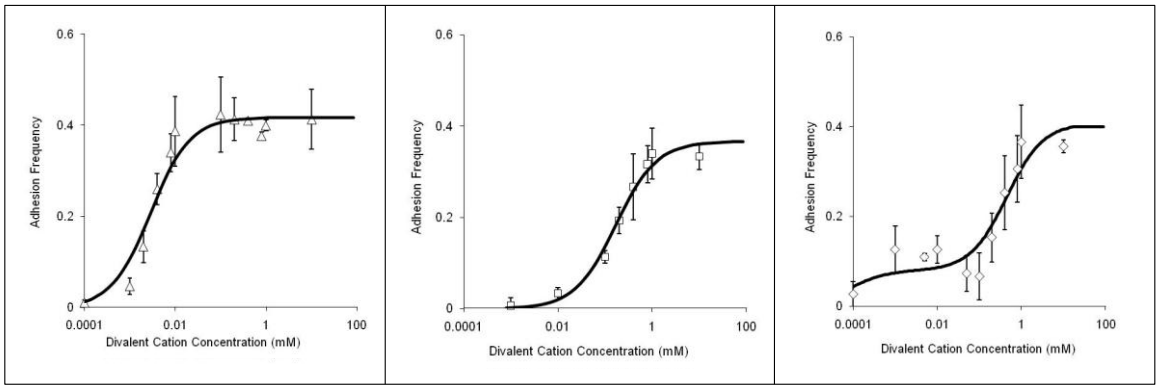

Figure 3-2. Model fits (curves) are compared to adhesion frequencies measured at 10 s contact time (points) in various concentrations of Mn^{2+} (A), Mg^{2+}(B) and Ca^{2+} (C) for locked open I domain.

To measure the dissociation rate of divalent cation binding to I domain, the total receptor density m_r in Equation 2-4 was replaced by $[\mathrm{I_{ion}}]_{\mathrm{initial}} \mathrm{e}^{-k_{rc}t}$, where $[\mathrm{I_{ion}}]_{\mathrm{initial}}$ is the

concentration of divalent cation bound I domain at t = 0, k_{rc} is the dissociation rate for divalent cations. The following model could be used to extract the reverse-rate,

$$P_a = 1 - \exp\left\{-A_c K_a m_l [I_{ion}]_{initial} e^{-k_{rc}t}\right\} \quad \text{Equation 3-7}$$

$[I_{ion}]_{initial}$ could be obtained from,

$$P_a = 1 - \exp\left\{-A_c K_a m_l [I_{ion}]_{initial}\right\} \quad \text{Equation 3-8}$$

The dissociation rate of divalent cation to I domain was extracted from the binding frequency data by fitting to Equation 3-7. The adhesion frequency data were fitted along with the known predictor variables (ligand surface site density m_l, contact time t, and $[I_{ion}]_{initial}$) (Figure 3-3).

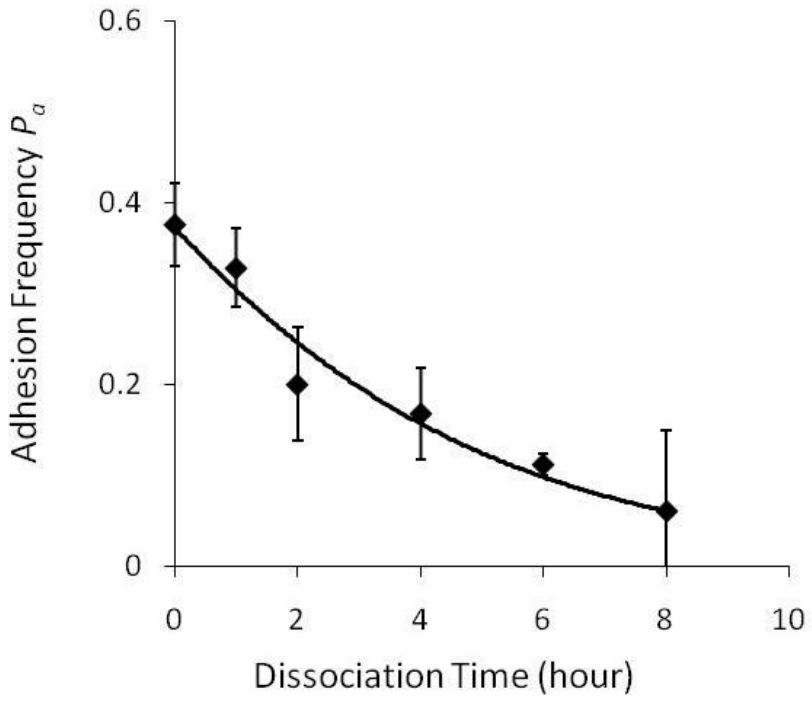

Figure 3-3. Model fits (curves) are compared to adhesion frequencies measured at different dissociation time (points) for the dissociation of Mg^{2+} from open I domain. Each point represents the average value of 5 pairs of cell for a contact time of 10 s.

CHAPTER 4

REGULATION OF 2D BINIDNG AFFINITIES AND KINETICS OF $\alpha_L\beta_2$ BY CONFORMATIONAL CHANGES OF THE α_L I DOMAIN

4.1 Introduction

Conformation change of integrin has been thought to be the most important mechanism for integrin regulation. The conformation of integrin affects a lot of biological functions. Ligand binding affinity and kinetics is the very immediate and the most important one. It has been suggested that different conformations of integrin correspond to different ligand binding affinities.

The regulation of ligand binding affinity and kinetics of $\alpha_L\beta_2$ by conformational changes has been examined using mutants that introduce a pair of cysteines to form a disulfide bond to lock the α_L I domain in either the closed, intermediate, or open conformation by altering the α7 helix position . The isolated locked I domain mutants exhibited low (6.3×10^2 M^{-1}), intermediate (3.3×10^5 M^{-1}), and high (6.7×10^6 M^{-1}) 3D affinities for ICAM-1 as measured by SPR [12, 50]. In The increase in on-rate (~50-60 folds) and decrease in off-rate (~100-250 folds) both contributed to the increase in binding affinity from the locked closed to the locked open I domains. The isolated locked open I domain was sufficient for full adhesive activity, since it had a 3D binding affinity for ICAM-1 (and mediated ICAM-1 dependent cell adhesion) at a level similar to those of fully activated wild-type (WT) $\alpha_L\beta_2$ [50, 52, 78].

While various lines of evidence have been obtained in support of the above models for affinity/kinetic regulation by conformational changes, previous measurements were made by SPR with one of the binding partners in the fluid phase, i.e., 3D kinetics

and affinity [12, 50, 78]. By comparison, for 2D interaction, such as cell-cell adhesion and cell-substrate adhesion, the binding affinity K_a is the ratio of equilibrium concentration of bonds to those of free receptors and ligands. However, concentration is measured as number of molecules per volume in 3D but number of molecules per area (i.e., surface density) in 2D, resulting in different units for K_a (M^{-1} in 3D and μm^2 in 2D). The kinetic on-rate k_{on} also has different units in different dimensions ($M^{-1}s^{-1}$ in 3D and $\mu m^2 s^{-1}$ in 2D). The 2D k_{on} is the rate of bond formation between unit densities of receptors and ligands that are respectively anchored on two apposing surfaces of unit area. By comparison, the 3D k_{on} is the rate of bond formation between unit concentrations of receptors and ligands in solution of unit volume. There has been increasing recognition that 2D binding parameters are not readily conversable from their 3D counterparts [79]. It is therefore important to directly measure in situ the more physiologically relevant 2D binding affinity and kinetic rates.

The regulation of 2D binding affinity and kinetics of the α_L I domain-ICAM-1 interaction by conformational changes has been investigated using the micropipette adhesion frequency experiment [53]. When expressed on cell surface, the locked open, intermediate, and closed I domains bind ICAM-1 with high, intermediate, and low affinities. Locking the I domain into high and intermediate conformations increased the binding affinities by ~8,000 and ~30 folds compared the locked closed I domain, which was on the same order of magnitude as the affinity of the WT I domain. Therefore, the alternation of the C-terminal α7 helix position was sufficient to regulate the ligand binding affinity of the I domain when expressed on cell surface, in agreement with the 3D SPR measurement [12, 50] and consistent with the cell binding measurement [55]. Surprisingly, differences

among the off-rates for the four isolated I domains were modest at best, with the locked open I domain having the smallest off-rate of 0.41 s^{-1} and the locked closed I domain having the largest off-rate of 0.71 s^{-1}, in sharp contrast to the 3D SPR measurement [12, 50].

In order the further investigate the regulation of $\alpha_L\beta_2$ ligand binding activity by the α_L I domain conformation, the 2D binding kinetics and affinities of $\alpha_L\beta_2$ containing a locked or WT α_L I domain was quantified using micropipette adhesion frequency assay. The results showed that the upregulation of ligand binding affinity of the $\alpha_L\beta_2$ was mostly due to the conformational changes in the I domain, which in turn was regulated by other domains by pulling down the I domain C-terminal α7 helix.

4.2 The Binding Affinities and Kinetics of $\alpha_L\beta_2$ Containing a WT or Locked I Domain

4.2.1 Measuring Specific $\alpha_L\beta_2$-ICAM-1 Binding

Expressed on cell surface, $\alpha_L\beta_2$ mediated sufficient level of adhesion with ICAM-1 reconstituted on RBC to be measured by the micropipette, which is capable of measuring interactions with affinities too low for many conventional adhesion assays to detect [80]. By sorting the K562 cells to express appropriate levels of $\alpha_L\beta_2$ and reconstituting appropriate levels of ICAM-1 on RBCs, the equilibrium frequencies of adhesion of each pair of interacting molecules were adjusted to mid-range levels, i.e. 0.2-0.8. To estimate reliably binding parameters, 2-3 curves were generated for each species by varying the site densities of integrin or ICAM-1 or both (Figure 3-1). The detected interactions were mostly specific, as the adhesion frequency between the K562 cells and

RBCs without ICAM-1 coupling was <0.06, which was deemed as nonspecific binding (Figure 3-1 and data not shown).

For all integrin molecules tested, measurement of specific ICAM-1 binding affinity and kinetics requires that the presence of divalent cations, as binding was reduced to the nonspecific level when measured in HBSS- with EDTA (Figure 4-1A). Washing the cells first with HBSS- containing EDTA then with HBSS- to remove EDTA and resuspending them in HBSS- for adhesion test also diminished binding to the nonspecific level (Figure 4-1B). Thus, after stripping the divalent cations with EDTA, no specific adhesion frequency above the noise level could be calculated, thereby preventing estimates of integrin-ICAM-1 binding affinity and kinetics from Equations 2-4 and 3-2. However, washing the cells previously exposed to divalent cations with, and then performing micropipette assay in, HBSS- without EDTA resulted in sufficiently high specific adhesion signals above noise. Therefore, a condition in which K562 cells were first allowed to bind divalent cations, washed with HBSS-, and then assayed for ICAM-1 binding in HBSS- was chosen to the baseline experimental condition. Inclusion of 2 mM Mn^{2+} or 2 mM Mg^{2+} in the chamber solution where micropipette adhesion assay was performed was chosen to be the activating experimental condition. The EDTA condition was not used because it did not allow specific ICAM-1 binding affinity and kinetics to be estimated by the experimental method.

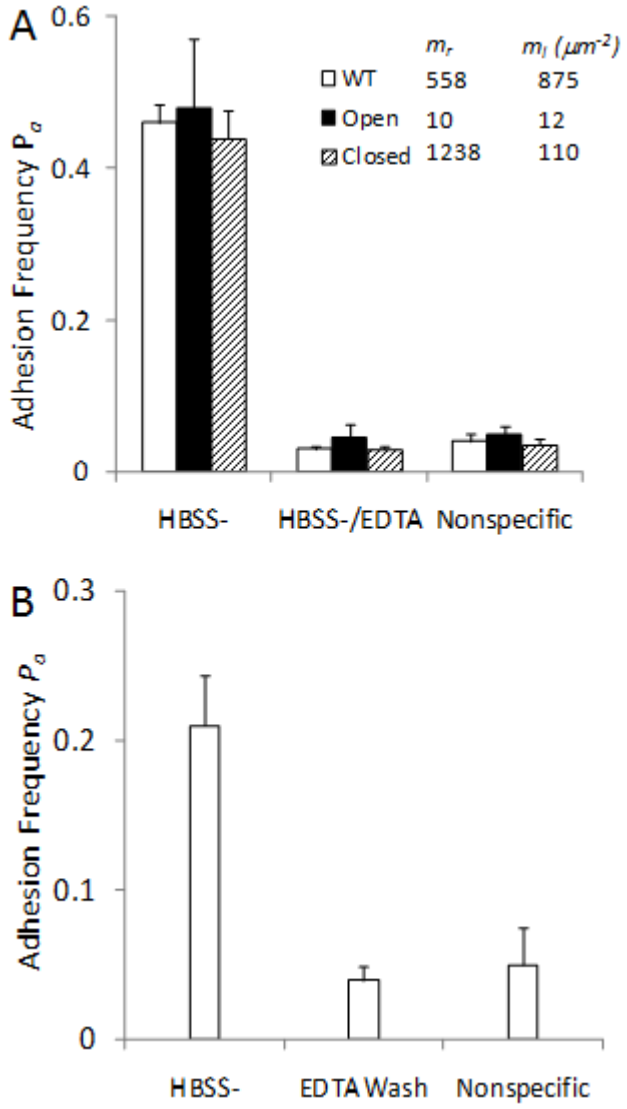

Figure 4-1. Divalent cation requirement for specific binding. (A) K562 cells expressing $\alpha_L\beta_2$ pre-bound with divalent cations were washed in HBSS- and assayed in HBSS- or HBSS-/EDTA by micropipette for adhesion to RBC reconstituted with ICAM-1. (B) K562 cells expressing WT $\alpha_L\beta_2$ pre-bound with divalent cations were washed in HBSS- or HBSS-/EDTA and assayed in HBSS- by micropipette for adhesion to RBC reconstituted with GPI-ICAM-1. To bring the specific adhesion frequencies of different interactions to a comparable, midrange level, different site densities (indicated) of integrin (m_r) and ICAM-1 (m_l) were used to compensate their different affinities. The nonspecific adhesions were measured using RBC not reconstituted with ICAM-1 ($m_l = 0$) to touch K562 cells expressing the same m_r values of the indicated integrins treated and tested under identical conditions. Data are presented as the mean adhesion frequency ± s.e.m. of 5 pairs of cells, 100 contacts per cell pair, and 5 second per contact.

In order to obtain reliable binding parameters, multiple binding curves were generated by altering the site densities of $\alpha_L\beta_2$ or ICAM-1 or both. To test whether the change in site density has effects on binding parameters, $\ln(1-P_a)^{-1}$, where P_a is the equilibrium adhesion frequency, was plotted against the product of receptor and ligand site densities ($m_r \times m_l$). An example of such plot for WT $\alpha_L\beta_2$ is shown in Figure 4-2. The $\ln(1-P_a)^{-1}$ increased linearly with the increase of $m_r \times m_l$. The slope of the fitted straight line gave the value of A_cK_a (4×10^{-6} μm^4) according to Equation 3-2.

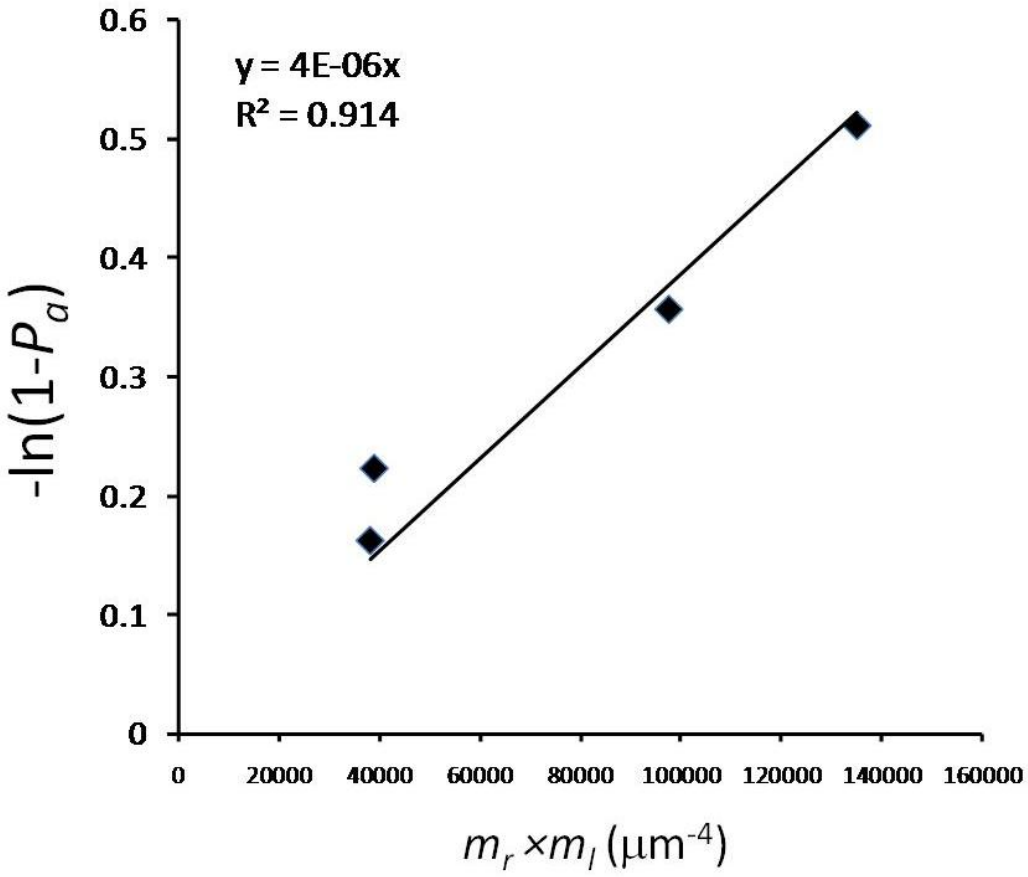

Figure 4-2. The value of $\ln(1-P_a)^{-1}$ increases linearly with the product of site densities of $\alpha_L\beta_2$ (m_r) and ICAM-1 (m_l). Four binding curves were generated by changing the site densities of WT $\alpha_L\beta_2$ and ICAM-1. The values of $\ln(1-P_a)^{-1}$ were calculated using equilibrium binding frequency of each curve.

4.2.2 $\alpha_L\beta_2$ containing a WT or locked I domain binds ICAM-1 with affinities comparable to the corresponding isolated I domain

To compare the 2D binding characteristics of the I domains in isolation and in the whole integrin, the binding affinity and kinetics of $\alpha_L\beta_2$ containing a WT or locked I domain were measured by micropipette under the baseline condition. Similar to the isolated I domains, the 2D ICAM-1 binding affinity of $\alpha_L\beta_2$ containing locked open or locked intermediate I domain was ~3000 or ~30 folds higher than that of $\alpha_L\beta_2$ containing locked closed I domain (Figure 4-3A and Table 1). The mutant $\alpha_L\beta_2$ containing a locked closed I domain had a 2D affinity for ICAM-1 similar to that of the inactive WT $\alpha_L\beta_2$ (Figure 4-3A and Table 1), suggesting that the WT I domain, assumes a closed conformation in the absence of activating agents. Without activation, the 2D ICAM-1 binding affinities of the intact $\alpha_L\beta_2$ mutants containing the locked I domains were on the same orders of magnitude as those of the isolated I domains locked at the corresponding conformations, indicating that the I domain has nearly the full ligand binding capacity and confers nearly the same ligand binding affinities without other domains of the integrin (Table 1). This is especially true for the locked open I domain, since expressing the open I domain in the whole $\alpha_L\beta_2$ did not further increase the binding affinity. The 2D off-rates of the four intact $\alpha_L\beta_2$ species (Figure 4-3B) were more distinct from each other (up to 6-fold differences) than the isolated I domains (<2 folds), revealing modest but clearly observable influences of other domains of the $\alpha_L\beta_2$ integrin (Table 1). Yet these 2D off-rates differed substantially from the 3D off-rate of ICAM-1 dissociating from activated $\alpha_L\beta_2$ [78].

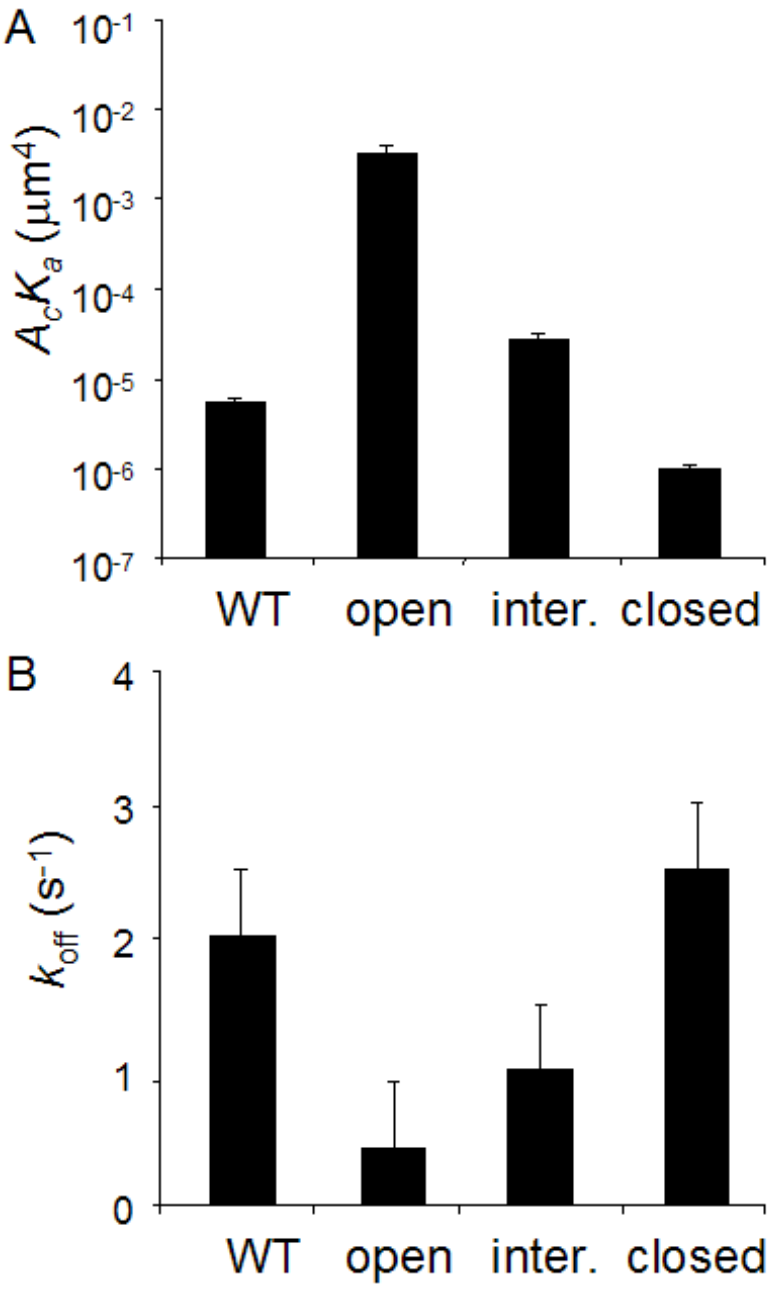

Figure 4-3. Binding parameters for $\alpha_L\beta_2$ integrins. The effective binding affinities (A) and off-rates (B) of the WT $\alpha_L\beta_2$, and $\alpha_L\beta_2$ mutants containing the locked open, locked intermediate, and locked closed I domains for ICAM-1 are shown. Two or three specific binding curves were measured for each $\alpha_L\beta_2$ species and Equation 2-4 was fit to each curve to evaluate an effective binding affinity and an off-rate for that curve. Binding parameters estimated from different curves for the same species were averaged and calculated for standard deviation as presented in the figure. All differences in A_cK_a values of different I domains are statistically significant ($P < 0.03$, student-t test) except that

between the WT $\alpha_L\beta_2$ and the $\alpha_L\beta_2$ mutant containing a locked closed I domain ($P > 0.08$). Statistically significant differences were found in k_{off} values between the WT $\alpha_L\beta_2$ and the $\alpha_L\beta_2$ mutant containing a locked open I domain ($P < 0.005$), between the $\alpha_L\beta_2$ mutants containing a locked open and a locked intermediate I domain ($P < 0.03$), and between the $\alpha_L\beta_2$ mutants containing a locked open and a locked closed I domain ($P < 0.007$) but not between other pairs ($P > 0.07$).

4.3 Movement of the I Domain α7 Helix Regulates Most of the $\alpha_L\beta_2$ Binding Affinity

The continuous presence of Mn^{2+} or Mg^{2+} in the test chamber increased the 2D binding affinities for ICAM-1 of the $\alpha_L\beta_2$ mutants containing locked I domains only by several folds from values measured in the baseline condition [53]. Thus, when the I domain pre-bound with a divalent cation was locked at the closed, intermediate, or open position, the 2D binding affinities for ICAM-1 were clamped at low, intermediate, or high levels with no (for isolated I domains) or a narrow range (for I domains contained in the whole $\alpha_L\beta_2$) of regulation by Mn^{2+} or Mg^{2+}. These data are consistent with the cell binding measurement [55]. Mn^{2+} and Mg^{2+} have been shown to induce the switchblade-like conformational change of the whole integrin and stabilize the integrin in an extended conformation, which moves the I domain ~10 nm upward further above the cell membrane [35]. Lengthening cell surface receptors has been shown to increase 2D binding affinity by enhancing its accessibility to ligands on the apposing cell surface [81]. In sharp contrast to the isolated WT I domain and to the mutant $\alpha_L\beta_2$ containing locked I domains, the 2D binding affinities of WT $\alpha_L\beta_2$ for ICAM-1 measured in Mn^{2+} or Mg^{2+} were increased ~1500 and ~380 folds, respectively, compared to the value measured in HBSS- (Figure 4-4A).

To exclude the possibility that the mutations in the I domain might have effects on $\alpha_L\beta_2$-ICAM-1 binding affinity other than preventing the I domain α7 helix movement, DTT was used to unlock the disulfide bonds. In the baseline condition, DTT treatment reduced the 2D ICAM-1 binding affinity of the mutant $\alpha_L\beta_2$ containing an open I domain 3-4 orders of magnitude to the level of that of the WT $\alpha_L\beta_2$, but had little effect on the affinity of the mutant $\alpha_L\beta_2$ containing a closed I domain, which was already similar to that of the WT $\alpha_L\beta_2$ (Fig. 4-4), indicating that these I domains returned to (or remained at) the inactive conformation after unlocking the disulfide bonds. In addition, DTT resumed the full 3-4 log range of affinity regulation of the mutant $\alpha_L\beta_2$ by Mn^{2+} and Mg^{2+}, yet had no adverse effects on the binding affinities of, and their divalent cation regulation thereof, the WT $\alpha_L\beta_2$ (Fig. 4-4B). Since WT and mutant $\alpha_L\beta_2$ with and without DTT treatment were able to bind ICAM-1 specifically in HBSS- but not in EDTA, the MIDAS of the I domain in the context of the whole integrin must be occupied by a divalent cation in HBSS-, just as it is in isolation. Affinity upregulation by several orders of magnitude requires the downward movements of the I domain α7 helix, since the isolated WT I domain and isolated mutant I domains unlocked with DTT were unable to be upregulated by Mn^{2+} or Mg^{2+} to a high affinity state [53]. Thus, the data suggested a coupling between the I domain conformation and the global conformation of the whole integrin, such that changes in the latter results in changes in the former, leading to changes in the α7 helix position.

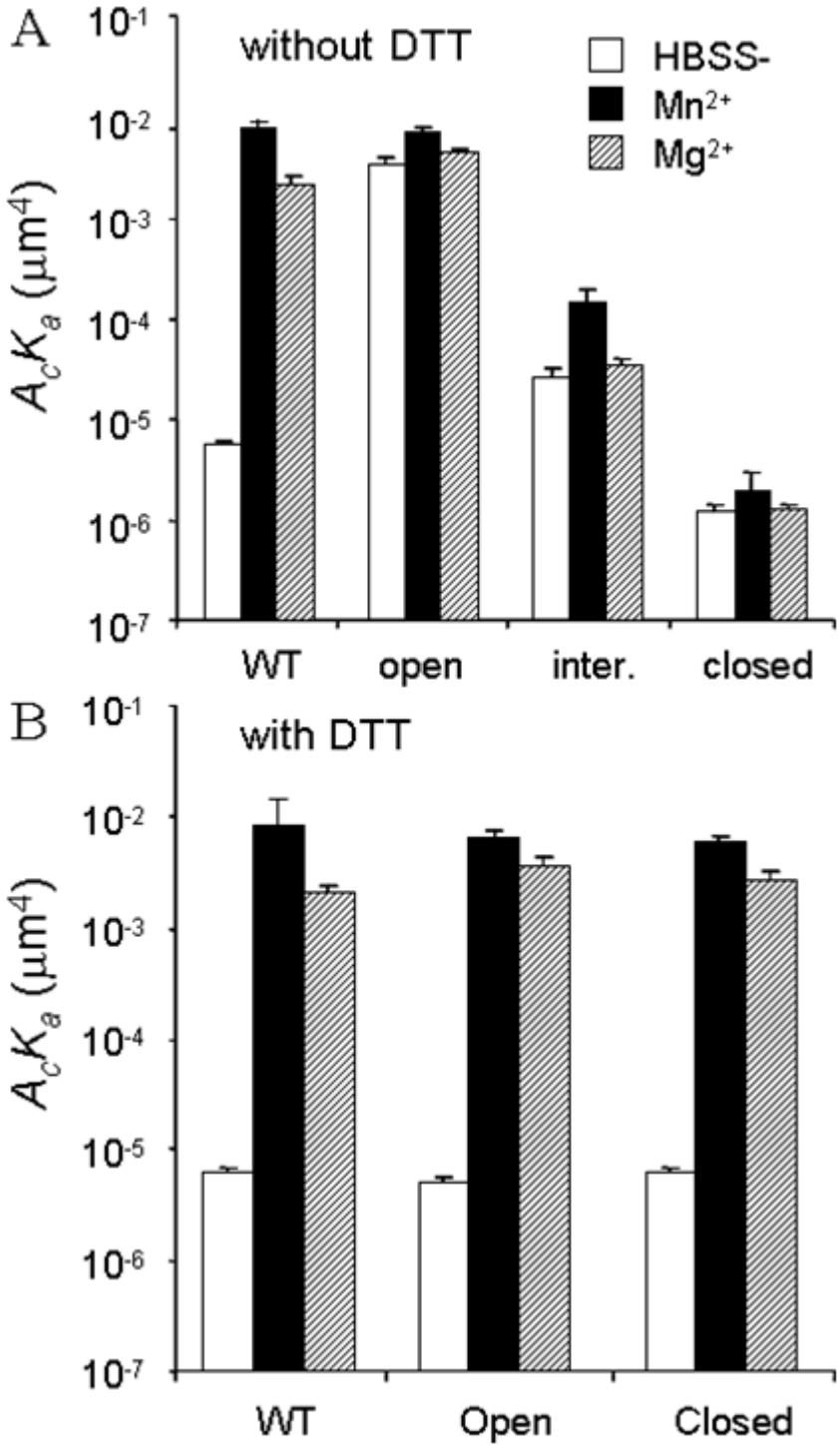

Figure 4-4. Regulation of $\alpha_L\beta_2$ affinity by Mn^{2+} and Mg^{2+}. Effective binding affinities for ICAM-1 of the WT $\alpha_L\beta_2$ and $\alpha_L\beta_2$ containing the locked open, locked intermediate, or locked closed I domain with or without 2 mM of Mn^{2+} or Mg^{2+} in the absence (A) or presence (B) of 10 mM DTT are shown. The adhesion frequencies of 5 pairs of cells were measured for a 10 s contact duration and the effective binding affinities were calculated from Eq. (2). Data are presented as mean ± s.e.m. Without DTT treatment, the differences

between WT A_cK_a values measured in HBSS- and in Mn^{2+} or Mg^{2+} are statistically significant ($P < 0.0008$, student-t test), but the differences between the mutant A_cK_a values measured in the absence and presence of Mg^{2+} are not statistically significant ($P > 0.25$) for any of the three $\alpha_L\beta_2$ integrins containing locked mutant I domains. Statistically significant differences were found between the A_cK_a values measured in the absence and presence of Mn^{2+} for mutant $\alpha_L\beta_2$ containing a locked intermediate ($P < 0.0008$) or locked closed ($P = 0.05$) I domain but not for mutant $\alpha_L\beta_2$ containing a locked open I domain ($P > 0.4$). With DTT treatment, the differences between A_cK_a values measured in HBSS- and in Mn^{2+} or Mg^{2+} are statistically significant ($P < 0.01$) for any of the three $\alpha_L\beta_2$ integrins.

4.4 Discrepancy of 2D and 3D Off-rate Measurements

The 2D off-rates of the various $\alpha_L\beta_2$ integrin constructs dissociating from ICAM-1 observed in this study fell in a narrow range from 0.2-2.5 s^{-1}. By comparison, the 3D off-rates of the corresponding I domain species measured by SPR spanned a much wider range, extending the high end by several folds and the low end by an order of magnitude (Table 1). To investigate potential reasons that could contribute to this discrepancy, a series of test and control experiments were carried out.

4.4.1 The Micropipette Adhesion Frequency Assay is Able to Measure Slow Off-rate

To demonstrate the ability of the micropipette adhesion frequency assay to analyze kinetic processes of slow off-rates, the 2D binding kinetics between $\alpha_L\beta_2$ containing the locked open I domain and an anti−$\alpha_L\beta_2$ adhesion-blocking mAb (clone 38) was measured, because antibodies in general dissociate very slowly from their antigens. It is evident from Figure 4-5 that the antibody-antigen binding curve represents a kinetic process much slower than that represented by the $\alpha_L\beta_2$-ICAM-1 binding curve. The adhesion frequency of the $\alpha_L\beta_2$-ICAM-1 interaction reached a steady-state in 5 s, whereas that of the $\alpha_L\beta_2$-mAb 38 interaction remained in the transient phase even when

the contact duration was as long as 60 s. Lengthening the contact duration further is possible but technically challenging because it would drastically prolong the experiment, as the contact cycle with long duration is to be repeated 100 times using the same pair of cells. Since only transient data before reaching steady-state were analyzed, the 0.03 s^{-1} k_{off} value obtained from fitting the incomplete binding curve likely overestimated the true off-rate (Table 2). Thus, the adhesion frequency assay is capable of measuring 2D off-rate on the order of 0.01 s^{-1}, which is as slow as the slowest 3D off-rate – that of the locked open I domain dissociating from ICAM-1 – measured in the previous SPR studies [50]. Therefore, the fast 2D off-rates of the locked open I domain and $\alpha_L\beta_2$ containing the locked open I domain (of the order of 0.1 s^{-1}) was not due to the inability of the experimental method to measure them.

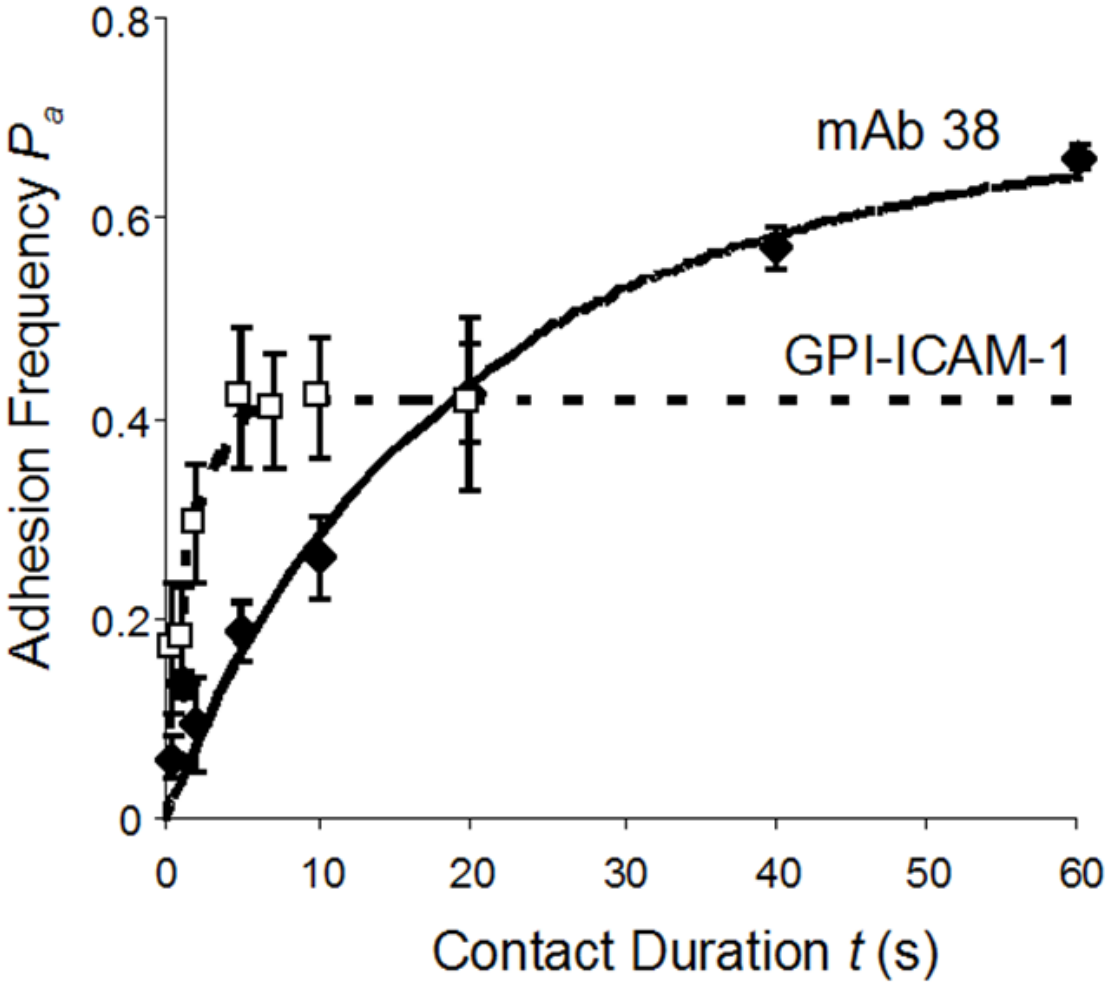

Figure 4-5. Slow and fast binding curves. Binding curves of $\alpha_L\beta_2$ containing the locked open I domain for mAb 38 (♦, solid curve) and for mouse GPI-ICAM-1 (□, dashed curve) are compared. The adhesion frequency of the $\alpha_L\beta_2$-mAb 38 interaction did not reach equilibrium even at 60 s, which was the longest contact duration for that experiment. By comparison, the adhesion frequency of the $\alpha_L\beta_2$-ICAM-1 interaction reached equilibrium at 5 s.

4.4.2 Mouse ICAM-1 and human ICAM-1 bind to human I domain and $\alpha_L\beta_2$ with similar binding affinities and kinetics

Although there are sequence differences between mouse and human ICAM-1, mouse ICAM-1 also binds specifically to human $\alpha_L\beta_2$ [1]. The kinetic parameters shown

in Figures. 4-4 and 4-5 (summarized in Table 1) were measured using mouse ICAM-1 because of its much higher availability. By comparison, the previous SPR studies used human ICAM-1 [12, 50, 78]. Therefore, whether ICAM-1 from different species dissociated at much different off-rates was tested by measuring the 2D kinetics of human $\alpha_L\beta_2$ containing the locked open I domain interacting with human ICAM-1. The binding parameters of $\alpha_L\beta_2$ for mouse and human ICAM-1s were very similar, especially the 2D A_cK_a (Figure 4-6). Although the 2D off-rates differed slightly (<2 folds), they were of the same order of 0.1 s^{-1} (Table 2), which is still an order of magnitude faster than the 3D off-rate measured in the previous SPR study [12, 50, 78]. Thus, the differences in the 2D and 3D off-rates were not caused by the different ICAM-1 species used.

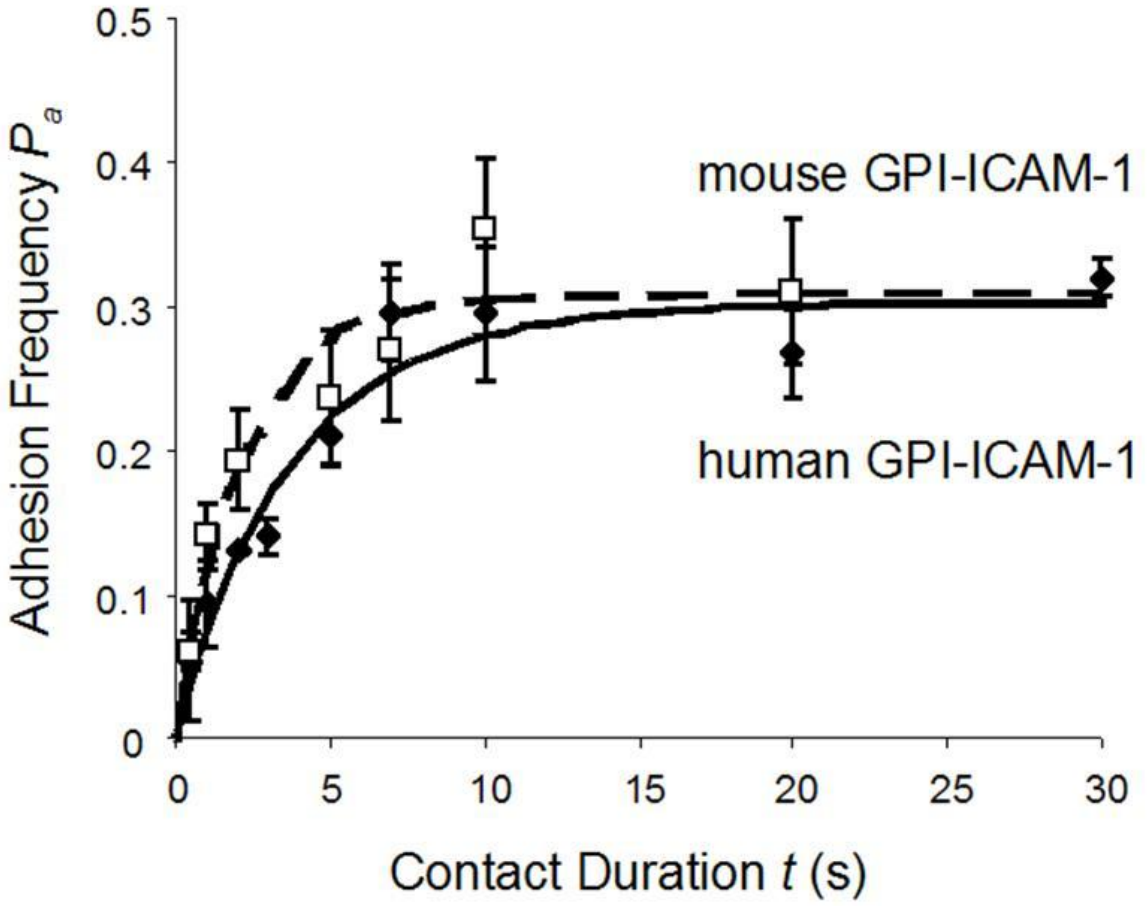

Figure 4-6. Binding curves for mouse and human ICAM-1. Binding curves of $\alpha_L\beta_2$ containing the locked open I domain for human GPI-ICAM-1 (♦, solid curve) and mouse GPI-ICAM-1 (□, dashed curve) are compared. The site density of $\alpha_L\beta_2$ was 8 μm^{-2} for both curves. Human and mouse ICAM-1 had comparable site densities of 20 and 14 μm^{-2}, respectively. The two curves had similar equilibrium adhesion frequencies and reached equilibrium level at nearly the same contact durations.

4.4.3 *ICAM-1 coupled to RBC via GPI anchor and via a capture mAb have similar off-rates*

Both the mouse and human ICAM-1 used to measure the kinetic rates shown in Figures. 4-1 to 4-5 were fusion proteins whose transmembrane and cytoplasmic domains were replaced by a GPI anchor for its easy reconstitution into the RBC membrane. To assess the effects of ICAM-1 presentation on the 2D off-rate, the kinetic measurement of

isolated locked open I domain for ICAM-1 captured by a nonblocking anti-ICAM-1 mAb pre-coated on the RBC surface using chromium chloride coupling was performed [67]. GPI-anchored human ICAM-1 was captured using mAb CA7, which bind to D5 domain of human ICAM-1. Due to the high affinity of antibody-antigen interaction, only submicrogram per milliliter concentration was required to capture enough ICAM-1 on the RBC surface. By comparison, submilligram per milliliter concentration was required for sufficient number of ICAM-1 to insert their GPI anchors into the RBC membrane. This 1000-fold difference in the required concentrations ensured that pre-coating CA7 was required for RBC to acquire from low concentration incubation a high enough ICAM-1 site density for specific $\alpha_L\beta_2$ adhesion. Indeed, control experiment using RBC not pre-coated with CA7 and incubated with submicrogram per milliliter concentration of ICAM-1 resulted in no more than background level of adhesion (data not shown). By comparison, incubating RBC pre-coated with CA7 with the same concentration of GPI-ICAM-1 enabled the measurement of a binding curve shown in Figure 4-7, which is comparable to that obtained using RBC without CA7 pre-coating but incubated with submilligram per milliliter concentration of GPI-ICAM-1. Thus, K562 $\alpha_L\beta_2$ had similar 2D affinities and off-rates for ICAM-1 regardless of the method by which it was coated on RBC (Figure 4-6 and Table 2), which is consistent with the knowledge that the binding site for $\alpha_L\beta_2$ resides on the D1 domain of ICAM-1, which is >20 nm distal to the membrane anchor [82], and that the first two Ig domains (D1-D2) of ICAM-1 is sufficient for I domain binding [12].

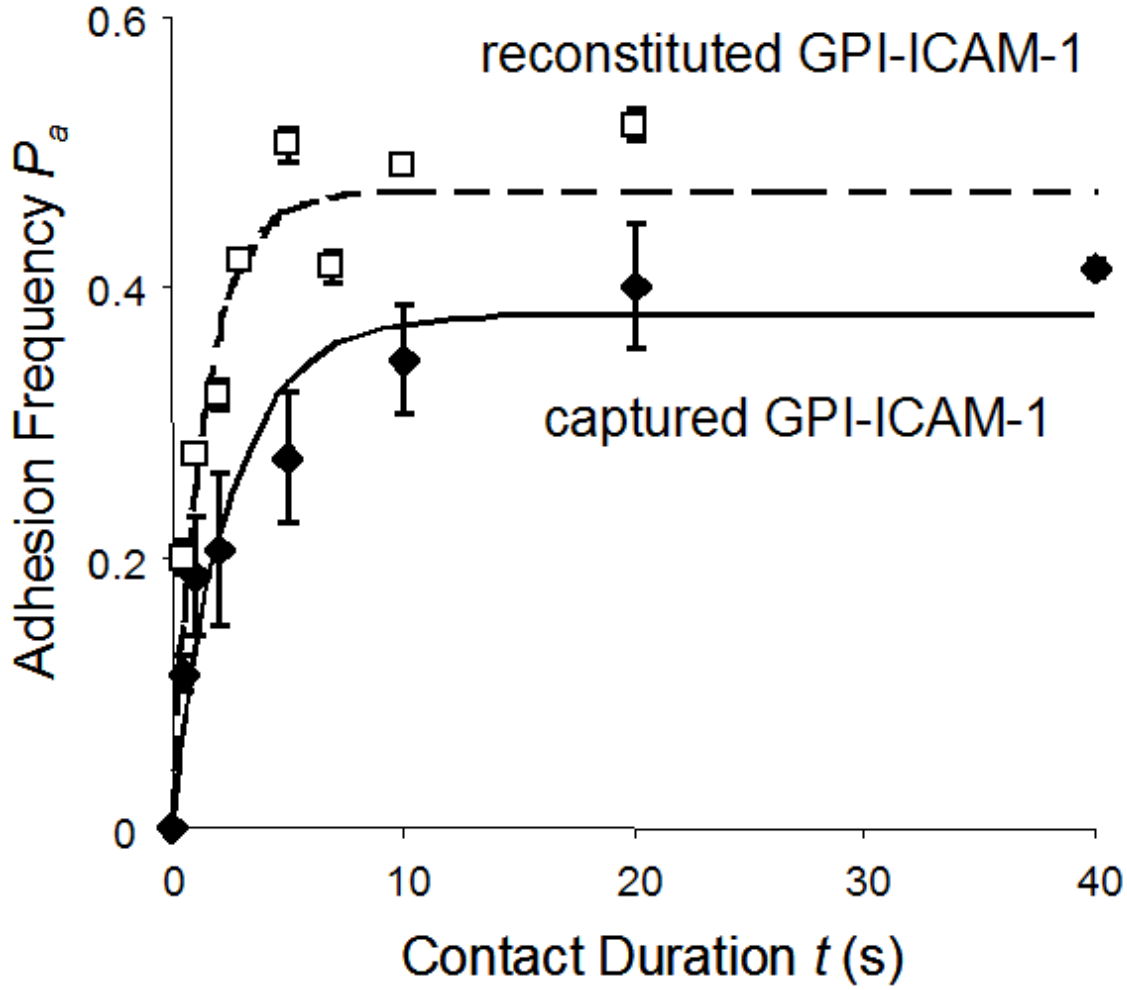

Figure 4-7. Binding curves for reconstituted and captured ICAM-1. Binding curves of the isolated locked open I domain for human GPI-ICAM-1 captured by CA7 precoated on RBC (♦, solid curve) and for mouse ICAM-1 reconstituted on RBC via GPI anchor (□, dashed curve) are compared. The respective site densities of open I domain and captured GPI-ICAM-1 were 40 and 12 μm^{-2}. The respective site densities of open I domain and reconstituted GPI-ICAM-1 were 8 and 20 μm^{-2}. The difference in the steady-state adhesion frequencies can be accounted for by the different $m_r \times m_l$ products in the two cases, but both curves achieved steady-state at a similar time, indicating similar off-rates for the two interactions.

4.5 Discussion

Using the micropipette adhesion frequency assay, additional evidence for the model for affinity regulation by conformational changes in integrins was obtained [51]. The binding affinities and kinetics of whole $\alpha_L\beta_2$ integrins containing locked I domains were

measured for the first time, although these mutants were previously studied for their ability to mediate cell adhesion [52]. The mutant $\alpha_L\beta_2$ containing a locked I domain, regardless of into which conformation it was locked, had the same orders of magnitude of binding affinity and off-rate as the corresponding values of the isolated I domain, indicating that the I domain has nearly the same ligand binding capacity as the intact $\alpha_L\beta_2$ heterodimer. When measured in the baseline condition, the WT $\alpha_L\beta_2$ bound ICAM-1 with a low affinity comparable to the $\alpha_L\beta_2$ mutant containing a locked closed I domain, similar to WT I domain in isolation. This suggests that, just as WT I domain in isolation, the low affinity conformation is the default conformation for the inactive WT $\alpha_L\beta_2$. Mn^{2+} and Mg^{2+} were able to increase the 2D ICAM-1 binding affinity of WT $\alpha_L\beta_2$ to a level comparable to that of the mutant $\alpha_L\beta_2$ containing a locked open I domain. The ability for Mn^{2+} and Mg^{2+} to substantially upregulate the ICAM-1 binding affinity of $\alpha_L\beta_2$ from the baseline condition was diminished when the position of the I domain α7 helix was locked, regardless of into which position it was locked. In the baseline condition, unlocking the α7 helix position by DTT returned the ICAM-1 binding affinities of the $\alpha_L\beta_2$ mutants to the level of inactive WT $\alpha_L\beta_2$. In addition, DTT treatment resumed the full range of affinity regulation of these locked $\alpha_L\beta_2$ heterodimers by Mn^{2+} and Mg^{2+}. Therefore, just as in isolation, the position of the α7 helix regulates most of the ligand binding affinity when the I domain is in the context of the whole $\alpha_L\beta_2$ heterodimer. Unlike in isolation, the presence of the whole $\alpha_L\beta_2$ context enables the position of the I domain α7 helix to be regulated, provided that it is not locked in fixed conformations. The conformations of other $\alpha_L\beta_2$ domains have only limited capacities to regulate the

ligand binding affinity and kinetics once the I domain is locked, most likely through regulating the distance of the I domain ligand binding site above the cell membrane. In other words, the regulation of ligand binding affinity and kinetics by other domains of WT $\alpha_L\beta_2$ is achieved mostly through their effects on the I domain. More specifically, the conformational changes in other domains have to propagate through the α7 helix (most likely resulting in an applied force that pulls the α7 helix downward) in order to regulate ligand binding affinity and kinetics. Mn^{2+} and Mg^{2+} must regulate the I domain conformation indirectly through the conformational changes in other domains of $\alpha_L\beta_2$ rather than directly binding to the I domain MIDAS.

The measured 2D binding affinity and kinetic rate constants also provide an opportunity to contrast these values with their 3D counterparts measured by SPR for the same molecular interactions [50]. Although the different units prevent direct comparison of the absolute values of 2D and 3D binding affinities, their correlation, or the lack thereof could be examed. The fold-increase in relative affinity from the locked closed to the locked open I domain measured by our 2D micropipette method (~8,000) agrees well with the previous 3D results obtained using SPR technique (~10,000). However, the affinities of the locked intermediate I domain relative to those of the locked closed and locked open I domains differ by an order of magnitude: the 2D values are ~25 folds increase from closed to intermediate and ~300 folds increase from intermediate to open whereas the corresponding 3D values are ~500 and ~25 folds increases.

Although the 2D and 3D off-rates agree well in one case (locked intermediate I domain), significant discrepancies between the micropipette and SPR measurements are seen in all other cases. Both cases exist for 2D k_{off} >> 3D k_{off} (locked open I domain and

$\alpha_L\beta_2$ integrin) and 2D k_{off} << 3D k_{off} (WT and locked closed I domain). It appears that the hundreds of folds of 3D off-rate differences among the different molecular species are greatly compressed into a much narrower ten fold range of 2D off-rate differences (Table 1). This results in a significant expansion of 2D on-rate differences among the different I domain conformers into a much broader range than that of 3D on-rate differences among the same set of I domain conformers, as the range of affinity differences are similar in 2D and 3D.

Table 4-1. 2D and 3D binding affinities and off-rates of isolated α_L I domain and $\alpha_L\beta_2$ integrin at different conformational states. All 2D data are from this study and the ligand was mouse GPI-ICAM-1. The 3D data for I domains interacting with human soluble ICAM-1 are from references [12], and the 3D data for $\alpha_L\beta_2$ interacting with human soluble ICAM-1 are from reference [78]. Data are presented as mean ± standard deviation.

Receptor		2D		3D	
		A_cK_a (μm^4)	k_{off} (s^{-1})	K_a (μM^{-1})	k_{off} (s^{-1})
I domain	WT	$1.31(\pm0.03)\times10^{-6}$	0.51±0.01	$6.74(\pm0.54)\times10^{-4}$	4.6±0.36
	Open	$4.05(\pm0.96)\times10^{-3}$	0.41±0.22	8.21±4.27	0.014±0.001
	Inter.	$1.32(\pm0.18)\times10^{-5}$	0.56±0.19	0.31±0.06	0.43±0.07
	Closed	$5.08(\pm1.04)\times10^{-7}$	0.71±0.25	$6.39(\pm0.75)\times10^{-4}$	3.6±0.34
$\alpha_L\beta_2$	WT	$5.46(\pm0.52)\times10^{-6}$	2.01±0.65		
	WT (Mn^{2+})	$8.57(\pm3.78)\times10^{-3}$	0.19±0.08	3.68±0.69	0.0459(±0.086)
	Open	$3.30(\pm0.62)\times10^{-3}$	0.42±0.19		
	Inter.	$2.68(\pm0.45)\times10^{-5}$	1.01±0.50		
	Closed	$9.85(\pm1.27)\times10^{-7}$	2.51±1.02		

It has been well known that removal of divalent cations prevents or rapidly detaches integrin-mediated cell adhesion [83]. It has also been observed that isolated WT I domain expressing K562 cells roll on ICAM-1 under flow but locking the I domain into the open, high-affinity state results in firm adhesion to ICAM-1 [55]. Cell detachment results from diminishing integrin-ligand bonds, which are caused by decreases in affinity, which can be due to either a decrease in on-rate, an increase in off-rate, or a combination thereof. Similarly, stable, continuous rolling requires the balance of bond formation and dissociation to maintain the same number of bonds. Either an increase in on-rate or a decrease in off-rate could result in more bond formation than dissociation, thereby reducing the rolling velocity and transiting rolling to firm adhesion. The data revealed that it is the tremendous regulation range of the 2D on-rate rather than the small regulation region of the 2D off-rate of the $\alpha_L\beta_2$-ICAM-1 interaction that underlies the above regulation of adhesion functions.

The discrepancies between the 2D and 3D off-rates are surprising because it has been proposed that the discrepant conversions between the 2D affinity and 3D affinity were due to on-rates, which have different units in 2D (per unit surface density per unit time) and 3D (per unit volumetric concentration per unit time) [79, 81, 84]. By comparison, off-rates were believed to have the same values regardless of whether they were measured in 2D or 3D because they have the same unit (per unit time) in either case [75, 81, 85-88]. In the present study, however, the off-rates were found drastically different in 2D and 3D, yet the fold-increases in binding affinity from the locked closed I domain to the locked open I domain are similar in 2D and 3D.

To examine the possible sources for the discrepancies between the 2D and 3D off-rates, several experiments were performed to rule out potential contributing mechanisms. The ability for the adhesion frequency assay to measure off-rate accurately has been questioned because all published 2D off-rates measured by this method fall in a narrow range (of orders between 0.1 and 1 s^{-1}) despite the fact that these off-rates govern dissociation of very different interactions [67, 77, 80, 81, 84, 88-91]. Micropipette adhesion frequency assay was performed to measure the slow kinetics of an $\alpha_L\beta_2$ mutant interacting with a blocking antibody. The results confirmed that the micropipette assay is capable of measuring 2D off-rates as slow as the 3D off-rates measured by SPR.

The adhesion frequency assay measures the likelihood of adhesion. For the assay to work well, the cell surface densities of the receptors and ligands have to be adjusted so that the repeated adhesion tests result in mid-ranged probabilities (~0.2-0.8). This limits the dynamic range of the assay, for a 0.2-0.8 probability range can be spanned by only a ~10-fold difference in affinities between two interactions with the same site densities. To measure the 3-4 orders of magnitude of differences in the ICAM-1 binding affinities of the open and closed α_L I domains, K562 cells were sorted to obtain high expression of locked closed I domain (~2000 μm^{-2}) and low expression of locked open I domain (~10 μm^{-2}). Any errors in the site density determination would propagate as errors in the affinity estimates; however, the off-rate estimates should not be affected.

Another potential problem may be transport limitations, which can cause problems in SPR measurements [92]. High affinity and fast on-rate interactions may deplete free receptors and ligands before transport brings in replacement, thereby lowering their local densities. The dissociated receptors/ligands may also rebind upon

dissociation, thereby prolonging the apparent lifetime (reciprocal off-rate). However, the former effect would have only impacted the on-rate. The latter effect would have underestimated the off-rate of the locked open I domain, thereby overestimating the "true" differences in the off-rates between the locked-open and locked-closed conformers.

The use of ICAM-1 from different species might be another potential cause for the discrepancies. However, direct comparison between mouse and human ICAM-1 in a back-to-back experiment showed that human α_L I domain and $\alpha_L\beta_2$ bind to ICAM-1 from the two species not only with the same specificity and the same divalent cation-dependency, but also with very similar binding affinity and kinetics (Table 2). Therefore, the use of mouse ICAM-1 did not cause the observed discrepancies between the 2D and 3D off-rates. Mouse ICAM-1 is a reasonable ligand for characterizing human $\alpha_L\beta_2$ binding and its regulation by conformational change.

Table 4-2. 2D binding affinities and off-rates of locked open α_L I domain and $\alpha_L\beta_2$ containing a locked open I domain for different ligands.

Receptor	Ligand	A_cK_a (μm^4)	k_{off} (s^{-1})
open I domain	reconstituted mouse GPI-ICAM-1	$4.05(\pm0.96)\times10^{-3}$	0.41±0.22
open I domain	CA7 captured human GPI- ICAM-1	$9.94(\pm0.19)\times10^{-4}$	0.37±0.21
open $\alpha_L\beta_2$	reconstituted mouse GPI-ICAM-1	$3.30(\pm0.62)\times10^{-3}$	0.42±0.19
open $\alpha_L\beta_2$	reconstituted human GPI-ICAM-1	$2.25(\pm0.31)\times10^{-3}$	0.24±0.09
open $\alpha_L\beta_2$	mAb 38	$1.32(\pm0.56)\times10^{-1}$	0.03±0.02

It has been shown that ligand binding kinetics of GPI-anchored receptor could be different from its transmembrane anchor counterpart [89]. ICAM-1 is known to exist as a dimer or multimer on cell surface [93, 94]. However, the GPI-ICAM-1 used in the present study likely expresses as a monomer on the cell surface [93]. Jun *et al.* demonstrated that a single ICAM-1 monomer contains a complete binding site for $\alpha_L\beta_2$ [95]. Therefore, the GPI-anchored ICAM-1 is able to bind $\alpha_L\beta_2$ with full competency. The monomeric nature of the present 2D GPI-ICAM-1 binding should not cause off-rate discrepancies, as the 3D interactions between the purified molecules in the previous SPR studies were also monomeric. It is also possible that GPI anchored ICAM-1 could be extracted from the RBC membrane, thereby reducing the number of ICAM-1 molecules in the contact area available for $\alpha_L\beta_2$ binding. But this would have only impacted on-rates but would not have influenced the 2D off-rates [67, 81, 84, 89]. In addition, GPI-anchor receptor may display a different lateral mobility on the cell membrane, which could affect its ligand binding kinetics. To assess this potential effect, we tested whether the GPI anchor of ICAM-1 had affected the binding parameters. We coupled ICAM-1 to RBCs by using a capturing mAb CA7. The binding between capture antibody and ICAM-1 is likely strong and long lasting; therefore the m_l will not decrease in this case. Micropipette measurements using GPI-anchored or antibody-captured ICAM-1 resulted in comparable binding affinities and off-rates, indicating that the use of GPI-ICAM-1 did not affect the binding parameters (Table 2).

The present results are also comparable to recently published 2D off-rates of β_2 integrin dissociating from ICAM-1 [91, 96, 97]. Lomakina and Waugh reported a 0.7 s^{-1} 2D off-rate of neutrophil integrin interacting with ICAM-1 in the presence of Mg^{2+} using

the micropipette adhesion frequency assay [91], which is comparable to our values but different from the 3D values. Using a flow chamber, Vitte et al. measured bond lifetimes of Jurkat cell integrins interacting with ICAM-1 in the absence and presence of Mg^{2+} or Mn^{2+} [96]. The dissociation curves exhibited at least two phases and hence cannot be interpreted using first-order kinetics. Nevertheless, the apparent off-rates (0.30-0.44 s^{-1}) of the initial phase (0-2 s) are comparable to our 2D values but not to the 3D values (Table 1, 8, 12, and 13). Interestingly, the apparent off-rates (0.032-0.094 s^{-1}) of the later phase (2-10 s), which involves bond strengthening, are comparable to the 3D off-rates of the locked open I domain and of the Mn^{2+}-upregulated WT $\alpha_L\beta_2$ dissociating from ICAM-1. Apparent off-rates of the initial (and later) phase exhibited <4 (and <10) folds of divalent cation regulation, which is consistent with our results, but not with the 3D results. Using atomic force microscopy, Zhang et al. measured rupture forces over a range of loading rates, which were analyzed by the dynamic force spectroscopy method to estimate 2D off-rates based on the Bell equation that assumes off-rate to increase exponentially with force [97]. The zero-force extrapolations of 2D off-rates of 0.17 and 4 s^{-1} for high- and low-affinity $\alpha_L\beta_2$ estimated from the low loading rates (20-10,000 pN/s) data are consistent with our values but are faster than the 3D off-rates of the high-affinity I domain and activated $\alpha_L\beta_2$. Corresponding values estimated from the high loading rates (10,000-50,000 pN/s) data are even faster (40 and 57 s^{-1}). Taking together, the differing 2D off-rates from their 3D counterparts are unlikely experimental artifacts as the 2D data were determined using three independent techniques by three different laboratories.

Discrepancies between 3D and 2D off-rate have been reported for other molecular systems as well. The off-rates of platelet glycoprotein Ibα dissociating from von

Willebrand factor-A1 domain was 0.0038 s^{-1} measured in 3D by radioimmunoassay [98] but were 3.21 s^{-1} and 5.66 s^{-1} measured in 2D by two independent flow chamber experiments [99, 100]. Merkel et al. determined 2D off-rates of biotin/(strept)avidin interactions by a biomembrane force probe [101]. The ~1 min 2D zero-force mean lifetime (= $1/k_{off}$) is orders of magnitude shorter than the 3D value of 35 hours [102]. Ludwig and Evans estimated a 2D apparent force-free mean lifetime of 30 s for extracting single diC 14 lipids from the surface of a lipid:cholesterol vesicle, which is 50-fold shorter than the 3D counterpart estimated from solution measurement [103, 104].

There are many differences between the 2D and 3D measurements, which could affect estimation of the kinetic parameters. Evans suggested that molecular attractions exterior to a binding site could significantly prolong association in solution yet escape detection in force probe tests because the peripheral interaction might be overwhelmed by small forces (e.g. <1 pN) [105]. Likewise, application of force could eliminate pathways available to spontaneous dissociation, which would yield a slower apparent off-rate. It was therefore concluded that there should be no reason to expect the apparent lifetime derived from extrapolation of rupture kinetics to zero force to match the lifetime measured for dissociation in solution [105]. In addition, unlike 3D experiments, where the receptors and ligands approach each other and separate apart by free diffusion, in the micropipette measurement, the molecules are brought together and apart by the movement of the cell membranes. Cell membranes, especially the flexible RBC membrane, undulate under thermal excitations throughout the experiment. The standard deviation of RBC membrane fluctuation is of the order of tens of nanometers, which may exert a small force on the molecular bond, especially when there is only one bond linking

RBC to the K562 cell, which is likely the case. Membrane undulations could also influence 2D binding in other ways, e.g., making the contact time discontinuous. Anchoring the molecule to the cell membrane places restriction not only on translational but also on rotational diffusion of the molecule, which may also impact 2D binding. Whether, and if so, how these mechanisms contribute to the discrepancies between the 2D and 3D off-rates observed in this work is not known at this point. However, the data prompt renewed interest in theoretical modeling and experiment investigation of the influences of these factors on the 2D binding parameters.

CHAPTER 5

THE REGULATION OF 2D BINDING AFFINITY AND KINETICS OF $\alpha_L\beta_2$ BY ACTIVATING ANTIBODIES AND SMALL MOLECULE ANTAGONISTS

5.1 Introduction

Evidences of integrin conformational change have largely emerged after the first crystal structure of integrin ectodomain. In the previous chapter, the effects of I domain conformational change on ligand binding of $\alpha_L\beta_2$ have been demonstrated. The conformational change of I domain could not take place without the presence of other domains. Two other conformational changes in the extracellular domains are suggested to be very important for the activation of whole integrin: the switchblade-like conformational change of integrin legs from bent to extended conformation, and the conversion of integrin headpiece between closed and open conformations [43, 106, 107].

In order to investigate the effects of conformational change on integrin structure and function, the conformation of integrin need to be precisely controlled. Various tools have been used for controlling integrin conformation *in vitro*. Mutations, such as point mutation, introducing a disulfide bond or a glycan wedge, have been showed to successfully generate integrins with various conformations [12, 52, 106-109]. Antibodies and small molecules that could alter integrin ligand binding activity through conformation changes are also widely used. mAb CBR LFA1/2 maps to β_2 I-EGF3 domain. It binds integrins in inactive state and actives them by acting like a wedge in the headpiece-stalk interface [61] (Figure 5-1A). Therefore, CBR LFA1/2 activates β_2 integrins by stimulating the switchblade-like bent to extended conformational change,

which is confirmed by a recent EM study showing that the binding of CBR LFA1/2 to $\alpha_L\beta_2$ and $\alpha_x\beta_2$ induced extension [60]. Binding of mAb MEM83 activates the ligand binding of α_L I domain. A recent study maps MEM83 epitope to Asp182 on the β3-α2 loop, and Glu218 at the end of the α4 helix of the α_L I domain (Figure 5-2) [110]. These residues are located on a face of the α_L I domain opposite from and distant from the MIDAS site, but is close the bottom of the I domain that interfaces with the β-propeller domain (Figure 5-1B).

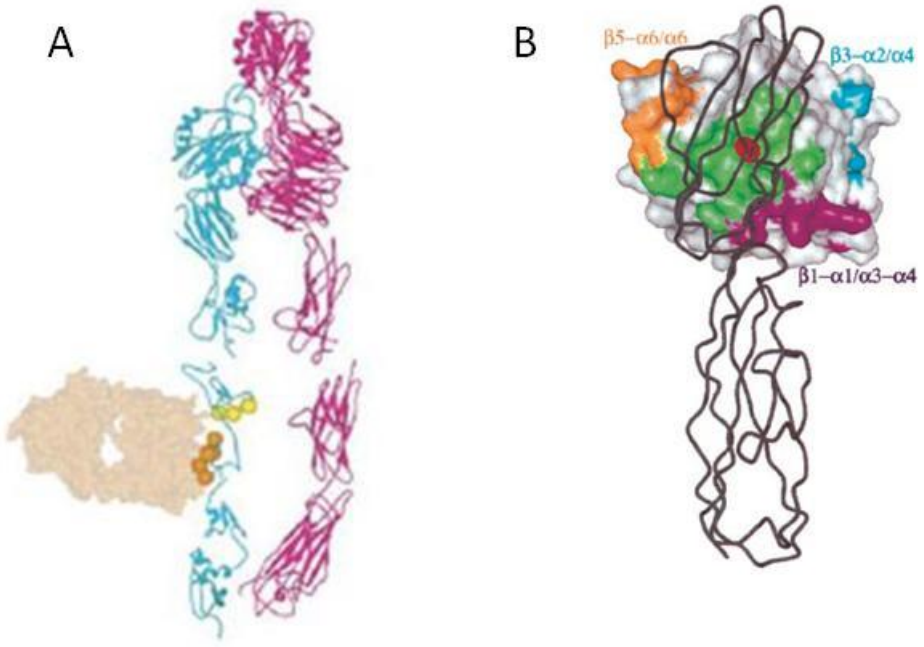

Figure 5-1. The epitopes of mAb CBR LFA1/2 and MEM83. (A) Ribbon diagrams of pseudoatomic $\alpha_x\beta_2$ in shown at the extended conformation. The α and β subunits are pink and cyan respectively. Residues comprising the epitopes of CBR LFA1/2 are orange spheres. CBR LFA1/2 Fab is shown as transparent surface representations [60]. (B) The α_L I domain is shown as a molecular surface and ICAM-1 is shown as a black Cα trace. Residues of MEM83 epitope is colored cyan [110]. (Figure and legend reproduced from references [60] and [110])

Recently, integrin becomes the most important class of cell adhesion molecules from a therapeutic point of view. Several small molecule integrin antagonists have been developed for clinical applications. The use of small-molecule antagonists has enhanced the understanding of integrin conformational change (reviewed in [111]). Based on their mechanism of action, small molecule antagonists fall into three different classes. One type of antagonist inhibits ligand binding directly by binding to the ligand binding site of I domain. However, others bind to sites distal to the MIDAS and inhibit ligand binding indirectly. These are called allosteric inhibition. BIRT377 is an allosteric I domain inhibitor (Figure 5-2A). It binds underneath the C-termical α-helix of the α_L I domain (Figure 5-2C). The binding of this antagonist stabilizes the closed conformation of the I domain, inhibits the conversion of $\alpha_L\beta_2$ to the high-affinity conformation, and therefore allosterically inhibits ligand binding to the MIDAS site in I domain. This action is confirmed by the fact that $\alpha_L\beta_2$ containing a locked open I domain is resistant to inhibition by BIRT377 [108]. Another antagonist, XVA143, however, inhibits ligand binding by perturbing the interface between the I domain and the I-like domain (Figure 5-2B and D). As described above, the I domain could be activated by the binding of I-like domain MIDAS to the intrinsic ligand, Glu310. It is suggested XVA143 binds to the I-like domain MIDAS as mimics of the intrinsic ligand and inhibits the binding of the intrinsic ligand in the I domain, and consequently leaves the I domain in the closed conformation. However, this antagonist could activate the rest of $\alpha_L\beta_2$ by stabilizing the I-like domain in active configuration. As a result, XVA143 induces and stabilizes the extended conformation of $\alpha_L\beta_2$.

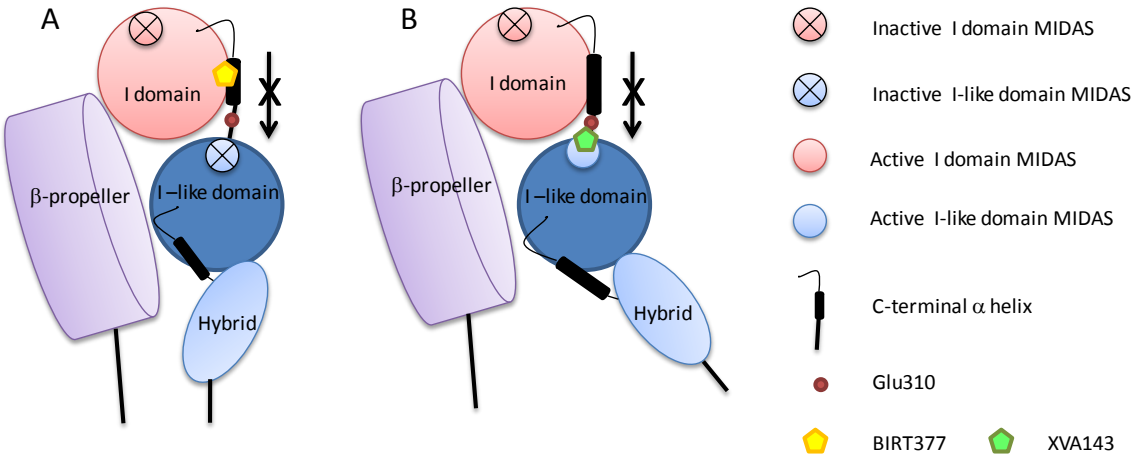

Figure 5-2. The inhibition of ligand binding of $\alpha_L\beta_2$ by BIRT377 and XVA143 [111, 112]. (A) BIRT377 inhibits the I domain activation by binding to the side of the C-terminal α7 helix and stabilizes the headpiece in closed conformation. (B) XVA143 competes with the intrinsic ligand (Glu-310) to bind to I-like domain MIDAS. It prevents the activation of I domain while activates the rest of the integrin.

Activation dependent antibodies, also called reporting antibodies, are wildly used to detect integrin conformational change on cell surface. The epitopes of these antibodies are only exposed in certain conformation of integrin. The exposure of mAb KIM127 epitope has been widely used to indicate the extended conformation of $\alpha_L\beta_2$. It maps to the I-EGF2 of β_2 subunit and the epitopes of KIM127 and CBR LFA1/2 actually locate on the opposite sides of β_2 leg [61, 113] (Figure 5-3). Although it has been reported to activate ligand binding [76], it preferentially binds to the activated forms of β_2 integrins [114].

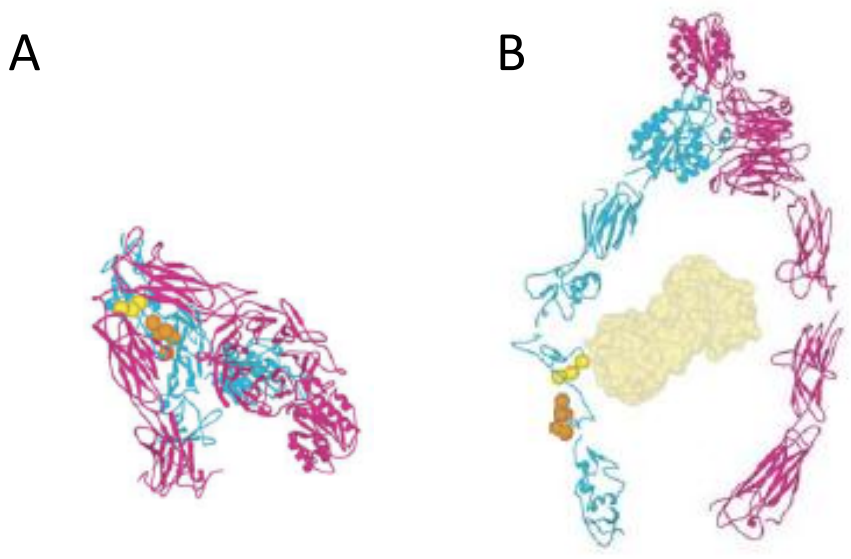

Figure 5-3. Reporting of extension of $\alpha_x\beta_2$ by KIM127 Fab. Ribbon diagrams of pseudoatomic $\alpha_X\beta_2$ in the bent conformation (A) and extended conformation (B). The α and β subunits are pink and cyan respectively. Residues comprising the epitopes of KIM127 and CBR LFA1/2 are yellow and gold spheres, respectively. KIM127 Fab is shown as transparent surface representations. (Figure and legend reproduced from reference [60])

It is essential to understand how the conformational changes affect the ligand binding affinity and kinetics $\alpha_L\beta_2$. It is well-known that activated $\alpha_L\beta_2$ has the high ligand binding affinity and inactive $\alpha_L\beta_2$ has low ligand binding affinity. However, there is so far no study investigated how conformational changes in I domain and in $\alpha_L\beta_2$ legs could have different effects on the regulation of binding affinity and kinetics. The conformational change of I domain from closed to open has been shown to increase the binding affinity and decrease the off-rate. It is not known the effects of leg extension on these binding parameters although it has been shown to facilitate cell rolling mediated by $\alpha_L\beta_2$ [112]. By controlling the conformation of $\alpha_L\beta_2$ carefully using mutation, activating antibodies, and small molecule antagonist, this study is able to investigate the distinct

effects of I domain conformational change and $\alpha_L\beta_2$ extension on ligand binding kinetics and affinity. The results showed that the switchblade-like conformational change of $\alpha_L\beta_2$ legs only affect the on-rate of $\alpha_L\beta_2$ binding. Without changing the conformation of I domain, the extension of $\alpha_L\beta_2$ alone increased the on-rate by ~ 3 to 4 fold, but did not affect the off-rate. The off-rate change of $\alpha_L\beta_2$ was mostly due to the conformational change of I domain. For WT $\alpha_L\beta_2$, the extension of integrin propagated the conformational change to I domain, and increased the binding affinity by ~ 30 fold. Moreover, this study provided useful information for the characterizations of multiple conformational states of $\alpha_L\beta_2$ regarding the binding affinity and kinetics.

5.2 The Effects of Activating Antibodies on $\alpha_L\beta_2$ Binding Affinity and Kinetics

Two activating antibodies, MEM83 and CBR LFA1/2, were used to regulate the binding kinetics and affinity of $\alpha_L\beta_2$. The adhesion frequency of WT or locked $\alpha_L\beta_2$ on K562 cell and ICAM-1 on RBCs were measured in the absence or presence of 10 μg/ml activating antibody in HBSS-. In the presence of MEM83, the binding affinity of WT $\alpha_L\beta_2$ increased ~ 22 fold with a 4 fold decrease in off-rate. However, MEM83 did not have significant effects on the binding kinetics and affinities of $\alpha_L\beta_2$ containing a locked I domain (Figure 5-4). CBR LFA1/2 also increased the binding affinity of WT $\alpha_L\beta_2$ for ~ 30 fold to a similar level of the binding affinity of MEM83 activated $\alpha_L\beta_2$. However, it only decreased the off-rate for less than 2 fold (Figure 5-4). For $\alpha_L\beta_2$ containing the locked open and intermediate I domains, CBR LFA1/2 increased the binding affinities by 3-4 fold without changing the off-rates (Figure 5-4).

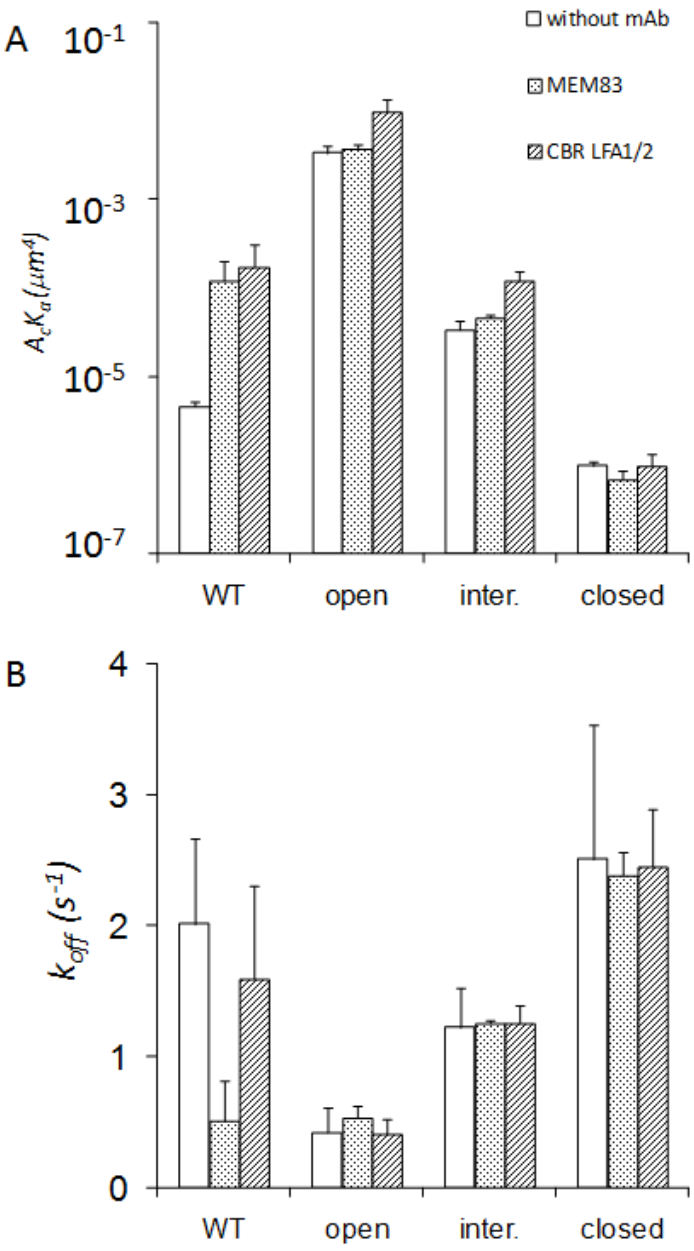

Figure 5-4. Regulation of $\alpha_L\beta_2$ affinity and off-rate by mAb MEM83 and CBR LFA1/2. Effective binding affinities (A) and off-rates (B) for ICAM-1 of the WT $\alpha_L\beta_2$ and $\alpha_L\beta_2$ containing the locked open, locked intermediate, or locked closed I domain with or without 10 μg/ml of MEM83 or CBR LFA1/2 are shown. The binding affinity and off-rate are shown as the mean ± s.e.m. of the parameters obtained from 2 to 3 binding curves with different site densities. MEM83 and CBR LFA1/2 both increased the binding affinity of WT $\alpha_L\beta_2$ ($P<0.0005$, student *t* test). MEM83 did not change the binding affinity of locked $\alpha_L\beta_2$ ($P>0.3$), while CBR LFA1/2 increased the affinities of open and intermediate $\alpha_L\beta_2$ by 3-4 fold ($P<0.07$). MEM83 decreased the off-rate of WT $\alpha_L\beta_2$ by 4 fold ($P=0.05$), but CBR LFA1/2 only reduced the off-rate slightly ($P=0.22$). Both of them did not change the off-rates of locked I domains ($P>0.52$).

To access the conformation of $\alpha_L\beta_2$ legs, the exposure of KIM127 epitope was examined using flow cytometry. The site density of total $\alpha_L\beta_2$ on K562 cells was measured by using mAb 7E4. Without activating antibodies, the binding of KIM127 was very low, less than 1/4 of the $\alpha_L\beta_2$ was able to bind KIM127 (Figure 5-5). In the presence of MEM83, the fraction of KIM127 bound $\alpha_L\beta_2$ was not significantly increased, indicating most of $\alpha_L\beta_2$ were in bent conformation, or at least with the KIM127 epitope buried. By contrast, in the presence of CBR LFA1/2, the fraction of KIM127 bound $\alpha_L\beta_2$ showed significant increase, ~ 75% of the total number of $\alpha_L\beta_2$ (Figure 5-5).

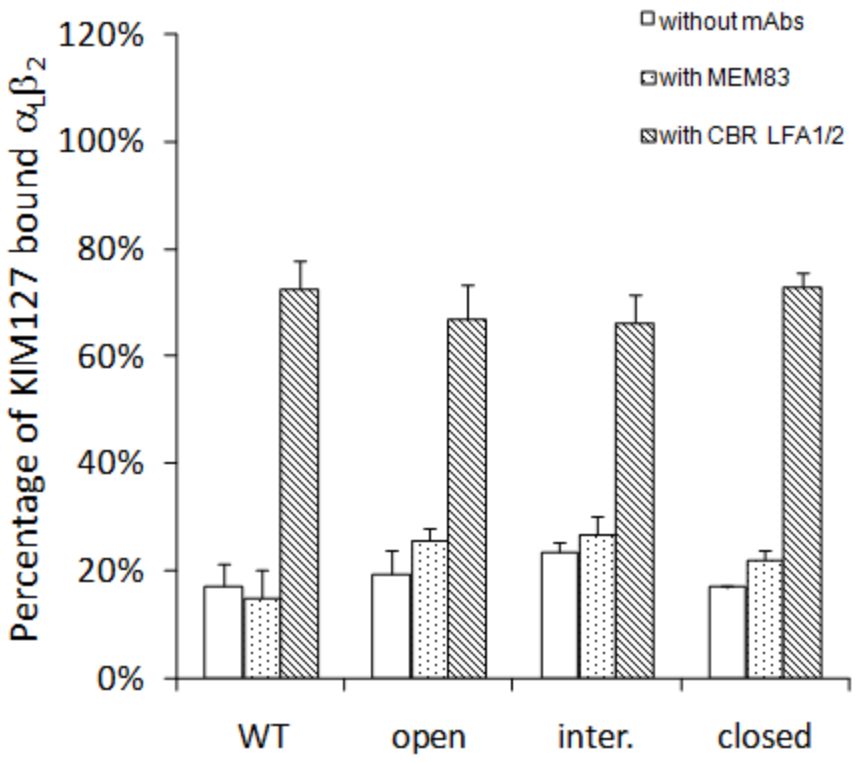

Figure 5-5. The binding of KIM127 to $\alpha_L\beta_2$ in the absence and presence of 10 μg/ml MEM83 or CBR LFA1/2. The total site density of $\alpha_L\beta_2$ were measured by mAb 7E4. The site density of KIM127 bound $\alpha_L\beta_2$ were measured in the absence and presence of MEM83 or CBR LFA1/2. The percentage of KIM127 bound $\alpha_L\beta_2$ was calculated by dividing the site density of KIM127 bound $\alpha_L\beta_2$ by the total site density. The values were shown as mean ± s.e.m. of two independent experiments.

5.3 The Effects of Small Molecule Antagonists on $\alpha_L\beta_2$ Binding Affinity and Kinetics

Small antagonists, BIRT377 and XVA143, were also used to control the conformation of $\alpha_L\beta_2$ and to regulate its binding affinity and kinetics. When Mg^{2+} (or CBR LFA1/2) and BIRT377 were both present in the chamber medium, the adhesion frequency of WT $\alpha_L\beta_2$ and ICAM-1 was very low (data now shown). Without other stimulation, BIRT377 decreased the binding affinity of WT $\alpha_L\beta_2$ by ~ 6 fold and to a level comparable to the locked closed $\alpha_L\beta_2$ (Figure 5-6). The binding affinities and kinetics of $\alpha_L\beta_2$ containing a locked I domain did not change with the presence of BIRT377 (Figure 5-6).

Similar to BIRT377, XVA143 decreased the binding affinity of WT $\alpha_L\beta_2$ by ~ 5 fold without a change in the off-rate (Figure 5-6). However, for $\alpha_L\beta_2$ containing locked open and intermediate I domains, BIRT377 was able to increase their binding affinities by ~ 5 fold. There is little, if there is any, effect of BIRT377 on the binding of locked closed $\alpha_L\beta_2$ (Figure 5-6).

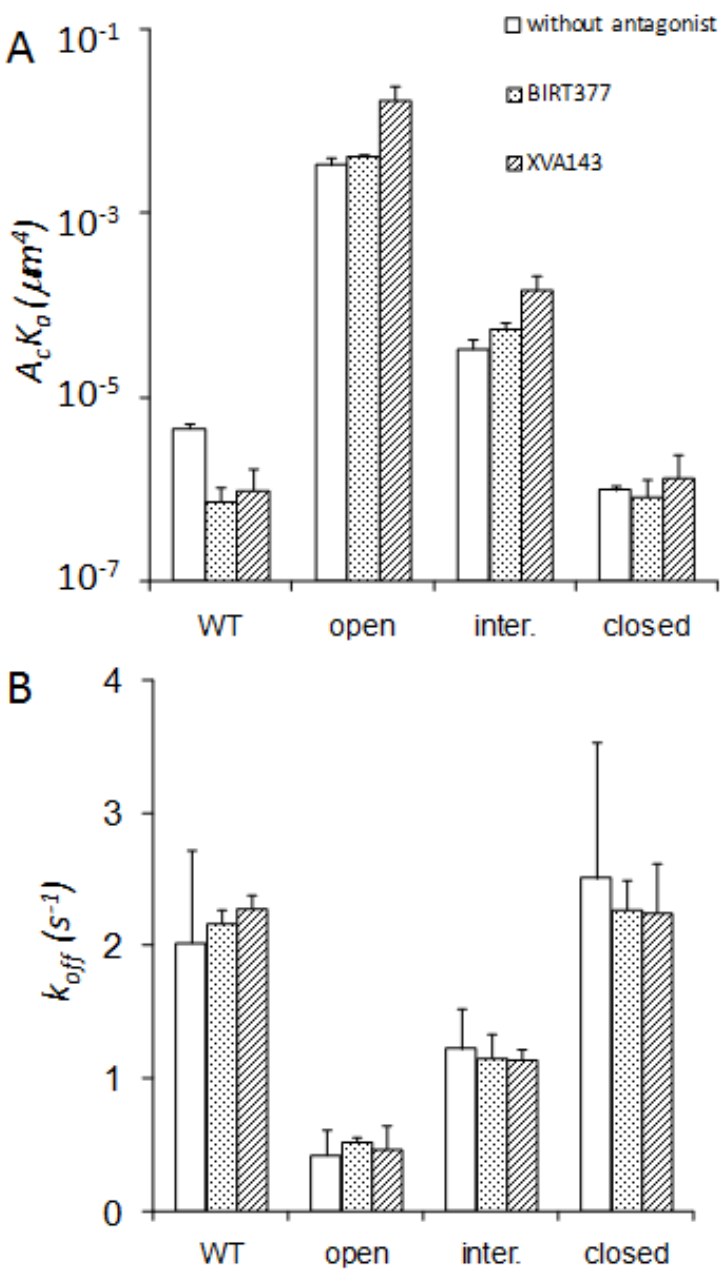

Figure 5-6. Regulation of $\alpha_L\beta_2$ affinity and off-rate by small antagonists BIRT377 and XVA143. Effective binding affinities (A) and off-rates (B) for ICAM-1 of the WT $\alpha_L\beta_2$ and $\alpha_L\beta_2$ containing the locked open, locked intermediate, or locked closed I domain with or without BIRT377 (10 μM) or XVA143 (1 μM). The binding affinity and off-rate are shown as the mean ± s.e.m. of the parameters obtained from 2 to 3 binding curves with different site densities. MEM83 and CBR LFA1/2 decreased the binding affinity of WT $\alpha_L\beta_2$ ($P<0.02$, student *t* test). They did not change the off-rate of WT and locked $\alpha_L\beta_2$ ($P>0.52$). MEM83 did not change the binding affinity of locked $\alpha_L\beta_2$ ($P>0.36$). XVA143 increased the binding affinity of locked open and intermediate $\alpha_L\beta_2$ by 5 fold ($P<0.06$).

Binding of KIM127 to $\alpha_L\beta_2$ with the presence or absence of BIRT377 and XVA143 was also measured. BIRT377 did not significantly increase the binding of KIM127 to $\alpha_L\beta_2$ (Figure 5-7). XVA143, however, greatly increased the number of KIM127 bound $\alpha_L\beta_2$ (Figure 5-7).

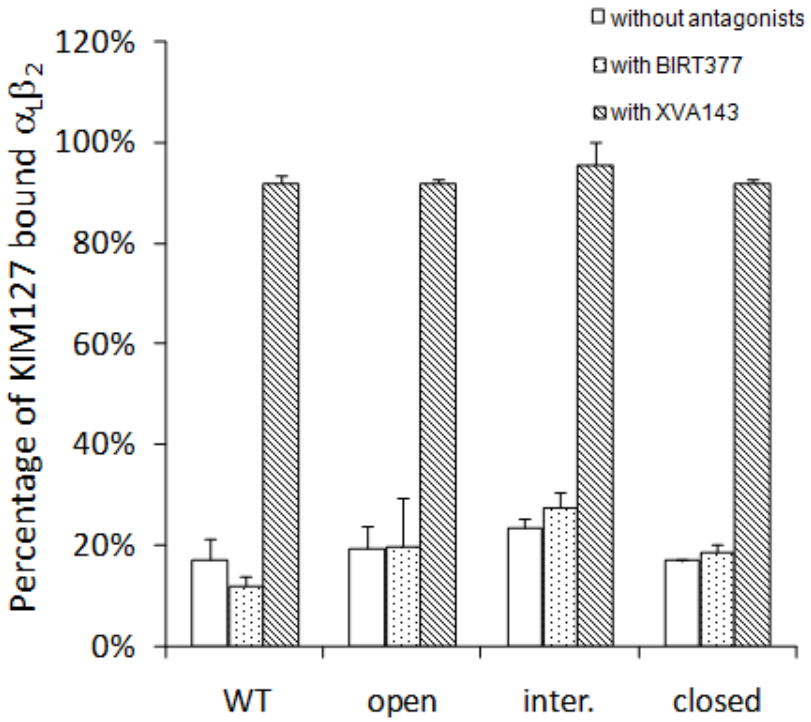

Figure 5-7. The binding of KIM127 to $\alpha_L\beta_2$ in the absence and presence of BIRT377 or XVA143. The total site density of $\alpha_L\beta_2$ were measured by mAb 7E4. The site density of KIM127 bound $\alpha_L\beta_2$ were measured in the absence and presence of BIRT377 (10 μM) or XVA143 (1 μM). The percentage of KIM127 bound $\alpha_L\beta_2$ was calculated by dividing the site density of KIM127 bound $\alpha_L\beta_2$ by the total site density. The values were shown as mean ± s.e.m. of two independent experiments.

5.4 Discussion

The difference in the effects of I domain conformational change and the extension of $\alpha_L\beta_2$ on 2D binding affinity and kinetics was studied for the first time in this study.

Activated by MEM83 or CBR LFA1/2, the binding affinity of WT $\alpha_L\beta_2$ was increased by ~ 30 fold and to a level comparable to locked intermediated $\alpha_L\beta_2$ (Table 3). MEM83 decreased the off-rate by ~ 4 fold; while CBR LFA1/2 did not affect the off-rate. This could be explained by different activating mechanisms of MEM83 and CBR LFA1/2. MEM83 increased the $\alpha_L\beta_2$ binding affinity by inducing conformation change in I domain [110]. However, MEM83 activated $\alpha_L\beta_2$ are at bent conformation because the exposure of KIM127 epitope was very low. In contrast, CBR LFA1/2 activates $\alpha_L\beta_2$ by inducing the extension of the legs, which is confirmed by the observation that the KIM127 bound $\alpha_L\beta_2$ was increased a lot in the presence of CBR LFA1/2. Therefore, the increase of binding affinity induced by MEM83 could be mainly due to conformational change of I domain. The off-rate of MEM83 activated $\alpha_L\beta_2$ was 0.51 s^{-1} and comparable to the off-rate of $\alpha_L\beta_2$ with a locked open I domain, indicating the I domain of MEM83 activated $\alpha_L\beta_2$ adapts open conformation. The off-rate of CBR LFA1/2 activated $\alpha_L\beta_2$ was 1.22 s^{-1} and on the same level of the intermediate I domain off-rate, indicating CBR LFA1/2 increased the binding affinity mainly by increasing the on-rate. EM study showed that the extension induced by CBR LFA1/2 could result in either closed or open headpiece in $\alpha_x\beta_2$ [60]. Thus, the I domain of CBR LFA1/2 activated $\alpha_L\beta_2$ could be a mixture of open, intermediate and closed conformation. These results strongly suggested conformations of $\alpha_L\beta_2$ activated by MEM83 and CBR LFA1/2 are different and have distinct characteristics regarding binding affinity and kinetics.

Mn^{2+} increases the binding affinity of WT $\alpha_L\beta_2$ to a higher level compared to activating antibodies in this study. The binding affinity of Mn^{2+} activated $\alpha_L\beta_2$ was ~ 50 fold higher than those of MEM83 and CBR LFA1/2 activated $\alpha_L\beta_2$. This difference may

be explained by the usage of cells and whole antibodies in this study. There might be steric hindrance for whole activating antibodies to access their epitopes on $\alpha_L\beta_2$ expressing on cell membrane. As a result, not all $\alpha_L\beta_2$ were bound by activating antibodies and the actual site density (m_r) were lower than the site density measured using flow cytometry, resulting a underestimated binding affinity. It is also possible that the purified proteins behave differently from cell surface expressing proteins in terms of antibody binding and conformational change. In fact, only ~ 70% of $\alpha_L\beta_2$ were extended when activated by CBR LFA1/2; while using Fab fragments and purified proteins, CBR LFA1/2 induced extension of > 90% of $\alpha_x\beta_2$ [60].

With conformation of I domain locked, MEM83 was not able to affect the binding of $\alpha_L\beta_2$. However, CBR LFA1/2 increased the binding affinity of locked open and intermediate $\alpha_L\beta_2$. This increase was mainly due to the on-rate increase (~ 3-4 fold), because the presence of CBR LFA1/2 did not change the off-rate at all. Therefore, the extension of $\alpha_L\beta_2$ could increase the ligand binding on-rate but has no effect on off-rate. This is further confirmed by using small molecule antagonists to regulate the binding affinity and kinetics of $\alpha_L\beta_2$. BIRT377 inhibits the ligand binding of $\alpha_L\beta_2$ by prevent pulling down of α7 helix of I domain without affect the conformation of integrin legs [65, 111]. As expected, BIRT377 did not change the binding affinities and kinetics of $\alpha_L\beta_2$ with a locked I domain. XVA143, on the other hand, increased the binding affinity of locked open and intermediated $\alpha_L\beta_2$ by increasing the on-rate by ~ 5 fold. The on-rate increase is exclusively due to extension of $\alpha_L\beta_2$ induced by the binding of XVA143 to the interface to α_L I domain and β I-like domain. After binding of XVA143, > 85% of $\alpha_L\beta_2$ changed to extended conformation as indicated by the exposure of KIM127 epitope.

Taken together, the extension of $\alpha_L\beta_2$ increased the ligand binding on-rate by 3-5 fold without affecting the off-rate. On cell surface, interaction between receptor and ligand is likely be influenced by the surface environmental factors, one of them is the distance that the binding pocket of the adhesion receptor extends outward from the cell surface. Extending the binding site above the surface by adding a polymer chain spacer generated a long range attractive force that may enhance the on-rate but would not affect the off-rate [115]. Another study showed reducing the molecular lengths of P- and L-selectin lowered the on-rate but not off-rate [72]. For $\alpha_L\beta_{2,}$ bent to extended conformational change extends the I domain outward from cell membrane by approximately 20 nm, which would greatly increase the accessibility of MIDAS binding site for ICAM-1.

For activation of $\alpha_L\beta_2$ by inside-out signaling, the extension of $\alpha_L\beta_2$ legs induce the swinging out of hybrid domain, resulting an open headpiece which in turn activate I domain by pulling down the $\alpha7$ helix. However, the extension of $\alpha_L\beta_2$ may not necessarily lead to an open headpiece and open I domain. EM studies showed that β_2 integrins could be extended with closed headpiece and I domain [60]. It is not known if this conformation is a stable state or just a transitional state during conformational change. Salas *et al.* demonstrated the importance of integrin extension in mediating cell rolling [112]. While inhibiting firm adhesion, XVA143 enhanced rolling mediated by $\alpha_L\beta_2$ by inducing the extension of molecule. Other studies also suggested that it may have physiological significance of supporting cell rolling [23, 55, 112]. Therefore, the extension of $\alpha_L\beta_2$ may play more roles than just being a transient step of conformational propagation from cytoplasmic domain to ligand binding site.

The present study also allows us to characterize the multiple conformational states of $\alpha_L\beta_2$ under different conditions by categorizing them according to binding affinity and kinetics (Table 5-1). As discussed above, the ligand binding affinity and off-rate are mainly determined by the conformational state of I domain. With an open I domain, the 2D binding affinity of $\alpha_L\beta_2$ is in the order of 10^{-3} μm^4, and the reverse-rate is ~ 0.5 s^{-1}. When the I domain is at intermediate state, the 2D binding affinity of $\alpha_L\beta_2$ is in the order of 10^{-5} μm^4, and the reverse-rate is ~ 1.2 s^{-1}. The 2D binding affinity of $\alpha_L\beta_2$ with a closed I domain is in the order of 10^{-7} μm^4, and the reverse-rate is larger than 2 s^{-1}. With the same conformation of I domain, the extended $\alpha_L\beta_2$ has few fold increase in the binding affinity compared to bent $\alpha_L\beta_2$, but the off-rate does not change.

Table 5-1. 2D binding affinity and orr-rates of $\alpha_L\beta_2$ regulated by MEM83, CBR LFA1/2, BIRT377, and XVA143.

I domain	$\alpha_L\beta_2$		A_cK_a (μm^4)	k_{off} (s^{-1})
Open	Bent	open $\alpha_L\beta_2$ (HBSS-)	$3.30(\pm0.62)\times10^{-3}$	0.42(±0.19)
		open $\alpha_L\beta_2$ (MEM83)	$3.71(\pm0.41)\times10^{-3}$	0.53(±0.10)
		open $\alpha_L\beta_2$ (BIRT 377)	$4.13(\pm0.19)\times10^{-3}$	0.52(±0.04)
		WT $\alpha_L\beta_2$ (MEM83)	$1.20(\pm0.80)\times10^{-4}$	0.51(±0.31)
	extended	open $\alpha_L\beta_2$ (CBR LFA1/2)	$9.78(\pm1.53)\times10^{-3}$	0.41(±0.11)
		open $\alpha_L\beta_2$ (XVA 143)	$1.67(\pm0.68)\times10^{-2}$	0.47(±0.18)
Inter.	Bent	Inter. $\alpha_L\beta_2$ (HBSS-)	$3.30(\pm0.88)\times10^{-5}$	1.23(±0.30)
		Inter. $\alpha_L\beta_2$ (MEM83)	$4.62(\pm0.25)\times10^{-5}$	1.26(±0.01)
		Inter. $\alpha_L\beta_2$ (BIRT 377)	$5.62(\pm0.95)\times10^{-5}$	1.16(±0.17)
	extended	Inter. $\alpha_L\beta_2$ (CBR LFA1/2)	$1.20(\pm0.32)\times10^{-4}$	1.26(±0.13)
		Inter. $\alpha_L\beta_2$ (XVA 143)	$1.47(\pm0.50)\times10^{-4}$	1.14(±0.08)
Closed	Bent	closed $\alpha_L\beta_2$ (HBSS-)	$9.85(\pm1.27)\times10^{-7}$	2.51(±1.02)
		closed $\alpha_L\beta_2$ (MEM83)	$6.98(\pm1.63)\times10^{-7}$	2.38(±0.18)
		closed $\alpha_L\beta_2$ (BIRT 377)	$8.47(\pm4.12)\times10^{-7}$	2.27(±0.23)
		WT $\alpha_L\beta_2$ (HBSS-)	$4.60(\pm0.52)\times10^{-6}$	2.01(±0.65)
		WT $\alpha_L\beta_2$ (BIRT 377)	$7.54(\pm0.29)\times10^{-7}$	2.17(±0.10)
	extended	closed $\alpha_L\beta_2$ (CBR LFA1/2)	$9.71(\pm0.35)\times10^{-6}$	2.45(±0.45)
		closed $\alpha_L\beta_2$ (XVA 143)	$1.36(\pm0.13)\times10^{-6}$	2.25(±0.37)
		WT $\alpha_L\beta_2$ (XVA 143)	$9.89(\pm0.70)\times10^{-7}$	2.28(±0.11)

CHAPTER 6

THE BINDING AFFINITIES AND KINETICS OF DIVALENT CATIONS TO α_L I DOMAIN AND $\alpha_L\beta_2$

6.1 Introduction

The receptor function of $\alpha_L\beta_2$ and other integrins depend on the presence of divalent cations. Divalent cations have multiple effects on $\alpha_L\beta_2$ mediated cell adhesion, such as enhancement and suppression of ligand binding activity. It is established that the nature of the divalent cation plays a critical role in regulation of ligand binding affinity of $\alpha_L\beta_2$ [116]. I*n vitro*, Mn^{2+} and Mg^{2+} have been shown to facilitate ligand binding to $\alpha_L\beta_2$, while Ca^{2+} inhibits the ligand binding at mM concentration. All three divalent cations are present in the extracellular environment (Mg^{2+} and Ca^{2+} at mM concentration; Mn^{2+} at μM concentration), and all are available to compete for binding to the integrin.

Although the mechanism of how these divalent cations regulate $\alpha_L\beta_2$ activity is not clear, it is believed that divalent cations regulate the ligand binding of $\alpha_L\beta_2$ either by directly coordinating into the binding site, or by binding into a metal ion coordination site to induce a conformational change of $\alpha_L\beta_2$. A very important metal ion coordination site of $\alpha_L\beta_2$ is the MIDAS on the top of the I domain. The divalent cation is central in the binding site and directly coordinates a Glu residue in the ligand [12, 42]. Conformational change of I domain clearly rearranged the coordination of divalent cation, including the amino acids that directly forming coordination and the position of surrounding loops [12] (Figure 2-7). Other than I domain MIDAS, there are many other metal ion binding sites

on $\alpha_L\beta_2$. Among them, the most important ones for conformational regulation might be the three divalent binding sites in I-like domain, I-like domain MIDAS, the adjacent MIDAS (ADMIDAS), and the ligand-induced metal binding site (LIMBS). For integrin without an I domain, I-like domain contains the ligand binding sites and these sites could directly affect the ligand binding. It has been shown that they have distinct roles in the regulation of $\alpha_4\beta_7$ mediated adhesion under different divalent cation conditions [117]. For integrins containing I domain, these metal ion coordination sites probably regulate the ligand binding by inducing or preventing conformational change. For example, I-like domain MIDAS, when activated, binds to an intrinsic ligand of I domain and thus pulls down the α7 helix to induce conformational change in I domain MIDAS. In fact, the mutation of intrinsic ligand Glu310 or I-like MIDAS residues Ala210 or Tyr115 to cysteine abolished I domain activation [64].

As divalent cations need to be coordinated into the metal ion binding sites in order to regulate integrin functions, the binding characteristics, such as binding affinity and kinetics, of the divalent cations to integrin is very important for understanding the mechanism of divalent cation regulation. Labadia *et al.* determined the binding affinity of Mg^{2+} and Mn^{2+} to $\alpha_L\beta_2$ using SPR [78]. The K_D of Mg^{2+} were 160 and 12 μM in the absence and the presence of Ca^{2+}, respectively; K_D of Mn^{2+} was 2 μM in the presence of Ca^{2+} [78]. Increasing Ca^{2+} into mM concentration range resulted in a competitive displacement of Mg^{2+}/Mn^{2+}. α_L I domain has been shown to bind to $^{54}Mn^{2+}$ in a conformation-dependent manner. Using $^{45}Ca^{2+}$ and $^{54}Mn^{2+}$ in direct binding studies, the K_D for the interactions between these cations and α_L I domain were estimated to be 50-60 and 10-20 μM, respectively [118]. In a recent study, Mg^{2+} and Ca^{2+} were shown to have

equivalent affinities to inactive α_M I domain. Activation induced a ~10-fold increase in the binding affinity of Mg^{2+} to α_M I domain with no change in that of Ca^{2+}. This study indicated that the affinity of divalent cations to integrins is itself regulated by the activation state of these receptors [119].

In these studies, $\alpha_L\beta_2$ and α_L I domain were purified proteins and their conformational state was not clearly addressed. Moreover, the binding kinetics, which is also important in order to characterize the divalent cation coordination, has not been measured. Here, the binding affinity and kinetics of Mn^{2+}, Mg^{2+}, and Ca^{2+} were measured in a more physiologic setup, using cell surface expressing I domains as well as $\alpha_L\beta_2$ (both WT and locked). Since $\alpha_L\beta_2$-ICAM-1 interaction is highly sensitive to the presence of divalent cations, a method using ligand binding to probe the binding affinity and kinetics of divalent cations to I domain and $\alpha_L\beta_2$ was employed. The results showed different cations bind to I domain MIDAS with different binding affinities and kinetics. Mn^{2+} has more than 30 fold higher binding affinity for all four types of I domains than Mg^{2+}. Ca^{2+} showed two binding affinities, a high one (K_D of μM) and a low one (K_D of mM), to I domain MDIAS. All three divalent cations dissociate from I domain MIDAS slowly with half lives of hours. Mn^{2+} dissociates slower than the other two divalent cations. The conformation of I domain also affects the binding affinity and kinetics of divalent cations. Open and intermediate I domains have similar binding affinities for Mn^{2+} and Mg^{2+}, which are higher than those of the WT and closed I domains.

With I domain MIDAS occupied with a divalent cation, the binding affinities of Mn^{2+} and Mg^{2+} for those metal ion binding sites that are important for conformational change of $\alpha_L\beta_2$ were also measured. Again, Mn^{2+} has a higher affinity than Mg^{2+}. Discard

the conformational difference in I domain, the binding affinity of Mn^{2+} and Mg^{2+} for WT and locked open $\alpha_L\beta_2$ were similar. In contrast to the slow dissociation of Mn^{2+} and Mg^{2+} from I domain MIDAS, these divalent cations dissociated from those metal ion binding sites that are important for conformational change very rapidly in less than minutes. These results provided new insights into the mechanism of $\alpha_L\beta_2$ regulation by divalent cations.

6.2 Binding Affinities of Divalent Cations to WT and Locked Isolated α_L I Domains

To measure the binding affinity of Mn^{2+}, Mg^{2+}, and Ca^{2+} for I domain MIDAS, K562 cells expressing WT or locked I domains and RBCs coated with ICAM-1 were used. Cells were washed with HBSS/EDTA to remove any preexisting divalent cations and then with HBSS- to wash away the EDTA. Cells were then suspended in HBSS- with desired concentrations of divalent cations. The adhesion frequencies of I domain and ICAM-1 were measured using micropipette adhesion frequency assay. The contact duration was chosen to be 10 seconds, which is long enough for the binding of I domain and ICAM-1 reaches equilibrium. Adhesion of I domain and ICAM-1 depended on the presence of divalent cations, because the adhesion frequency was at background level when no divalent cations were added after washing (data not shown). Moreover, the RBCs without ICAM-1 coated gave background level binding with the presence of divalent cations (data not shown).

The adhesion frequency was plotted against the concentration of divalent cations, and the binding affinity of divalent cation to I domain MIDAS were extracted by fitting the data into Equation 3-5. Plotting of adhesion frequency against concentrations of Mn^{2+}

or Mg^{2+} gave sigmoidal curves (Figure 3-2). The K_D of Mn^{2+} binding was at μM order and was several tens of fold higher than that of Mg^{2+} (Figure 6-1). For Ca^{2+}, a double sigmoidal curve was observed, and two binding affinities were obtained from the fitting using Equation 3-6 (Figure 3-2, Figure 6-1). One of the two binding affinities of Ca^{2+} was very high with K_D at μM order, and the other one is much lower with K_D at mM level (Figure 6-1). Locked open and intermediate I domains have similar binding affinities to divalent cations; whereas the binding affinities of WT and locked closed I domains were comparable (Figure 6-1). Furthermore, the binding affinities of divalent cations for open and intermediate I domains were higher than those of WT and closed I domains, especially for Mn^{2+} and $Ca^{2+}_{(1)}$ (Figure 6-1).

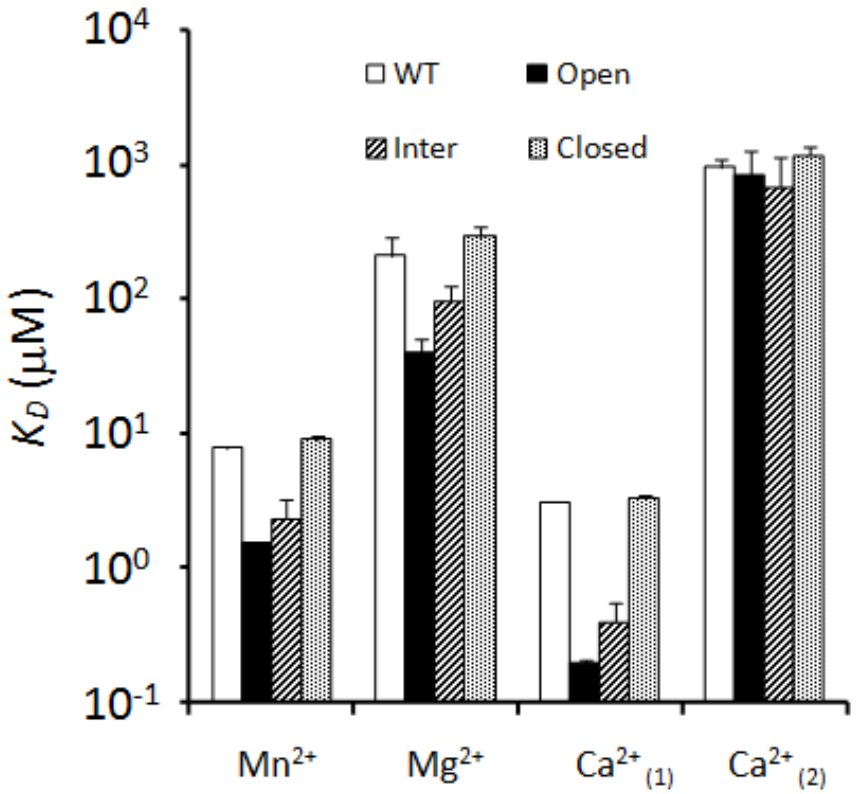

Figure 6-1. The K_D of Mn^{2+}, Mg^{2+}, and Ca^{2+} to MIDAS of WT and locked I domains. The values are presented as mean ± s.e.m. of the K_D obtained from three independent experiments. Mn^{2+} binds to I domain MIDAS with higher affinity than Mg^{2+} ($P \leq 0.05$ for all four types of I domains). Ca^{2+} has two binding affinities to I domain MIDAS, one with a K_D at μM order and one at mM order. Open and intermediate I domains have comparable binding affinities for Mn^{2+}, and Mg^{2+} ($P>0.6$); while WT and closed I domains have similar binding affinities for Mn^{2+}, and Mg^{2+} ($P>0.85$). Open and intermediate I domains have higher binding affinities for Mn^{2+} than WT and closed I domains ($P<0.007$ for Mn^{2+}). For Ca^{2+}, open and intermediate I domains have higher binding affinity for Ca^{2+} at conformation (1) than WT and closed I domains ($P<0.006$); however, the four types of I domains have comparable binding affinity for Ca^{2+} at conformation (2) ($P>0.52$).

6.3 Divalent Cations Dissociate from α_L I Domain MIDAS Very Slowly

When K562 cells were washed with and then suspended in HBSS-, the adhesion frequency between isolated I domain and ICAM-1 is still measurable (data from Chapter 4 and 5). This indicates that without using EDTA, the divalent cations pre-bound to I

domain remained bound for hours in HBSS- to enable specific binding. In order to investigate the dissociation of divalent cations form I domain MIDAS, cells were washed with HBSS/EDTA and then HBSS- to get rid of all preexisting divalent cations. The cells were then suspended in HBSS- containing Mn^{2+}, Mg^{2+}, or Ca^{2+} at saturating concentration, i.e., 2mM Mn^{2+}, 5mM Mg^{2+}, or 5mM Ca^{2+}, and incubated for 1 hour at room temperature. The divalent cations were then washed away and cells were suspended in HBSS- for micropipette measurement. The adhesion frequency of I domain and ICAM-1 were measured at different time points after the divalent cations were washed away, i.e. 0 hr, 0.5 hr, 1.5 hr, etc. The adhesion frequency of I domain and ICAM-1 decreased very slowly after washing, indicating divalent cations dissociated from I domain MIDAS very slowly (Figure 6-2). It is unlikely that K562 cells secrete divalent cations during experiment to bind to I domain MIDAS and support adhesion, because cells washed with HBSS/EDTA then washed and resuspended in HBSS- did not show specific adhesion for at least 8 hours (Figure 6-2). On the other hand, in the presence of divalent cations at saturating concentration, the adhesion frequency remained constant for 8 hours, indicating the decrease of adhesion frequency could not be due to receptor downregulation or other cellular environment changes (Figure 6-2).

The adhesion frequency was plotted against the dissociation time in order to extract the dissociation rate of divalent cation from I domain MIDAS using Equation 3-7 (Figure 3-3). The differences in dissociation rates of Mn^{2+}, Mg^{2+}, and Ca^{2+} were not dramatic. Mn^{2+} dissociated form I domain MIDAS with a little slower rate compared to Mg^{2+} (Figure 6-4). Mn^{2+}, Mg^{2+}, and Ca^{2+} had faster dissociation rates for open and intermediate I domains than for closed I domain. The dissociation rates of Mn^{2+}, Mg^{2+},

and Ca^{2+} for WT I domain were in between of those for open I domain and closed I domain (Figure 6-3).

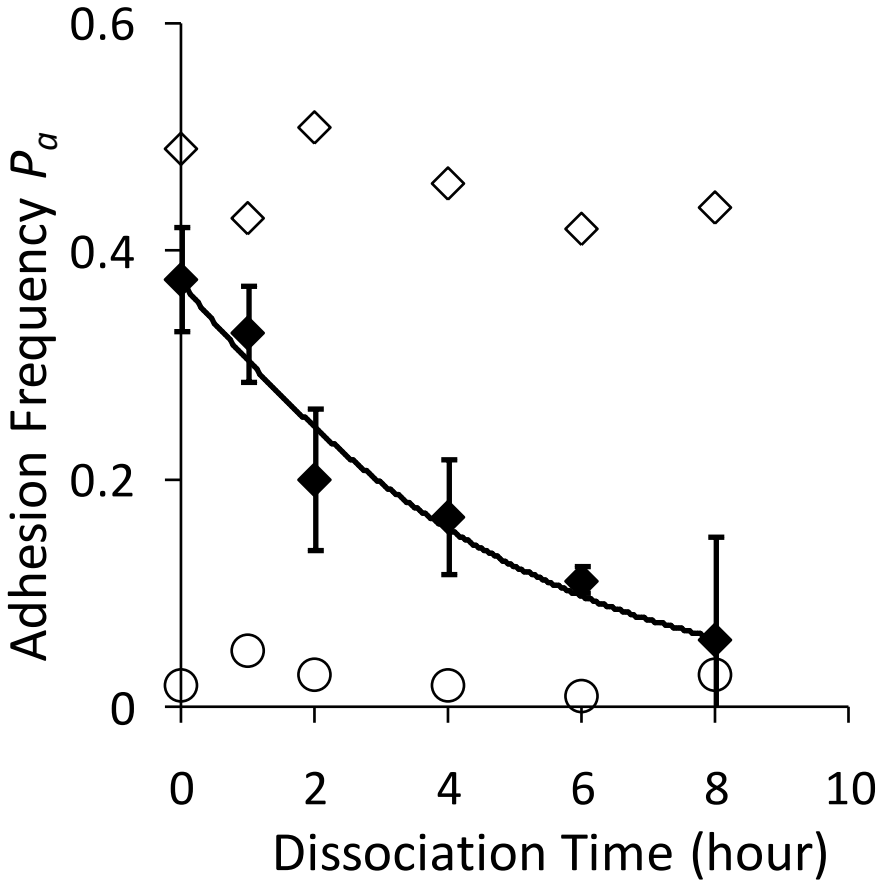

Figure 6-2. The adhesion frequency of open I domain and ICAM-1 with different divalent cation conditions. Cells were washed with HBSS/EDTA and then HBSS-. With the presence of 2mM Ca^{2+}, the adhesion frequency remained constant for 8 hours (◊). After the Ca^{2+} was washed and cells were suspended in HBSS-, the adhesion frequency decreased gradually (♦). Without incubating with Ca^{2+}, the adhesion frequency of open I domain and ICAM-1 was at background level and did not increase for 8 hours (○).

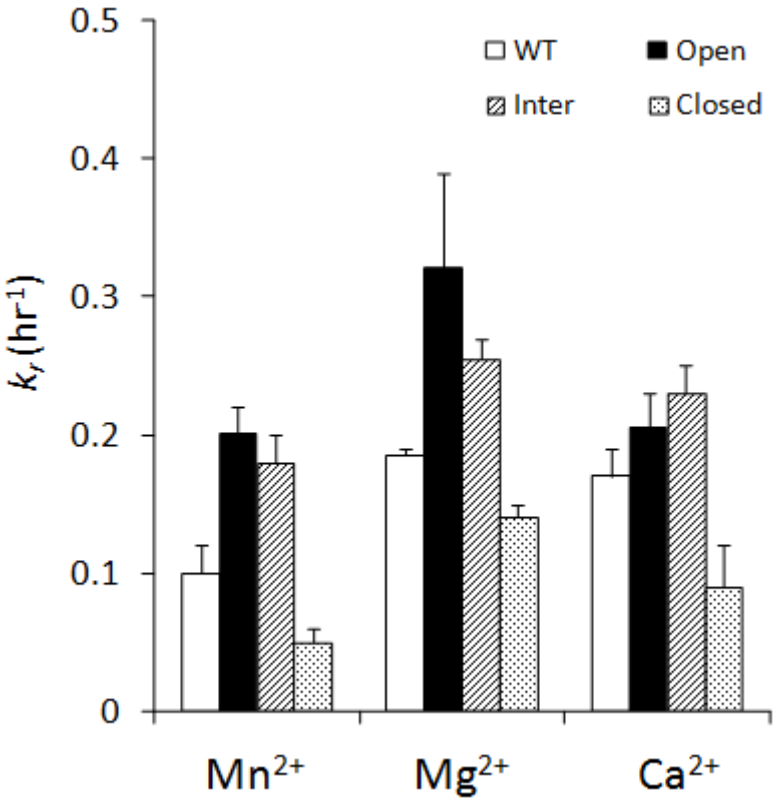

Figure 6-3. The dissociation rates (k_r) of Mn^{2+}, Mg^{2+}, and Ca^{2+} to MIDAS of WT and locked I domains. The values are presented as mean ± s.e.m. of the dissociation rates obtained from two independent experiments. Mn^{2+} dissociates from I domain MIDAS slower compared to Mg^{2+} for all four types of I domains ($P<0.05$). Closed I domain has slower dissociation rate for Mn^{2+}, Mg^{2+}, and Ca^{2+} compared to open and intermediate I domains ($P<0.03$ for Mn^{2+} and Mg^{2+}, $P<0.09$ for Ca^{2+}). The dissociation of Mn^{2+}, Mg^{2+}, and Ca^{2+} from WT I domain is slightly slower than from open and intermediate I domains without statistically significance ($P>0.1$).

6.4 Divalent Cations Dissociate Rapidly from the Metal Ion Binding Sites that are Important for $\alpha_L\beta_2$ Conformational Change

I domain MIDAS is the site directly participating the ligand binding; however, it is other metal ion binding sites in $\alpha_L\beta_2$ play important roles in conformational regulation. The dissociation measurements suggested once I domain MIDAS coordinates with a divalent cation, the divalent cation remains bound for hours. However, this is not the case for other metal ion binding sites, or at least not for those sites that are important for

conformational regulation. When prebound divalent cations were washed away prior to micropipette experiments, WT $\alpha_L\beta_2$ have very low binding affinity to ICAM-1 (Figure 4-4). Adding Mn^{2+} or Mg^{2+} increased the binding affinities of WT $\alpha_L\beta_2$ for hundreds of fold. Therefore, divalent cations must dissociate from those metal ion binding sites critical for inducing conformational change during the wash; otherwise, WT $\alpha_L\beta_2$ would also show high binding affinity even after the divalent cations were washed.

The rapid dissociation of divalent cations to the sites that are important for conformational regulation was further confirmed here. K562 cells expressing open and WT $\alpha_L\beta_2$ were incubated with saturating concentrations of Mn^{2+} (2mM) or Mg^{2+} (5mM) to make sure that the I domain MIDAS is occupied by a divalent cation. After that, the divalent cations were washed away with HBSS- and the adhesion frequency of $\alpha_L\beta_2$ and ICAM-1 were immediately measured in HBSS-. For open $\alpha_L\beta_2$, the adhesion frequency of the first pair of cells after washing decreased a lot compared to the frequency measured in the presence of saturating concentration of divalent cations and remained constant afterwards at a basal level that is several fold lower (Figure 6-4 A, B). The basal level adhesion frequency is comparable to the frequency between $\alpha_L\beta_2$ and ICAM-1 with cells washed with HBSS- only, a condition that $\alpha_L\beta_2$ should be bent (data not shown). This indicates that divalent cations dissociated from those metal ion binding sites that are important for conformational change, most possibly for $\alpha_L\beta_2$ extension, during the wash. The adhesion frequency of WT $\alpha_L\beta_2$ also decreased rapidly to a background level after the washing (Figure 6-4 C, D). The dissociation rates could be obtained by fitting this data using Equation 3-5. However, most of the decreasing phase was missing due to the rapid dissociation, and thus the dissociation rates estimated using this method may not be

accurate. Nevertheless, this observation strongly suggested the rapid dissociation of divalent cations from those sites that are important for conformational change of $\alpha_L\beta_2$.

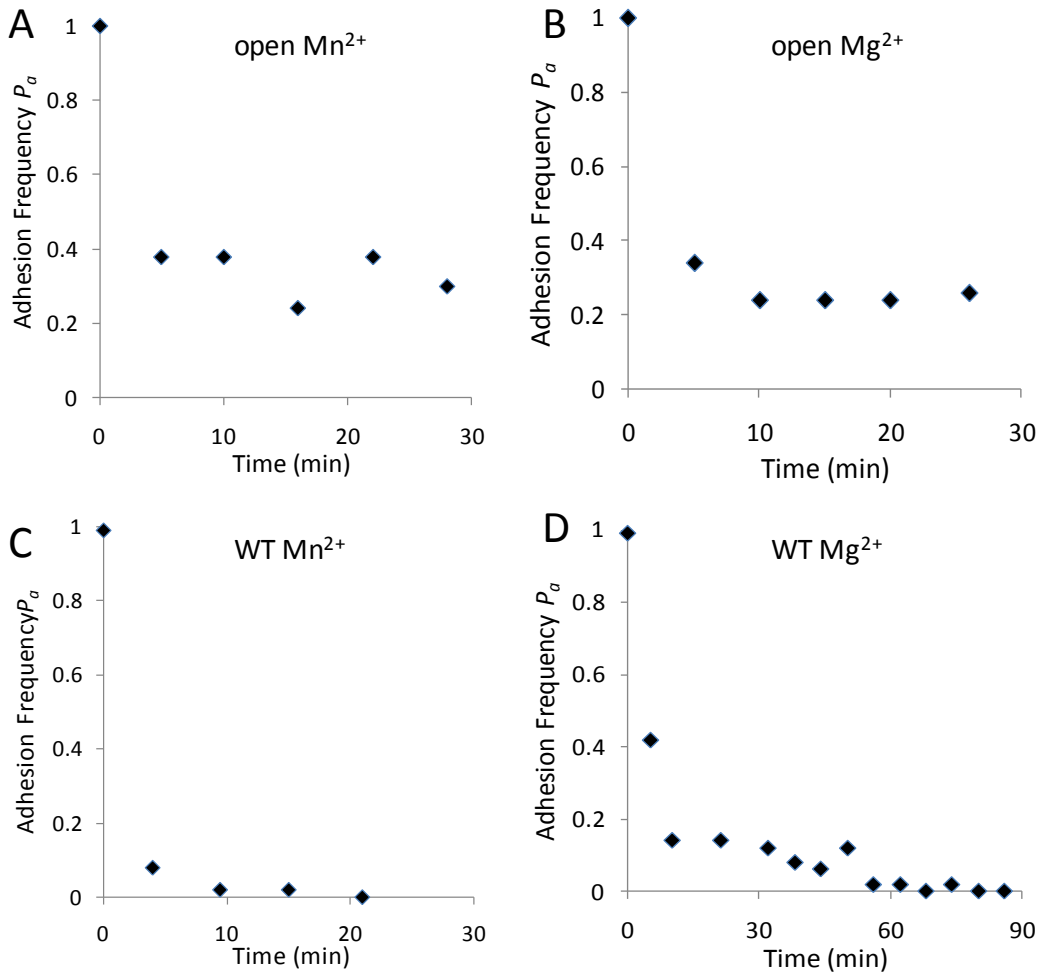

Figure 6-4. The adhesion frequency of open and WT $\alpha_L\beta_2$ after Mn^{2+} and Mg^{2+} were washed away. In the presence of Mn^{2+} and Mg^{2+}, the adhesion frequencies of open and WT $\alpha_L\beta_2$ and ICAM-1 were 100%, showing as the first points at time 0 in all four panels. After Mn^{2+} and Mg^{2+} were washed, the adhesion frequency was measured using micropipette. The adhesion frequencies dropped rapidly to basal or background level and the decreasing phase of the curve could not be obtained.

6.5 Binding Affinities of Divalent Cations to the metal ion binding Sites that are Important for $\alpha_L\beta_2$ Conformational Change

Divalent cations dissociate from I domain MIDAS slowly but dissociate rapidly form those metal ion binding sites that are important for $\alpha_L\beta_2$ conformational regulation. This experimental observation gives rise to a possibility of measuring the binding affinity of divalent cations to those other sites without the influence of I domain MIDAS. After pre-bound divalent cations were washed, cells were incubated with saturating concentration of Mn^{2+} or Mg^{2+} to allow the I domain MIDAS being occupied with a divalent cation. The divalent cations were then washed away so that those other metal ion binding sites of interesting should not be occupied. Cells were resuspended in HBSS-containing known concentrations of Mn^{2+} or Mg^{2+}, and the adhesion frequency between WT, or open $\alpha_L\beta_2$ and ICAM-1 were measured. The binding affinity of Mn^{2+} for those metal ion binding sites was hundred fold higher than that of Mg^{2+} (Figure 6-5). Although the conformation of I domains are different, the binding affinity of Mn^{2+} and Mg^{2+} for those critical metal ion binding sites for conformational change in WT and open $\alpha_L\beta_2$ were comparable (Figure 6-5).

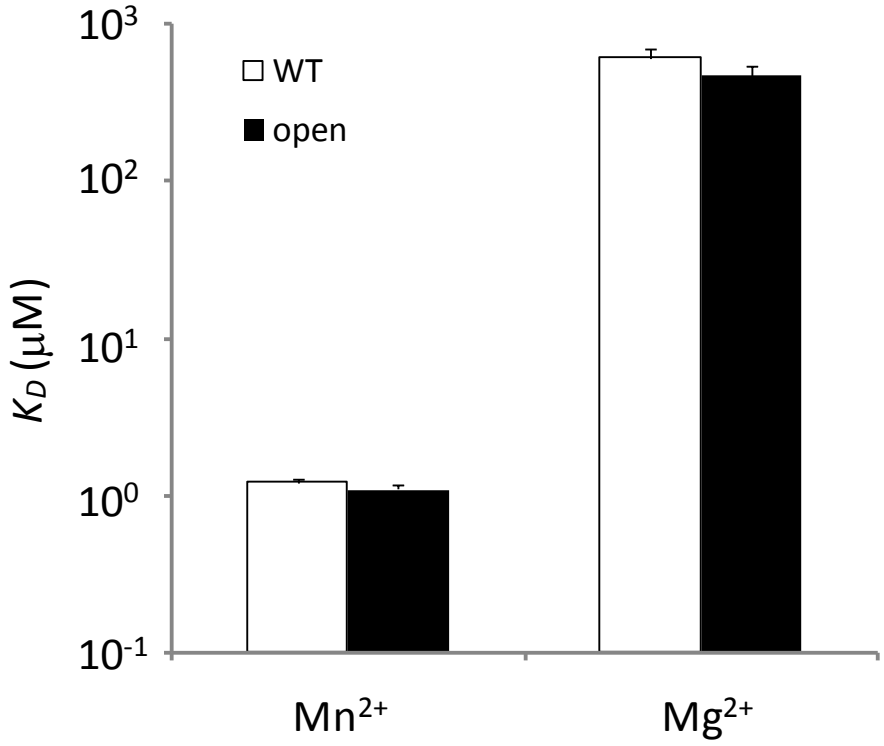

Figure 6-5. The K_D of Mn^{2+} and Mg^{2+} for divalent cation coordination sites important for conformational change of $\alpha_L\beta_2$. The values are presented as mean ± s.e.m. of the K_D obtained from two independent experiments. These sites in WT and open $\alpha_L\beta_2$ have comparable binding affinity for Mn^{2+} (P=0.21) and Mg^{2+} (P=0.23). Mn^{2+} has higher affinity compared to Mg^{2+} ($P \leq 0.01$).

6.6 Discussion

Divalent cation has been recognized as a very important player in integrin regulation for a long time, but the mechanism of regulation is not very clear. Using micropipette adhesion frequency assay, the binding affinity and dissociation rate of Mn^{2+}, Mg^{2+}, or Ca^{2+} for WT or locked I domain MIDAS were measured.

Mn^{2+} binds to I domain MIDAS with higher affinity and the K_D was about several μM. In comparison, the binding affinity of Mg^{2+} to I domain MIDAS was ~ 40 fold

lower, with K_D of tens to hundreds of μM. These results are consistent with previous studies using purified proteins [78, 118].

Ca^{2+} is unique in its binding by exhibiting two affinities for I domain MIDAS, a high binding affinity (μM) and a low binding affinity (mM). It is suggested there are two distinct classes of Ca^{2+} binding sites that differ in their affinity in integrin. An equilibrium dialysis study with purified platelet integrin $\alpha_{IIb}\beta_3$ has provided evidence for one high affinity (μM) and three to four low affinity (mM) Ca^{2+} sites [120]. A similar two site model for Ca^{2+} regulation of purified $\alpha_L\beta_2$ binding to ICAM-1 has also been proposed [78]. However, there is no evidence to show I domain contains more than one divalent cation coordination site. Therefore, the two affinities could not be explained by Ca^{2+} binding to two different sites. Here, the results is interpreted by assuming I domain adapts two different conformational states with the presence of Ca^{2+}. These two states have distinct Ca^{2+} binding affinities and there is an equilibrium between these two conformations. Another possibility is that extra Ca^{2+} was secreted by cells during the experiments. However, using cells washed with HBSS/EDTA and then HBSS-, no specific adhesion was detected even after the cells were put in HBSS- for 8 hours. Thus, the first plateau of the curve could not be due to Ca^{2+} secreted by K562 cells unless the secretion depends on the presence of Ca^{2+}.

Open and intermediate I domains had comparable binding affinities for Mn^{2+} and Mg^{2+}. WT and closed I domains had similar binding affinities for Mn^{2+} and Mg^{2+}, which were lower than those of open and intermediate I domains. Changing of I domain conformation from closed to open I domain increased the binding affinity for Mn^{2+} by ~ 6 fold and for Mg^{2+} by ~ 7 fold, indicating the divalent cation binding is regulated by I

domain conformation. Consistently, activation of α_M I domain increased the binding of Mg^{2+} by ~ 10 fold [119]. The comparability of divalent cation binding affinities of open and intermediate I domains suggests the conformation of MIDAS of these two I domains are very close. Similarly, WT and closed I domain MIDAS should have structures resemble each other. Similar results were found in α_M I domain. Mg^{2+} and Ca^{2+} were shown to have equivalent affinities to inactive α_M I domain [119]. Activation of the I domain induced a ~10-fold increase in the binding affinity of Mg^{2+} to α_M I domain with no change in that of Ca^{2+}. Previous studies measured the binding of divalent cations to I domain directly, meaning that the divalent cation is the ligand for I domain in these binding studies [118, 119, 121]. However, the ligand for I domain in this study is ICAM-1 and the binding of divalent cations to I domain was measured indirectly using ICAM-1 binding as an indicator. An important assumption for this experiment is that the conformation of I domain MIDAS would not be changed by the binding of ICAM-1, especially for the WT I domain; otherwise, the measured binding affinity of divalent cations is not the affinity for WT I domain MIDAS anymore. Using NMR, Huth *et al.* showed that the presence of ICAM-1 actually induced changes in the chemical shifts of two clusters of residues in I domain, one is in the MIDAS site and the other one is in the C-terminal α7 helix, indicating the ICAM-1 binding can change the conformation of I domain [121]. However, the fact that the binding affinities of divalent cations for WT I domain is comparable to their binding affinities for closed I domain suggested this is not the case for this study. Furthermore, the ICAM-1 binding affinity of the WT I domain is similar to that of the closed I domain [53].

A surprising finding of this study is the slow dissociation of divalent cations from I domain MIDAS. Mn^{2+}, Mg^{2+} and Ca^{2+} all bind to I domain MIDAS with half lives of hours. However, these divalent cations were shown to have fast dissociation rates for other metalloproteins with half lives from sub seconds to tens of seconds [122-124]. With the measured binding affinities and dissociation rates, the association rates are less than $2.5x10^3$ $M^{-1}s^{-1}$, which is very small compare to normal range of metal ion association rates, 10^{5-7} $M^{-1}s^{-1}$ [125]. An explanation for the abnormal association rate could be some unknown mechanisms to prevent the dissociation of divalent cation after it binds I domain MIDAS, such as structure rearrangement of the coordination site. If this is the case, the association rate is not simply the product of binding affinity and dissociation rate.

Mn^{2+} and Mg^{2+} increased the 2D binding affinity of WT $\alpha_L\beta_2$ by hundreds of fold, but only increased the binding affinity of isolated WT I domain by several fold. This suggests that the binding of Mg^{2+} or Mn^{2+} to MIDAS does not induce conformational change of I domain significantly enough to affect ligand binding affinity. Therefore, Mg^{2+} or Mn^{2+}must bind to other metal ion binding sites on $\alpha_L\beta_2$ in order to induce the conformation change and subsequently increase the ligand binding affinity. With I domain occupied with divalent cation, adding (removing) divalent cations from $\alpha_L\beta_2$ increased (decreased) the adhesion frequency. The increase/decrease in adhesion frequency should be due to conformational change induced by the association/dissociation of divalent cations to those sites that are critical for $\alpha_L\beta_2$ conformational regulation. Thus, the binding affinity and kinetics measured should be the binding parameters of divalent cations for those sites. When I domain was occupied with

a divalent cation, open $\alpha_L\beta_2$ was able to mediate specific adhesion with ICAM-1 without the addition of Mn^{2+} or Mg^{2+}. This basal frequency is several fold lower than the frequency with saturating concentration of Mn^{2+} or Mg^{2+}, indicating the binding of divalent cations induced the extension of $\alpha_L\beta_2$. The binding affinities of Mn^{2+} and Mg^{2+} for those other sites are comparable for WT and open $\alpha_L\beta_2$. Mn^{2+} has higher affinity (K_D of ~ 1 μM) compared to Mg^{2+} (K_D of ~ 400 μM). The stronger activation of $\alpha_L\beta_2$ by Mn^{2+} than Mg^{2+} could be explained by the higher affinity of Mn^{2+} for those metal ion binding sites. Indeed, Mn^{2+} induced extension of a larger number of $\alpha_L\beta_2$ than Mg^{2+} (data not shown). Taken together, these results strongly suggest that the importance of the divalent cation binding affinity in $\alpha_L\beta_2$ conformational regulation.

In strong contrast to I domain MIDAS, Mn^{2+} and Mg^{2+} much faster dissociate from those metal ion binding sites important for $\alpha_L\beta_2$ conformational change. Using the experiment method in this study, the initial phase of dissociation could not be accessed and as a result, the dissociation rate would not be accurate. Even so, the results clearly showed the dramatic difference in the dissociation rates of divalent cations for I domain MIDAS and for other metal ion binding sites. Therefore, different metal ion binding sites have their own characteristics regarding divalent cation binding affinity and kinetics, which may be an important mechanism for the regulation of $\alpha_L\beta_2$ by divalent cations.

CHAPTER 7

UPREGULATION OF β2 INTEGRIN AFFINITY BY ENGAGEMENT OF E-SELECTIN LIGANDS ON NEUTROPHIL

7.1 Introduction

During inflammation, neutrophils are recruited to infected or injured tissue sites and migrate across the blood vessel wall. The capture and recruitment of neutrophils is mediated by multiple cell surface adhesion molecules, most importantly selectins and integrins. Neutrophils are captured from blood stream and roll on the blood vessel wall through binding to endothelial cell selectins [126, 127]. When injured tissue releases chemokines, endothelial cells respond with upregulated E-selectin and P-selectin expression. These selectins bind to their ligands on neutrophils, including PSGL-1, with rapid binding kinetics [128, 129].

During rolling, neutrophil β_2 integrins become activated by chemokines and mediate firm adhesion of neutrophils to endothelial cells [130, 131]. It is suggested other signaling pathways could also induce the activation of β_2 integrins during the rolling. E-selectin engagement is proposed to be one of them [23, 132]. When neutrophils are rolling on substrate coated with E-selectin and ICAM-1 together, they roll first and then become arrested on the substrate; while E-selectin along only mediates cell rolling, and cells do not roll or arrest on ICAM-1 substrate [132, 133]. Using neutrophils in whole blood instead of isolated neutrophils, studies showed increased number of rolling cells without firm adherent cells and decreased rolling velocity when ICAM-1 was co-immobilized with E-selectin [23]. The activation of β_2 integrins by E-selectin binding

was blocked by MAPK inhibitors, indicating that this activating signaling pathway is different from and independent of the chemokine activation pathway, which involves G-proteins and protein kinase-C (PKC) [21, 23, 132-135].

E-selectin could engage multiple ligands on neutrophils. The signaling molecules for β_2 integrin activation by E-selectin binding have not yet been identified, although some candidates have been proposed. Upon cross-linking with mAbs, both PSGL-1 and L-selectin have been shown to trigger several important signaling events, including activation of MAPK signaling pathways [136-138]. Previously, it is suggested that both PSGL-1 and L-selectin play roles in the activation of β_2 integrin activation and there might be other unknown ligands for E-selectin on neutrophil to transduce signaling and activate β_2 integrins [132]. However, a recent study identified PSGL-1 as the main ligand for E-selectin binding and signaling molecules for subsequent β_2 integrin activation [139].

Although the activation of β_2 integrin by E-selectin binding has been demonstrated by previous studies, there are still important aspects remaining unsolved. Previous results were obtained using flow chamber technique or cell aggregation analysis, which have poor temporal resolution for the activation events. It is reported that after cross-linking of L-selectin, the phosphorylation of tyrosine peaks within 1 minute, which is a time frame that required for the activation and clustering of β_2 integrins. Moreover, neutrophil β_2 integrins shifted to activating state and formed clustering within seconds of E-selectin binding [21]. Therefore, the time of signaling transduction and conformational transition could be very short. However, there is so far no accurate

estimate of the timescale of β_2 integrin activation by the engagement of E-selectin ligands on neutrophils.

In the present study, the activation of neutrophil β_2 integrins by E-selectin engagement is investigated using micropipette adhesion frequency assay. The results showed that when neutrophils were in contact with RBCs coated with both E-selectin and ICAM-1, β_2 integrins were activated by the E-selectin binding. When the contact duration of the two cells was shorter than 5 seconds, the adhesion was mainly mediated by E-selectin and the adhesion frequency reached equilibrium at around 1 second; however, when the contact duration was longer than 5 seconds, a graduate increase in adhesion frequency rather than a plateau in the binding curve was observed, exhibiting a two-step binding curve phenomenon. Therefore, the two cells need to be kept in contact for at least 5 seconds before the signaling can be initiated by E-selectin binding and transduced to β_2 integrins. The results also indicate that the accumulation of E-selectin binding is required to induce the activating signaling.

7.2 2D Binding Kinetics of E-selectin to Neutrophils

To understand the characteristics of E-selectin binding to its ligands on neutrophils, the 2D binding affinity and kinetics were measured using micropipette adhesion frequency assay (Figure 7-1). Human E-selectin Ig chimera was captured onto RBC surface by a biotinylated capture antibody coated through biotin-steptavidin reaction. The adhesion detected was specific between E-selectin and its ligands, because the adhesion frequency is at background level when using RBCs with capture antibody but no E-selectin (Figure 7-1). Moreover, the adhesion was abolished after Ca^{2+} was

stripped with 5mM EDTA (Figure 7-1). E-selectin binds to neutrophils with a fast off-rate of 5.68±1.03 s^{-1}.

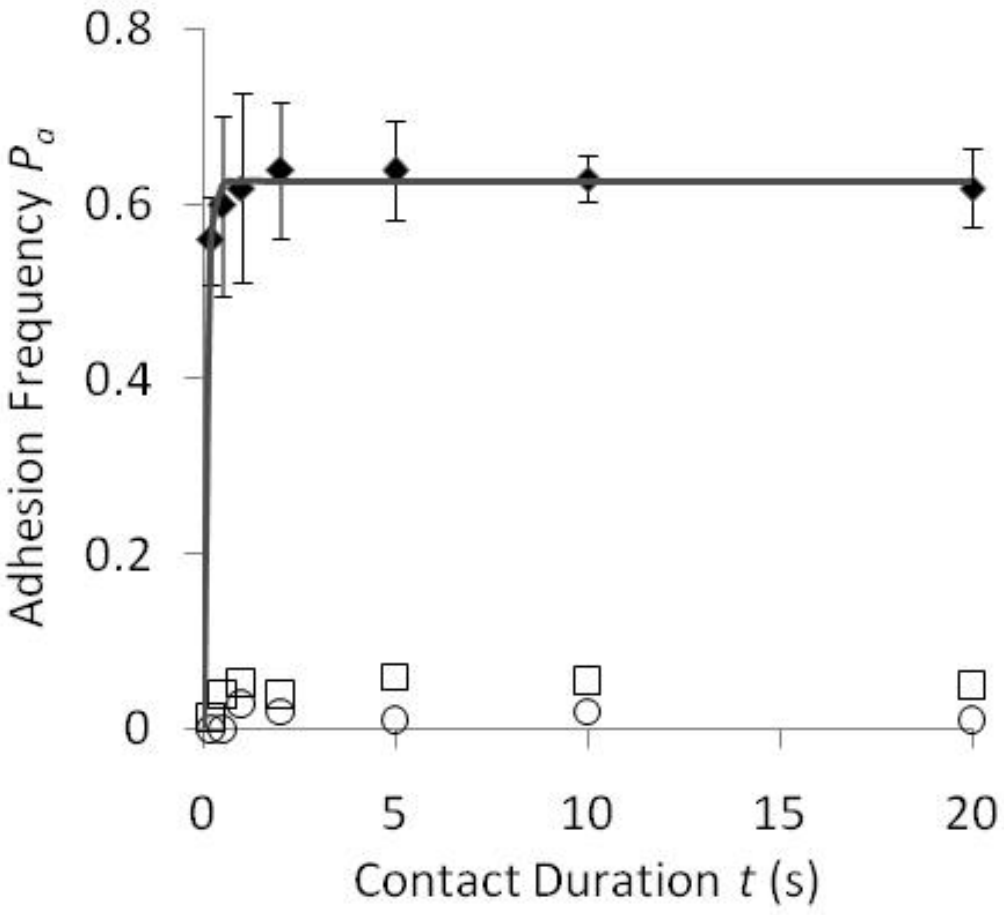

Figure 7-1. Binding of neutrophils with RBCs coated with E-selectin Ig chimera alone. The adhesion frequency quickly reached equilibrium at ~ 1 second and resulted in fast binding kinetics for E-selectin and its ligands (♦, solid curve). The binding between neutrophils and RBCs coated with capture antibody but without E-selectin is at background level (□). The addition of 5mM EDTA abolishes the binding between E-selectin and its ligands on neutrophils (○).

7.3 Binding of E-selectin Activates β_2 Integrins on Neutrophils

In order to investigate the activation of β_2 integrins by E-selectin binding, E-selectin Ig chimera and ICAM-1 Ig chimera were both coated onto RBCs (E-selectin/ICAM-1 RBCs). The binding frequency reached equilibrium at 1 second and stayed at the equilibrium level till ~ 5 seconds. At contact duration of 5 seconds, the binding frequency started to increase gradually and reached a second equilibrium at contact duration of ~ 10 seconds (Figure 7-2). Thus, the adhesion frequency vs. contact duration binding curve appears to be a two-step curve with two plateaus. Blocking E-selectin with ES-1 Fab totally abolished the binding of both steps (Figure 7-2). Treating the first step binding as a complete binding curve, the binding kinetics and affinity could be extracted. The binding kinetics and affinity of the first step binding were comparable to those of E-selectin-ligand interaction (Figure 7-3). Therefore, the first step binding is mediated by E-selectin and its ligands.

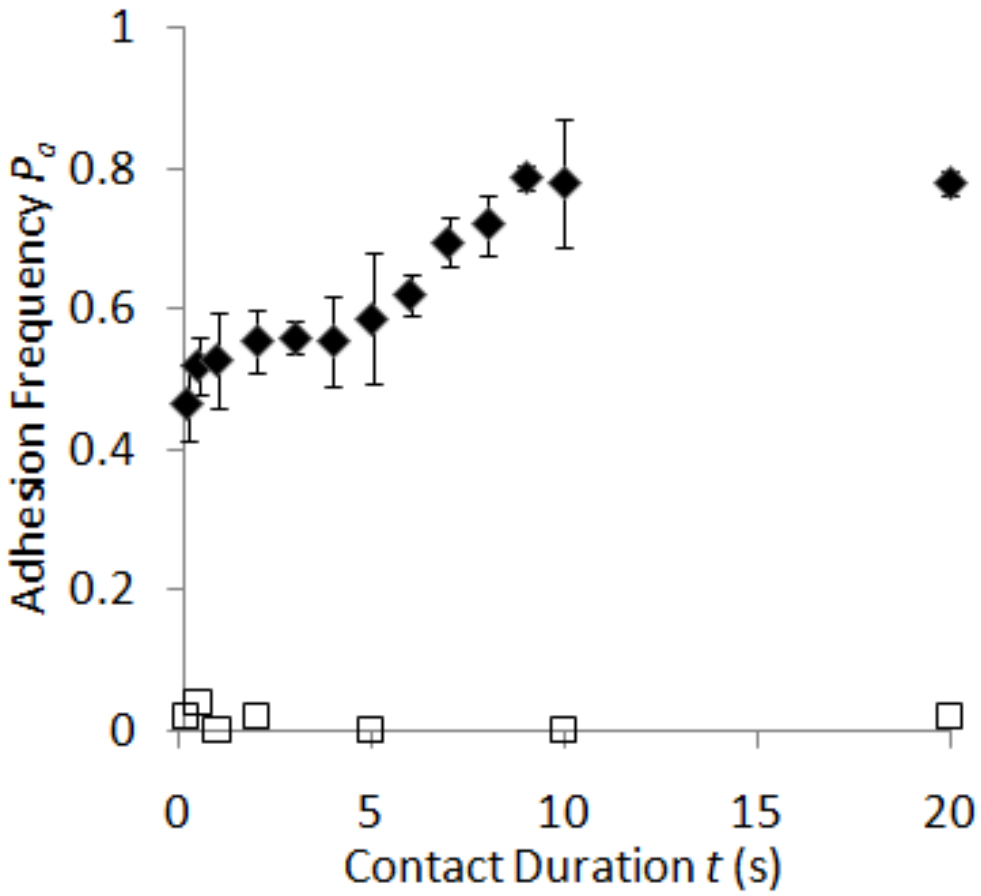

Figure 7-2. Two-step binding curve of E-selectin/ICAM-1 RBCs to Neutrophils. Four curves generated by using E-selectin/ICAM-1 RBCs all showed two-step binding phenomenon and one of them is shown in the figure. The binding of E-selectin to neutrophils activated β_2 integrins and resulted in an increase of the adhesion frequency at around 5 seconds (♦).The binding of both steps were totally blocked by an E-selectin blocking antibody ES-1 (□).

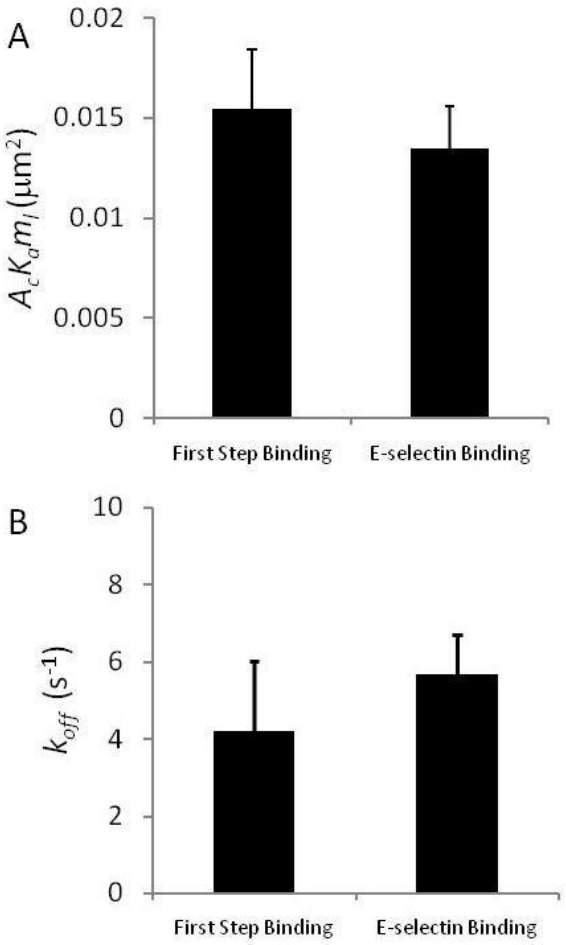

Figure 7-3. The binding parameters of the first step of two-step binding curve are compared to those of E-selectin binding to neutrophils. Because it is not clear which ligand(s) are responsible for E-selectin binding and signaling in this study, the site density of ligand (m_l) is also lumped together with A_cK_a as one parameter $A_cK_am_l$ (A). The off-rates are also compared (B). The data were presented as mean ± s.e.m. of three different binding curves. The parameters extracted from the first step binding of the two-step curve and E-selectin binding curve were very similar to each other.

The increase of adhesion frequency in the second step is contributed by β_2 integrin-ICAM-1 adhesion. When β_2 integrins were blocked with a β_2 subunit blocking antibody, 7E4, the second step of the binding curve no longer existed (Figure 7-4). Furthermore, using RBCs coated with E-selectin alone, the binding curve was a typical 2^{nd} order binding curve with only one plateau (Figure 7-1). The activation of β_2 integrins

requires the presence of E-selectin. Using RBCs with ICAM-1 alone on the surface with similar site density of ICAM-1 on the E-selectin/ICAM-1 RBCs, the adhesion frequency was at background level, indicating without activation, β_2 integrins are not able to support binding to ICAM-1 at the given site density (Figure 7-5). Adding of 2mM Mg^{2+}/EGTA was able to activate β_2 integrins and increase the adhesion frequency to ~ 0.3 (Figure 7-5).

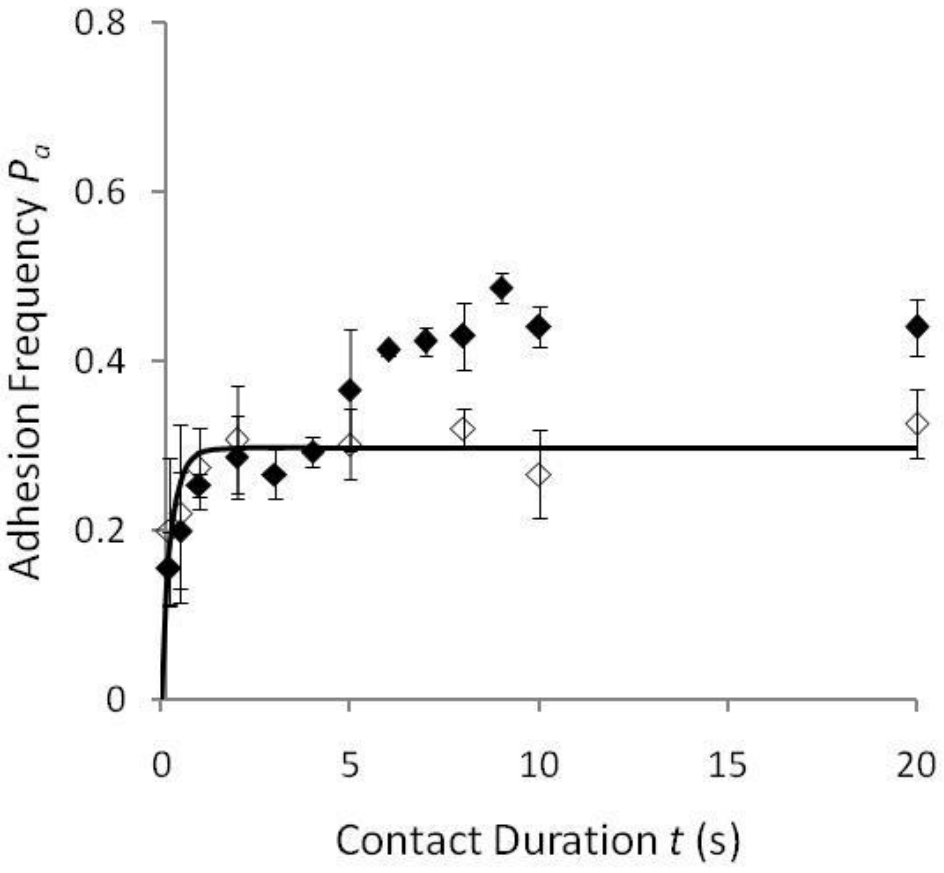

Figure 7-4. The binding of neutrophils to E-selectin/ICAM-1 RBCs with (◊) or without (♦) β_2 integrin blocking mAb 7E4. In order to show the effect of blocking more clearly, the data with antibody blocking was fitted to Equation 2-4. This binding curve showed only one plateau without a second step.

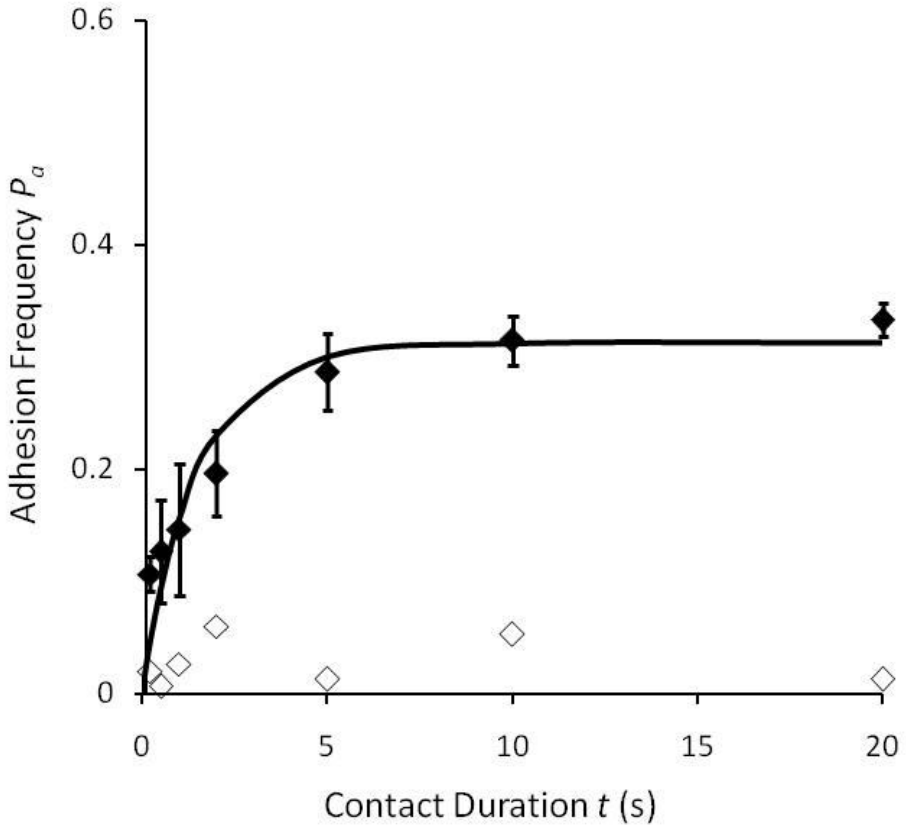

Figure 7-5. Binding of neutrophils to RBCs coated with ICAM-1 Ig chimera alone. With the coated site density of 11 molecules/μm^2, the adhesion frequency is at background level (◊). However, the addition of 2mM Mg^{2+}/EGTA activated β_2 integrins and increased the adhesion frequency (♦).

The activation of β_2 integrins by E-selectin binding is further confirmed by using E-selectin in solution instead of coated on RBC surface. ICAM-1 was coated on RBCs at a site density that is low enough, so that there is no adhesion when β_2 integrins are inactive (Figure 7-6). After the neutrophils and ICAM-1 coated RBCs were added to the chamber, E-selectin Ig chimera was added at a concentration of 10 μg/ml and the adhesion between neutrophils and RBCs was measured immediately after the E-selectin Ig chimera was added. The adhesion between the first pair of cell was very low, indicating it takes some time for E-selectin Ig in solution to bind to its ligands. After

about 5 minutes, the adhesion frequency had an obvious increase (data not shown) and the average frequency was ~ 0.4 and ~ 2 fold lower than the adhesion frequency when 2mM Mg^{2+}/EGTA was in presence. In contrast, monomeric E-selectin failed to activate β_2 integrins and to increase the adhesion frequency with same condition (Figure 7-6). Furthermore, nonspecific human IgG was not able to increase the adhesion frequency as well, indicating that the activation of β_2 integrins was induced by E-selectin but not by the human IgG Fc portion in the Ig chimera (Figure 7-6).

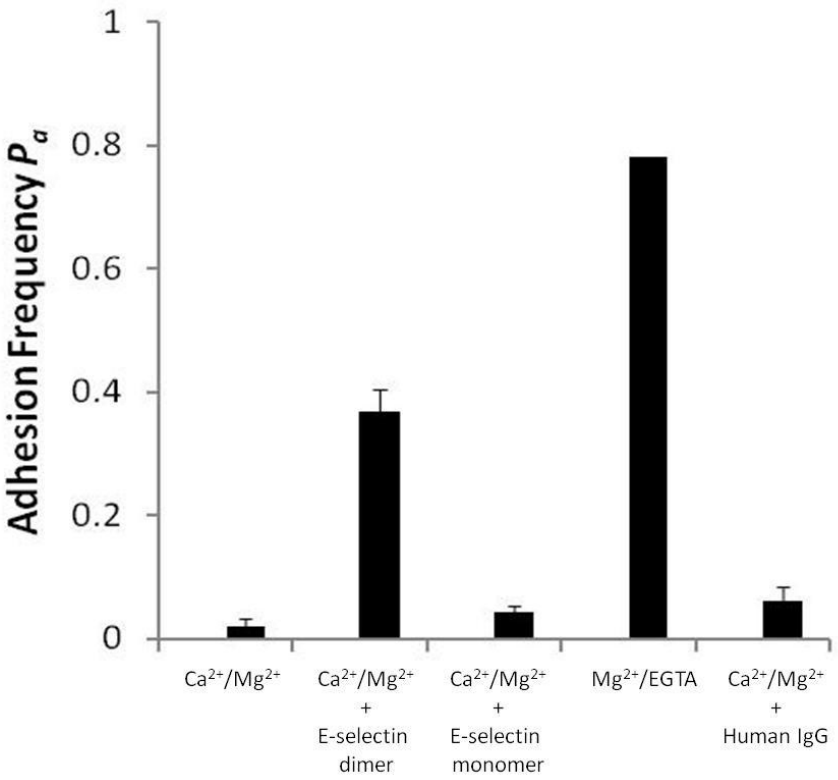

Figure 7-6. The binding of neutrophil β_2 integrins to RBCs coated with ICAM-1 Ig chimera was activated in the presence of 10 μg/ml E-selectin Ig chimera or replacing Ca^{2+}/Mg^{2+} with Mg^{2+}/EGTA. β_2 integrins were not activated by the presence of monomeric E-selectin or the activation is far weaker than that of E-selectin Ig chimera. The activation of β_2 integrins by E-selectin Ig chimera is not due to the human IgG Fc portion, because a nonspecific human IgG did not increase the adhesion frequency.

7.4 Binding Affinity of β_2 Integrins Activated by E-Selectin Binding is at Intermediate Level

Different two-step curves were obtained with RBCs with various site densities of E-selectin and ICAM-1. It is not known how the availability of E-selectin in the contact area affects the activation and ligand binding affinity of β_2 integrins. One possibility is that the larger the E-selectin site density, the stronger the activation signaling and therefore the higher the binding affinity of β_2 integrins. It is also possible that there is a threshold for activation signaling, once the threshold is reached, the ligand binding affinity of β_2 integrins remain the same no matter how high the site density of E-selectin reaches. The binding affinity of activated β_2 integrins could be calculated from the two-step binding curves. Assuming E-selectin binding and β_2 integrin binding do not cooperate with each other after β_2 integrins are activated, the equilibrium adhesion frequency of β_2 integrins and ICAM-1 can be obtained by subtracting the equilibrium adhesion frequency of the 1st step from the 2nd step, and the binding affinity (A_cK_a) can be calculated.

In order to study the relationship between E-selectin site density and ligand binding affinity of activated β_2 integrins, the equilibrium adhesion frequency of the 1st and 2nd steps are measured using RBCs coated with E-selectin and ICAM-1 at different site densities. The contact durations were chosen to be 3 seconds and 15 seconds, at which the binding curve reaches 1st and 2nd equilibrium respectively. The total site density of β_2 integrins on neutrophil is ~ 100 molecules/μm^2, but the accurate site density (m_r) is difficult to be determined for these experiments, because it is not clear whether all or a fraction of β_2 integrins are activated by E-selectin binding. Therefore, $A_cK_am_r$ is used

as a parameter to indicate the binding strength of activated β_2 integrins to ICAM-1. The plotted $A_cK_am_r$ of β_2 integrins vs. E-selectin site density appeared to be a saturation curve (Figure 7-7). $A_cK_am_r$ of β_2 integrins increased as E-selectin site density increased up to ~ 12 molecules/μm^2, and then reached an equilibrium of ~ 0.01 μm^2 (Figure 7-7).

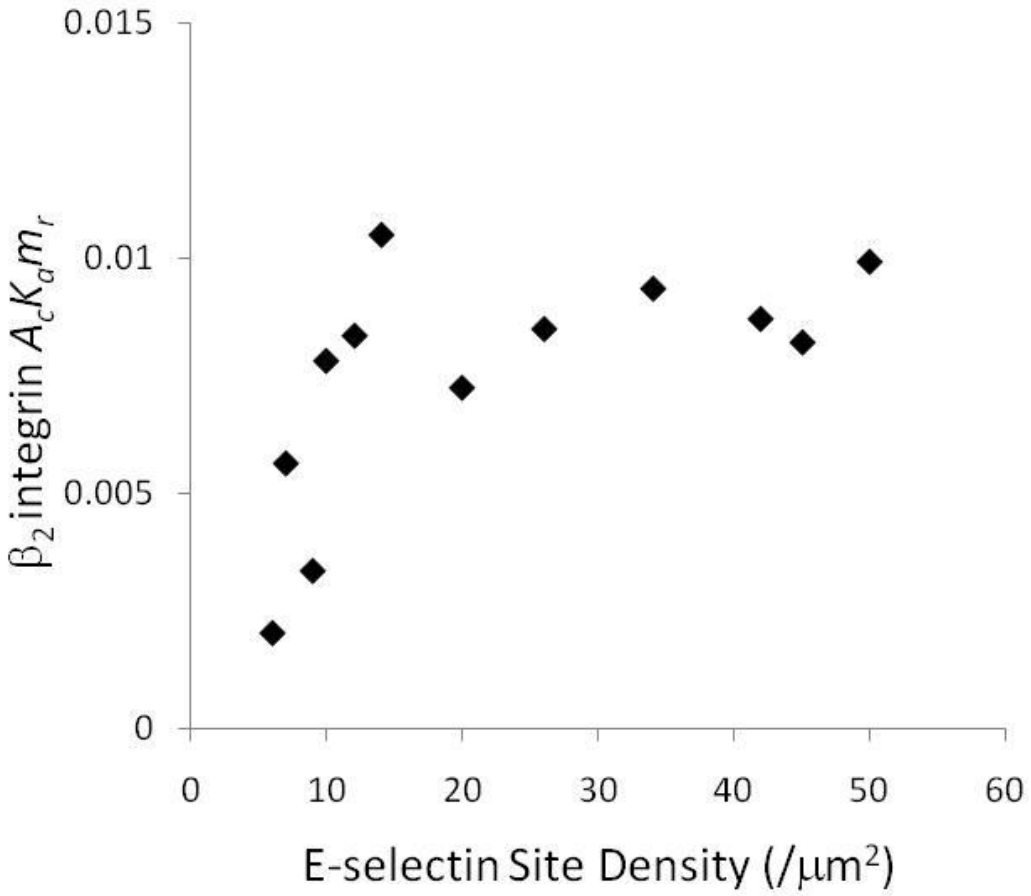

Figure 7-7. $A_cK_am_r$ of β_2 integrins vs. E-selectin site density curve appears to be a typical saturation curve. $A_cK_am_r$ of β_2 integrins initially increased as E-selectin site density increased and reached equilibrium when E-selectin site density was ~ 12 molecules/μm^2.

Depending on the stimulation, activated β_2 integrins could adapt different conformations with distinct ligand binding kinetics and affinities. To understand the

characteristics of the β_2 integrins activated by E-selectin binding, $A_cK_am_r$ of the β_2 integrins activated by E-selectin binding was compared to that of the β_2 integrins activated by Mg^{2+}/EGTA and Mn^{2+}. The $A_cK_am_r$ of β_2 integrins activated by binding of E-selectin Ig chimera coated on RBCs and in solution were comparable, and they were ~ 3 fold lower than that of the β_2 integrins activated by Mg^{2+}/EGTA and ~ 7 fold lower than that of the β_2 integrins activated by Mn^{2+}, indicating β_2 integrins activated by E-selectin are at a conformational state with its ligand binding affinity could be further increased (Figure 7-8).

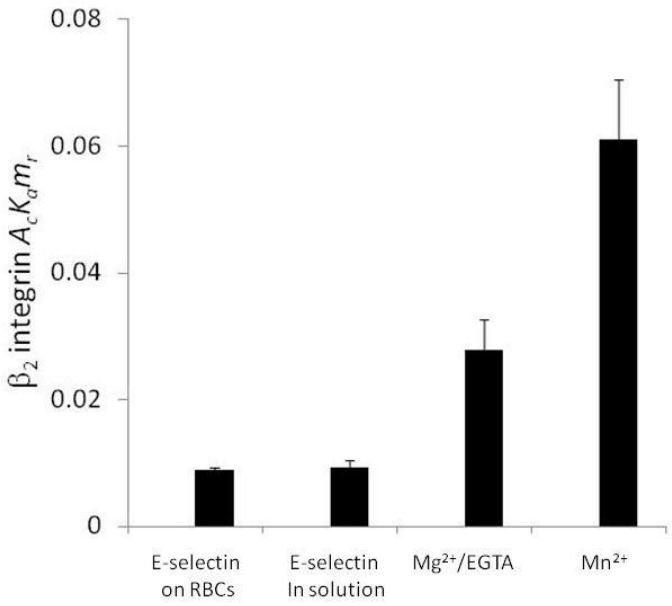

Figure 7-8. $A_cK_am_r$ of β_2 integrins activated by E-selectin Ig chimera binding, Mg^{2+}/EGTA, and Mn^{2+}. The $A_cK_am_r$ of β_2 integrins activated by E-selectin coated on RBCs were obtained from averaging the $A_cK_am_r$ values in the curve of Figure 7-7 with E-selectin site density at 12 molecules/μm^2 and higher.

7.5 P-selectin and L-selectin Binding did not Activate Neutrophil β_2 Integrins

Because P-selectin and L-selectin also bind to PSGL-1, one of the most important E-selectin ligands on neutrophils, it is possible that their binding could activate β_2 integrins as well. In order to test whether the ability to activate β_2 integrins is unique for E-selectin or universal for all three selectins, P-selectin or L-selectin Ig chimera was coated onto RBCs together with ICAM-1 Ig chimera, and the adhesion between the coated RBCs and neutrophils was measured.

The binding of neutrophils to RBCs coated with P-selectin alone or with both P-selectin and ICAM-1 showed no difference (Figure 7-9A). They were all typical 2^{nd} order binding curves with one plateau. The binding kinetics and affinities of the curves with both P-selectin and ICAM-1 on RBCs were comparable to that of the P-selectin alone (Figure 7-9B&C). Similarly, coating L-selectin together with ICAM-1 on RBCs was not able to activate β_2 integrins either (Figure 7-10A). The binding kinetics and affinities of the curves with both L-selectin and ICAM-1 on RBCs were comparable to that of the cruves with L-selectin alone on RBCs (Figure 7-10B&C). Therefore, P-selectin and L-selectin binding to neutrophils were not able to induce β_2 integrin activation, at least not to the same extend as the activation induced by E-selectin binding.

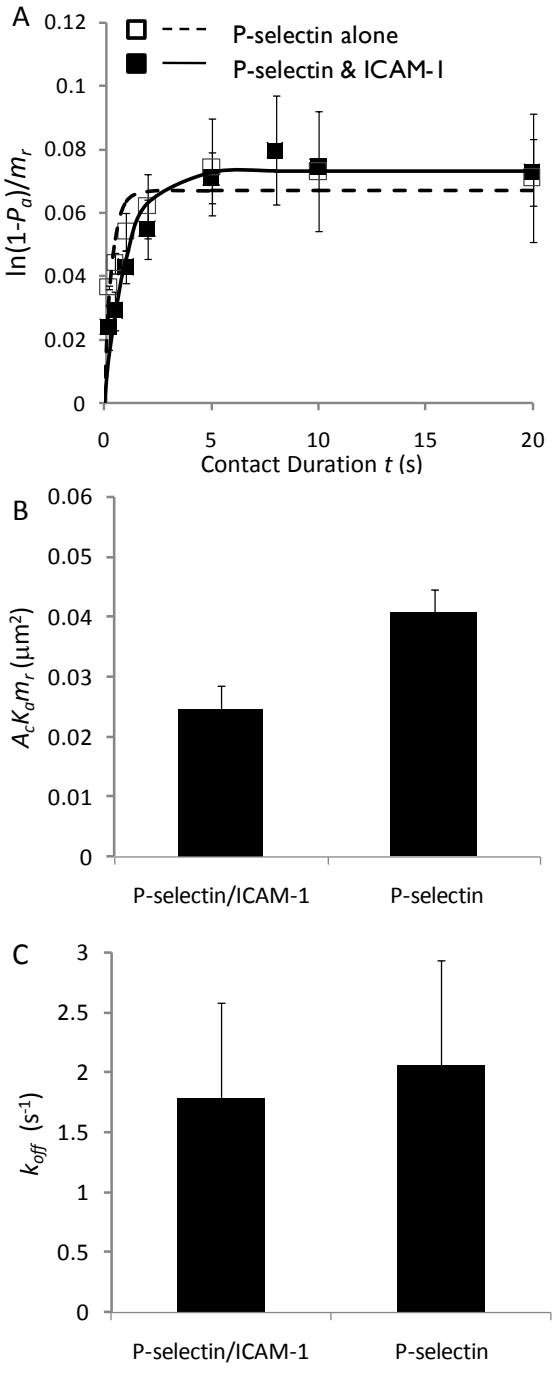

Figure 7-9. P-selectin binding is not able to activate β_2 integrins with current experimental setting. The binding curves of neutrophils to RBCs coated with P-selectin/ICAM-1 (■ and solid curve) or with P-selectin alone (□ and dashed curve) are shown with the adhesion frequency normalized by site density of P-selectin (A). Both of them only had one plateau and without second step. Binding parameters, $A_cK_am_l$ (B) and k_{off} (C), for neutrophils to RBCs coated with P-selectin/ICAM-1 or P-selectin alone were comparable. The data are shown as mean±s.e.m. of binding parameters of 2-3 binding curves.

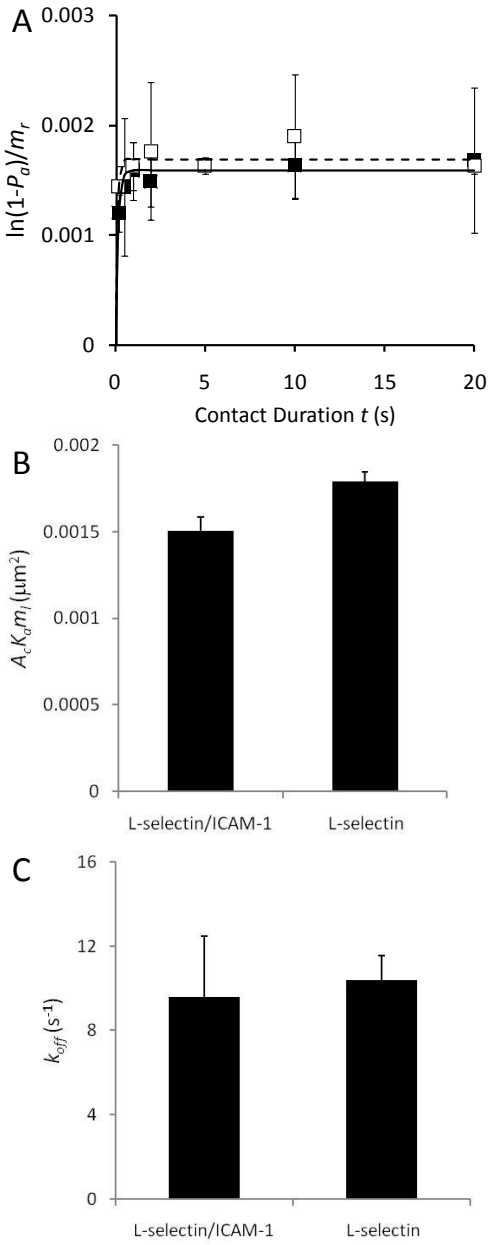

Figure 7-10. L-selectin binding is not able to activate β_2 integrins with current experimental setting. The binding curves of neutrophils to RBCs coated with L-selectin/ICAM-1 (■ and solid curve) or with L-selectin alone (□ and dashed curve) are shown with the adhesion frequency normalized by site density of L-selectin (A). Both of them only had one plateau and with no second step. Binding parameters, $A_c K_a m_l$ (B) and k_{off} (C), for neutrophils to RBCs coated with L-selectin/ICAM-1 or L-selectin alone were comparable. The data are shown as mean±s.e.m. of binding parameters of 2-3 binding curves.

7.6 Discussion

For the recruitment and migration of neutrophils during inflammation, β_2 integrins need to be activated in order to mediate firm adhesion. Recently, it is suggested E-selectin may play more roles than just an adhesion molecule for mediating neutrophil rolling, it might also trigger a signaling to activate β_2 integrins [21, 23, 132]. In the present study, the activation of β_2 integrins by E-selectin binding to neutrophils is investigated using micropipette adhesion frequency assay. The results showed β_2 integrins are activated by the engagement of E-selectin ligands on neutrophils to a state with intermediated level ligand binding affinity. It takes about 5 seconds for the activation to take place. Among the three selectins, E-selectin is the only one being able to activate β_2 integrins; P- and L-selectins failed to induce the activation of β_2 integrins with current experimental conditions. Moreover, the activation of β_2 integrins seems to require crosslinking of E-selectin ligands on neutrophils.

This is the first estimation of the timescale for E-selectin binding to activate β_2 integrins on neutrophils. The results showed that after the two cell membranes were in contact for 5 seconds or longer, β_2 integrins were activated to bind its ligand with higher affinity. Depending on the site densities of E-selectin, the first step binding reached equilibrium at adhesion frequency of 0.3-0.6. With an off-rate of ~ 5.7 s^{-1}, the cellular on-rate was estimated to be 2.0-5.2 s^{-1}. That means during the contact duration of 5 seconds, E-selectin should be able to form bonds with its ligands for 10-26 times on average and each bond needs to wait averagely for 0.19-0.5 second to form. The average lifetime of E-selectin bond is ~0.18 second. It is possible that the engagement of E-selectin ligands is not continuous and the effect of E-selectin ligand engagement accumulates over time

until it is strong enough to trigger the activation of β_2 integrins. If the contact duration is not long enough for the signaling to build up, β_2 integrins could not be activated. The observation that the second step binding initiated at ~ 5 seconds and reached equilibrium at ~ 10 seconds indicated that a latent time is required for β_2 integrins to be activated. This latent time, 5 seconds in this experiment, might be the minimum length of time for activation events to take place, including E-selectin binding, initiating of the signaling, transduction of signaling to β_2 integrins, and conversion of β_2 integrins into a state with higher ligand binding affinity. In the binding curve, the increase of the 2nd step is gradual. This might be due to the increased number of activated β_2 integrins for the signaling strength is further increased with a longer contact duration. It is also possible that the signaling strength reaches a threshold and does not increase with futher E-selectin ligands engagement. If this is the case, the gradual increase of the 2nd step should be the transient phase of the binding curve for activated β_2 integrins and ICAM-1.

In the present study, ligand binding ability ($A_cK_am_r$) of activated β_2 integrins increases as E-selectin site density increases up to 12 molecules/μm^2 and then leveled off. More E-selectin in the contact area may increase the chance of E-selectin engagement, and therefore increase the activating signaling; but once the signaling reaches its maximum strength, further increased E-selectin site density has no effect any more. The equilibrium $A_cK_am_r$ of β_2 integrins activated by E-selectin binding is ~ 3 folds lower than that of the β_2 integrins activated by Mg^{2+} and ~ 7 fold lower than that of the β_2 integrins activated by Mn^{2+}. The difference in $A_cK_am_r$ might be due to the numbers of β_2 integrins activated by E-selectin binding, Mg^{2+}, and Mn^{2+} are different, which results in different m_r. It is also possible that the binding affinities (K_a) of β_2 integrins activated in different

ways are not the same. Or, both of them could be different. Nevertheless, these results indicated that E-selectin binding could not fully activate β_2 integrins. Experimental evidences suggested that the increased adhesion of β_2 integrins to ICAM-1 after E-selectin binding could be due to clustering or conformational change of β_2 integrins. Binding of E-selectin induced coclustering of L-selectin and PSGL-1, and subsequent clustering of β_2 integrins [21]. The conformational change of β_2 integrins is also be very important. It is reported that E-selectin binding activated $\alpha_L\beta_2$ to an intermediate state, i.e., an extended conformation with a closed I domain [139]. Extended $\alpha_L\beta_2$ supports cell rolling when I domain is closed and mediates firm adhesion when I domain is open [12, 112]. Therefore, it is speculated that E-selectin binding to neutrophils activates the β_2 integrins into intermediate conformational state to mediate slow rolling, which facilitate chemokines to further activate β_2 integrins into full active state to mediate firm adhesion.

The crosslinking of E-selectin ligands seems to be important for β_2 integrin activation. E-selectin Ig chimera in solution activated β_2 integrins on neutrophils; while monomeric E-selectin could not. Consistently, previous study showed E-selectin dimer binding induced coclustering of L-selectin and PSGL-1, but E-selectin monomer binidng induced much less clustering [21]. The activation of β_2 integrins also requires continuous engagement of E-selectin. If the signaling for β_2 integrin activation keeps “on” once induced by E-selectin binding, β_2 integrins should be able to maintain in active state even after the E-selectin-ligand bonds dissociate. Therefore, after β_2 integrins become activated, it should be easier for the following contact test to have a positive outcome and this will result in clustering of adhesion events in the micropipette adhesion assay. But the clustering of adhesion events was not observed; instead, the adhesion events were

distributed rather randomly. Therefore, it seems that β_2 integrins are no longer activated once the two cells are taken apart, and there is no "memory" of the previous contact. Therefore, the adhesion events are independent of each other. Indeed, when neutrophils were rolling in the flow chamber with half of it coated with E-selectin/ICAM-1 and the other half with ICAM-1, they rolled on E-selectin/ICAM-1 but immediately detached after entering the ICAM-1 only zone [139].

Normally, neutrophils are considered to be activated by chemotactic factors of different origins and proinflammatory cytokines. Neutrophils fully activated by these regulators have enhanced production of reactive oxygen intermediates, increased respiratory burst, up-regulation of $\alpha_M\beta_2$, and fully activated β_2 integrins with high ligand binding affinity to mediate firm adhesion. However, the requirement of continuous engagement of E-selectin and the intermediate ligand binding affinity of the activated β_2 integrins indicate the β_2 integrins activated by E-selectin binding is rather in a transient activation state and is different than the full activated state that is triggered by ligation of G protein-coupled chemotactic receptors (GPCRs) [24, 140]. Indeed, the activation of b2 integrins by E-selectin engagement only slowed down the rolling velocity of neutrophils on the substrate coated with both E-selectin and ICAM-1; while TNF-α was able to induce neutrophil adhesion to the same substrate through CXCR2 and $G_{\alpha i}$ [139]. Similarly, P-selectin binding to PSGL-1 on neutrophils activated integrin $\alpha_M\beta_2$ by partially enhancing its function and the binding of P-selectin only triggered an intermediate state of neutrophil activation. Platelet-activation factor (PAF) and interleukin (IL)-8 further enhanced the activation of $\alpha_M\beta_2$ in concert with P-selectin [141].

Among the three selectins, E-selectin seems to be unique in its ability to activate β_2 integrins with current experimental setting. However, some studies showed conflicting results questioning the stimulatory effect of E-selectin binding to neutrophils [142-144]. The present study showed that only E-selectin, but not P- and L-selectin, when coated together with ICAM-1, induced a second step binding mediated by β_2 integrins and ICAM-1. E-selectin differentiates itself by its ability of binding monovalent sLe^x with greater affinity than P- and L-selectin. The binding of E-selectin to a wide variety of sLe^x ligands is sulfation independent, compared with P- and L-selectin [145]. E-selectin also exhibits different binding kinetics. It supports neutrophil rolling rates on the order of a leukocyte diameter per second, an order of magnitude slower than that of P- and L-selectin [146]. Therefore, E-selectin bonds under stress may survive longer than P- and L-selectin bonds, and this may increases the contact time and effective contact area on the rolling neutrophils. It is controversial in the literature about the ability of P-selectin to activate β_2 integrins. There are reports on the binding of PSGL-1 by purified P-selectin failed to show integrin activation on human neutrophils [147-149]. But it was reported that when bound to P-selectin fusion protein, PSGL-1 on mouse neutrophils trigged the stimulation of β_2 integrin mediated homotypic neutrophil aggregation [150]. Moreover, a recent study suggested PSGL-1 engagement by P-selectin induced an intermediate state of $\alpha_M\beta_2$ activation [141]. It is possible that P-selectin induced activation signaling is not as strong as that of E-selectin; therefore, in the micropipette assay, the site density of P-selectin needs to be largely increased in order to induce the activation of β_2 integrins. However, too high site density of P-selectin would result in a 100% adhesion frequency; as a result, it is not possible to detect further increase in frequency even if the β_2 integrins

are activated. Therefore, this technique limitation prevented us from investigating the activation of β_2 integrins by P-selectin with current experimental setting.

CHAPTER 8

CONCLUSIONS AND RECOMMENDATIONS

Integrin has been extensively studied; however, a very important feature of integrin, the regulation of integrin, has not yet been totally understood. Among the mechanisms that have been proposed for integrin regulation, conformational regulation is the most important one. The relationship between conformational change and $\alpha_L\beta_2$ function is the focus of this study. Ligand binding is the very first step for $\alpha_L\beta_2$ to mediate various important biological processes; and therefore one of the most important ways to regulate $\alpha_L\beta_2$ activity is to change the binding affinity and kinetics. The present study investigated the conformational change of $\alpha_L\beta_2$ and the regulation of $\alpha_L\beta_2$ ligand binding by conformational change. Mutation and a variety of reagents, including antibodies, small molecule antagonists, and divalent cations were used to change the binding affinity and kinetics of $\alpha_L\beta_2$ through inducing conformational changes of the molecule. In order to further investigate the regulation of $\alpha_L\beta_2$ in a more physiological environment, the activation of $\alpha_L\beta_2$ and other β_2 integrins on neutrophil by E-selectin binding was also studied.

This study employed micropipette adhesion frequency assay to measure the binding affinity and kinetics. This technique is very reliable for 2D binding affinity and kinetics measurement. The most important advantage of this assay is that it allows direct observation of the bonds of molecules. The proteins in this study are expressed on cell surface instead of in solution, which is more close to physiological conditions. Besides directly measuring receptor-ligand binding affinity and kinetics, this assay can be

modified for other measurements. In this study, the micropipette assay was also used for measuring the divalent cation binding affinity and dissociation from integrin. Another advantage of the micropipette assay is the high temporal resolution. It is this feature on which the experiments for studying the activation of β_2 integrins by E-selectin binding are based. Using this method, we have detected the activation of β_2 integrins in a real-time fashion and thus obtained an accurate estimation of the timescale that other techniques are not able to achieve.

In order to investigate the regulation of $\alpha_L\beta_2$ ligand binding by I domain conformational change and the extension of $\alpha_L\beta_2$, the binding kinetics and affinity of $\alpha_L\beta_2$ at different conformational states were measured. The conformational change of I domain from closed to open and intermediate conformations increased the binding affinity of $\alpha_L\beta_2$ by ~ 3000 and ~ 30 fold, respectively. The off-rate, on the other hand, only changes several fold. The off-rate is mainly regulated by the conformation of I domain, which contain the ligand binding site. With an open I domain, the 2D binding affinity of $\alpha_L\beta_2$ is in the order of 10^{-3} μm^4, and the reverse-rate is ~ 0.5 s^{-1}. When the I domain is at intermediate state, the 2D binding affinity of $\alpha_L\beta_2$ is in the order of 10^{-5} μm^4, and the reverse-rate is ~ 1.2 s^{-1}. The 2D binding affinity of $\alpha_L\beta_2$ with a closed I domain is in the order of 10^{-7} μm^4, and the reverse-rate is larger than 2 s^{-1}. I domain conformational change requires the presence of other domains. The extension of $\alpha_L\beta_2$ leg propagates the conformational change to ligand binding site by pulling down the C-terminal helix of the I domain. However, the extension itself, without affecting the I domain conformation, only increases the on-rate of ligand binding by several fold and has no effect on off-rate.

Therefore, different conformational changes could have distinct effects on ligand binding of $\alpha_L\beta_2$.

The conformation of $\alpha_L\beta_2$ could not be directly accessed by the experiments. The extension of $\alpha_L\beta_2$ is detected by a reporting antibody KIM127. Since the conformations of WT $\alpha_L\beta_2$ I domain when treated with different agents are not clear, a reporting antibody for I domain conformation would be very useful. Moreover, the conformation of $\alpha_L\beta_2$ headpiece, i.e. open or closed, is also important. But this information is totally missing in the study. Therefore, defining the conformation of WT I domain and headpiece of $\alpha_L\beta_2$ would definitely provide more accurate information. This study used divalent cations, activating antibody, and small molecule antagonists to control the conformation of $\alpha_L\beta_2$ *in vitro*. It is therefore essential to correlate these results with *in vivo* situation, where conformational change of $\alpha_L\beta_2$ could be very complicated.

The binding affinity and kinetics of divalent cations, Mn^{2+}, Mg^{2+}, and Ca^{2+}, are also measured. I domain MIDAS coordinates a divalent cation in order to mediate ligand binding, but the binding of divalent cation to MIDAS does not induce a downward movement of the α7 helix of I domain. Mn^{2+} has the higher binding affinity and slower dissociation rate for WT or locked I domains than Mg^{2+}. Ca^{2+} shows two different binding affinities for I domain, which may be due to two different conformations that MIDAS adapts after Ca^{2+} binding. Besides I domain MIDAS, there are multiple other metal ion binding sites in $\alpha_L\beta_2$ that play critical role in conformational regulation. The binding of Mn^{2+} and Mg^{2+} for these sites were also characterized. Mn^{2+} has the higher binding affinity and slower dissociation rate for these sites compared to Mg^{2+}. One interesting finding is that divalent cations dissociate from I domain fairly slowly but from

those binding sites that are important for ICAM-1 binding of $\alpha_L\beta_2$ rapidly. This different binding characteristics of divalent cations for I domain MIDAS and these other sites may indicate the different roles of sites in $\alpha_L\beta_2$ binding and regulation.

The rapid dissociation of divalent cations from those metal ion binding sites that are critical for $\alpha_L\beta_2$ ICAM-1 binding was observed in the study. However, divalent cations dissociate so fast that most of the declining phase of the dissociation curve was missing, which prevent an accurate estimation of the rate. Therefore, a different technique or experimental design with better resolution may be required to obtain those dissociation rates. The isolated I domain provide a great module for studying the divalent cation binding for it only contains one metal ion coordination site. However, $\alpha_L\beta_2$, there are more than 10 metal ion binding sites. The binding affinity of divalent cations to the metal ion binding sites that are important for for ICAM-1 binding of $\alpha_L\beta_2$ were measured assuming the ligand binding affinity change of $\alpha_L\beta_2$ is due to the divalent cation binding to those sites. Moreover, the effects of the multiple metal ion sites were lumped together. Therefore, it would be very interesting to identify and isolate the specific metal ion binding sites that are critical for specific conformational changes and study them one by one using mutagenesis.

On neutrophil, $\alpha_L\beta_2$ and other β_2 integrins are activated to have an intermediate ligand binding affinity by E-selectin binding. Within ~ 5 seconds, the binding of E-selectin Ig chimera coated on RBCs induced neutrophil β_2 integrins binding to ICAM-1 which is coated together with E-selectin. The activation signaling is accumulative and may be induced by the crosslinking of E-selectin ligands.

It is not clear which ligand(s) is responsible for the activation of β_2 integrins. Antibody blocking experiments could be carried out to determine the key E-selectin ligand(s). The results would provide very useful information on the ligand side to characterize current experimental system. It is also of interest to investigate how the change of E-selectin binding kinetics would affect the characteristics of E-selectin ligand engagement during the contact. For example, a slower E-selectin binding off-rate would increase the length of time for ligand engagement. As a result, the activation signaling strength is expected to be stronger.

The results presented in this study certainly contribute to our current understanding of integrin regulation. First of all, the measurement of 2D binding affinity and kinetics of whole $\alpha_L\beta_2$, especially the ones containing a locked I domain, is one of the very first studies that provided these binding parameters. The effect of $\alpha_L\beta_2$ extension on ligand binding affinity and kinetics has never been reported before. Therefore, the binding affinity and kinetics data add to our current knowledge of binding parameters of $\alpha_L\beta_2$. Moreover, the results certainly help to reveal different roles of different conformational change in the regulation of $\alpha_L\beta_2$. The measurement of divalent cation binding affinity and dissociation rate for $\alpha_L\beta_2$ metal ion binding sites is also among the very few studies that reported these parameters. Instead of using purified molecules and directly measuring the divalent cation binding, this study used ligand binding as an indicator for divalent cation binding based on the understanding of the special properties and conformational regulation of I domain and $\alpha_L\beta_2$. The data could contribute to the understanding of the mechanisms of $\alpha_L\beta_2$ regulation by divalent cations. Furthermore, the results confirmed the sophistication and sensitivity of the experimental design and thus

micropipette adhesion frequency assay could be a very useful tool for this type of measurements in the future. This study also emphasized the importance of intracellular signaling in the regulation of $\alpha_L\beta_2$ by studying the activation of $\alpha_L\beta_2$ and other β_2 integrins by E-selectin binding on neutrophils. The activation of $\alpha_L\beta_2$ and other β_2 integrins by E-selectin binding was studied using a novel experiment design. This design takes advantage of the high temporal resolution of micropipette technique and allows an accurate estimation of the timescale of the activation event. Indeed, this study is the first one to report the timescale of and β_2 integrins activation by E-selectin binding on neutrophils. Overall, this study investigated the regulation of $\alpha_L\beta_2$ conformation and ligand binding activity and successfully provided useful information for the understanding of the mechanisms for $\alpha_L\beta_2$ regulation.

However, there are still a lot of questions waiting to be answered regarding the conformational regulation of integrins. One of the most intriguing questions is how the conformational change is initiated in the cytoplasmic tail of integrin and how it is transmitted to the very remote ligand binding site. Another challenge is to understand the dynamics of integrin conformational change, i.e., how fast integrins can switch to another conformation. So far, several models for integrin conformational change have been proposed based on experimental evidence. However, most of the experimental evidence for integrin conformational change is static snapshots of multiple conformational states instead of real-time dynamic conversion of between different conformers. The wide range of integrin activators and inhibitors also adds complexity to the picture of integrin regulation. Since there are multiple pathways of integrin activation or inhibition, it is very

interesting to understand how these pathways or mechanisms interact and coordinate with each other in order to accurately control and regulate integrin functions.

Although micropipette assay has a lot of advantages that other technique lacks, a more sophisticated technique may be required when it comes to study more complicated questions of integrin regulation and to provide larger volume of information. Micropipette assay provides binding affinity and kinetic information by detecting whether there is a bond formation upon the separation of the two cell membranes. However, when the two cell membranes are in contact prior to separation, bonds could already be formed and dissociated for several times. This information could not be obtained by micropipette assay, which makes the technique very time-consuming because the assay can only observe one bond for one whole contact duration. Micropipette assay also omits all the information that could be very important to characterize a bond, such as bond force, bode lifetime, and etc. Therefore, a technique that provides solution to the above problems yet still inherits all the advantage of micropipette would be more appropriate for future experiments in integrin study. Biomembrane Force Probe (BFP) is an ideal candidate. The setup of BFP is very similar to micropipette except that it uses a bead attaching to a RBC as a probe. The position of the edge of the bead is tracked by a high-speed camera and thus any displacement of the bead could be accurately calculated. When a bond formed between the molecules on the bead and the opposite cell/bead, the force of the bond could be calculated from the displacement of the bead and the spring constant of the RBC. Therefore, BFP is a more powerful tool than micropipette for the purpose of studying integrin conformation and ligand binding properties on single molecule level. Using BFP, the force of the bonds formed at different conformational

states could be characterized. The dynamics of integrin conformational change, especially the bent to extended change (or vice versa), could be directly observed. These experiments would reveal more detailed information of integrin regulation that could never been obtained by other methods.

In conclusion, this work provided valuable information of the regulation of $\alpha_L\beta_2$ conformational change and its ligand binding affinity and kinetics. It shed lights on the mechanisms of $\alpha_L\beta_2$ regulation by conformational change, divalent cations, and intracellular signaling. The results could also be applied to understand the activation and regulation of $\alpha_L\beta_2$ in normal or abnormal situations *in vivo*.

REFERENCES

1. Johnston, S.C., M.L. Dustin, M.L. Hibbs, and T.A. Springer, *On the Species Specificity of the Interaction of LFA-1 with Intercellular Adhesion Molecules.* J Immunol, 1990. 145(4): P. 1181-7.
2. Humphries, M.J., *Integrin Structure.* Biochem Soc Trans, 2000. 28(4): P. 311-39.
3. Hynes, R.O., *Integrins: Versatility, Modulation, and Signaling in Cell Adhesion.* Cell, 1992. 69(1): P. 11-25.
4. Sanchez-Madrid, F., P. Simon, S. Thompson, and T.A. Springer, *Mapping of Antigenic and Functional Epitopes on the Alpha- and Beta-Subunits of Two Related Mouse Glycoproteins Involved in Cell Interactions, LFA-1 And Mac-1.* J Exp Med, 1983. 158(2): P. 586-602.
5. Crowley, C.A., J.T. Curnutte, R.E. Rosin, J. Andre-Schwartz, J.I. Gallin, M. Klempner, R. Snyderman, F.S. Southwick, T.P. Stossel, and B.M. Babior, *An Inherited Abnormality of Neutrophil Adhesion. Its Genetic Transmission and Its Association with a Missing Protein.* N Engl J Med, 1980. 302(21): P. 1163-8.
6. Gahmberg, C.G., M. Tolvanen, and P. Kotovuori, *Leukocyte Adhesion--Structure And Function of Human Leukocyte Beta2-Integrins and Their Cellular Ligands.* Eur J Biochem, 1997. 245(2): P. 215-32.
7. Hogg, N., M. Laschinger, K. Giles, and A. Mcdowall, *T-Cell Integrins: More than Just Sticking Points.* J Cell Sci, 2003. 116(Pt 23): P. 4695-705.
8. Gahmberg, C.G., L. Valmu, S. Fagerholm, P. Kotovuori, E. Ihanus, L. Tian, and T. Pessa-Morikawa, *Leukocyte Integrins and Inflammation.* Cell Mol Life Sci, 1998. 54(6): P. 549-55.
9. Dustin, M.L., R. Rothlein, A.K. Bhan, C.A. Dinarello, and T.A. Springer, *Induction By IL 1 and Interferon-Gamma: Tissue Distribution, Biochemistry, and Function of a Natural Adherence Molecule (ICAM-1).* J Immunol, 1986. 137(1): P. 245-54.
10. Altman, L.C., G.H. Ayars, C. Baker, and D.L. Luchtel, *Cytokines And Eosinophil-Derived Cationic Proteins Upregulate Intercellular Adhesion Molecule-1 on Human Nasal Epithelial Cells.* J Allergy Clin Immunol, 1993. 92(4): P. 527-36.
11. Look, D.C., S.R. Rapp, B.T. Keller, and M.J. Holtzman, *Selective Induction of Intercellular Adhesion Molecule-1 by Interferon-Gamma in Human Airway Epithelial Cells.* Am J Physiol, 1992. 263(1 Pt 1): P. L79-87.
12. Shimaoka, M., T. Xiao, J.H. Liu, Y. Yang, Y. Dong, C.D. Jun, A. Mccormack, R. Zhang, A. Joachimiak, J. Takagi, J.H. Wang, and T.A. Springer, *Structures of the Alpha L I Domain and Its Complex with ICAM-1 Reveal a Shape-Shifting Pathway for Integrin Regulation.* Cell, 2003. 112(1): P. 99-111.
13. Springer, T.A., *Traffic Signals for Lymphocyte Recirculation and Leukocyte Emigration: The Multistep Paradigm.* Cell, 1994. 76(2): P. 301-14.
14. Grakoui, A., S.K. Bromley, C. Sumen, M.M. Davis, A.S. Shaw, P.M. Allen, and M.L. Dustin, *The Immunological Synapse: A Molecular Machine Controlling T Cell Activation.* Science, 1999. 285(5425): P. 221-7.
15. Moore, K.L., N.L. Stults, S. Diaz, D.F. Smith, R.D. Cummings, A. Varki, and R.P. McEver, *Identification af a Specific Glycoprotein Ligand for P-Selectin (Cd62) on Myeloid Cells.* J Cell Biol, 1992. 118(2): P. 445-56.

16. Sperandio, M., M.L. Smith, S.B. Forlow, T.S. Olson, L. Xia, R.P. McEver, and K. Ley, *P-Selectin Glycoprotein Ligand-1 Mediates L-selectin-dependent Leukocyte Rolling In Venules.* J Exp Med, 2003. 197(10): P. 1355-63.
17. Xia, L., M. Sperandio, T. Yago, J.M. Mcdaniel, R.D. Cummings, S. Pearson-White, K. Ley, and R.P. McEver, *P-Selectin Glycoprotein Ligand-1-Deficient Mice Have Impaired Leukocyte Tethering to E-Selectin Under Flow.* J Clin Invest, 2002. 109(7): P. 939-50.
18. Yang, J., T. Hirata, K. Croce, G. Merrill-Skoloff, B. Tchernychev, E. Williams, R. Flaumenhaft, B.C. Furie, and B. Furie, *Targeted Gene Disruption Demonstrates that P-Selectin Glycoprotein Ligand 1 (PSGL-1) is Required for P-selectin-Mediated But Not E-Selectin-Mediated Neutrophil Rolling And Migration.* J Exp Med, 1999. 190(12): P. 1769-82.
19. Springer, T.A., *Traffic Signals on Endothelium For Lymphocyte Recirculation And Leukocyte Emigration.* Annu Rev Physiol, 1995. 57: P. 827-72.
20. Rainger, G.E., A.C. Fisher, and G.B. Nash, *Endothelial-Borne Platelet-Activating Factor And Interleukin-8 Rapidly Immobilize Rolling Neutrophils.* Am J Physiol, 1997. 272(1 Pt 2): P. H114-22.
21. Green, C.E., D.N. Pearson, R.T. Camphausen, D.E. Staunton, and S.I. Simon, *Shear-Dependent Capping of L-selectin And P-selectin Glycoprotein Ligand 1 By E-Selectin Signals Activation of High-Avidity Beta2-Integrin On Neutrophils.* J Immunol, 2004. 172(12): P. 7780-90.
22. Hidari, K.I., A.S. Weyrich, G.A. Zimmerman, and R.P. McEver, *Engagement of P-selectin Glycoprotein Ligand-1 Enhances Tyrosine Phosphorylation And Activates Mitogen-activated Protein Kinases In Human Neutrophils.* J Biol Chem, 1997. 272(45): P. 28750-6.
23. Chesnutt, B.C., D.F. Smith, N.A. Raffler, M.L. Smith, E.J. White, and K. Ley, *Induction of LFA-1-Dependent Neutrophil Rolling On ICAM-1 By Engagement Of E-Selectin.* Microcirculation, 2006. 13(2): P. 99-109.
24. Warnock, R.A., S. Askari, E.C. Butcher, and U.H. Von Andrian, *Molecular Mechanisms of Lymphocyte Homing to Peripheral Lymph Nodes.* J Exp Med, 1998. 187(2): P. 205-16.
25. Dustin, M.L., S.K. Bromley, Z. Kan, D.A. Peterson, and E.R. Unanue, *Antigen Receptor Engagement Delivers a Stop Signal to Migrating T Lymphocytes.* Proc Natl Acad Sci U S A, 1997. 94(8): P. 3909-13.
26. Monks, C.R., B.A. Freiberg, H. Kupfer, N. Sciaky, and A. Kupfer, *Three-Dimensional Segregation of Supramolecular Activation Clusters in T Cells.* Nature, 1998. 395(6697): P. 82-6.
27. Bachmann, M.F., K. Mckall-Faienza, R. Schmits, D. Bouchard, J. Beach, D.E. Speiser, T.W. Mak, and P.S. Ohashi, *Distinct Roles for LFA-1 and Cd28 during Activation of Naive T Cells: Adhesion Versus Costimulation.* Immunity, 1997. 7(4): P. 549-57.
28. Iezzi, G., K. Karjalainen, and A. Lanzavecchia, *The Duration of Antigenic Stimulation Determines the Fate of Naive and Effector T Cells.* Immunity, 1998. 8(1): P. 89-95.
29. Pardi, R., J.R. Bender, C. Dettori, E. Giannazza, and E.G. Engleman, *Heterogeneous Distribution and Transmembrane Signaling Properties of*

Lymphocyte Function-Associated Antigen (LFA-1) in Human Lymphocyte Subsets. J Immunol, 1989. 143(10): P. 3157-66.
30. Van Seventer, G.A., Y. Shimizu, K.J. Horgan, and S. Shaw, *The LFA-1 Ligand Icam-1 Provides an Important Costimulatory Signal for T Cell Receptor-Mediated Activation of Resting T Cells.* J Immunol, 1990. 144(12): P. 4579-86.
31. Hynes, R.O., *Integrins: A Family of Cell Surface Receptors.* Cell, 1987. 48(4): P. 549-54.
32. Yusuf-Makagiansar, H., M.E. Anderson, T.V. Yakovleva, J.S. Murray, and T.J. Siahaan, *Inhibition of LFA-1/ICAM-1 And VLA-4/VCAM-1 As A Therapeutic Approach To Inflammation And Autoimmune Diseases.* Med Res Rev, 2002. 22(2): P. 146-67.
33. Kim, M., C.V. Carman, and T.A. Springer, *Bidirectional Transmembrane Signaling by Cytoplasmic Domain Separation in Integrins.* Science, 2003. 301(5640): P. 1720-5.
34. Shamri, R., V. Grabovsky, J.M. Gauguet, S. Feigelson, E. Manevich, W. Kolanus, M.K. Robinson, D.E. Staunton, U.H. Von Andrian, and R. Alon, *Lymphocyte Arrest Requires Instantaneous Induction of an Extended LFA-1 Conformation Mediated by Endothelium-Bound Chemokines.* Nat Immunol, 2005. 6(5): P. 497-506.
35. Takagi, J., B.M. Petre, T. Walz, and T.A. Springer, *Global Conformational Rearrangements in Integrin Extracellular Domains in Outside-in and Inside-out Signaling.* Cell, 2002. 110(5): P. 599-11.
36. Giancotti, F.G. and E. Ruoslahti, *Integrin Signaling.* Science, 1999. 285(5430): P. 1028-32.
37. Hato, T., N. Pampori, and S.J. Shattil, *Complementary Roles for Receptor Clustering and Conformational Change in the Adhesive and Signaling Functions of Integrin AlphaIIb Beta3.* J Cell Biol, 1998. 141(7): P. 1685-95.
38. Springer, T.A., *Folding of the N-Terminal, Ligand-Binding Region of Integrin Alpha-Subunits Into a Beta-Propeller Domain.* Proc Natl Acad Sci U S A, 1997. 94(1): P. 65-72.
39. Goodman, T.G. and M.L. Bajt, *Identifying The Putative Metal Ion-Dependent Adhesion Site in the Beta2 (CD18) Subunit Required for Alphalbeta2 and Alphambeta2 Ligand Interactions.* J Biol Chem, 1996. 271(39): P. 23729-36.
40. Dickeson, S.K. and S.A. Santoro, *Ligand Recognition by the I Domain-Containing Integrins.* Cell Mol Life Sci, 1998. 54(6): P. 556-66.
41. Leitinger, B. and N. Hogg, *Effects of I Domain Deletion on the Function of the Beta2 Integrin Lymphocyte Function-Associated Antigen-1.* Mol Biol Cell, 2000. 11(2): P. 677-90.
42. Lee, J.O., P. Rieu, M.A. Arnaout, and R. Liddington, *Crystal Structure of the A Domain from the Alpha Subunit of Integrin CR3 (CD11b/CD18).* Cell, 1995. 80(4): P. 631-8.
43. Shimaoka, M., J. Takagi, And T.A. Springer, *Conformational Regulation of Integrin Structure and Function.* Annu Rev Biophys Biomol Struct, 2002. 31: P. 485-516.

44. Lee, J.O., L.A. Bankston, M.A. Arnaout, and R.C. Liddington, *Two Conformations of the Integrin A-domain (I-domain): a Pathway for Activation?* Structure, 1995. 3(12): P. 1333-40.
45. Emsley, J., C.G. Knight, R.W. Farndale, M.J. Barnes, and R.C. Liddington, *Structural Basis of Collagen Recognition by Integrin Alpha2beta1*. Cell, 2000. 101(1): P. 47-56.
46. Kallen, J., K. Welzenbach, P. Ramage, D. Geyl, R. Kriwacki, G. Legge, S. Cottens, G. Weitz-Schmidt, and U. Hommel, *Structural Basis for LFA-1 Inhibition Upon Lovastatin Binding to the CD11a I-Domain.* J Mol Biol, 1999. 292(1): P. 1-9.
47. Legge, G.B., R.W. Kriwacki, J. Chung, U. Hommel, P. Ramage, D.A. Case, H.J. Dyson, and P.E. Wright, *Nmr Solution Structure of the Inserted Domain of Human Leukocyte Function Associated Antigen-1*. J Mol Biol, 2000. 295(5): P. 1251-64.
48. Qu, A. and D.J. Leahy, *Crystal Structure of The I-Domain From The CD11a/CD18 (LFA-1, Alpha L Beta 2) Integrin.* Proc Natl Acad Sci U S A, 1995. 92(22): P. 10277-81.
49. Qu, A. and D.J. Leahy, *The Role of the Divalent Cation in the Structure of the I Domain from the CD11a/CD18 Integrin.* Structure, 1996. 4(8): P. 931-42.
50. Shimaoka, M., C. Lu, R.T. Palframan, U.H. Von Andrian, A. Mccormack, J. Takagi, and T.A. Springer, *Reversibly Locking a Protein Fold in an Active Conformation with a Disulfide Bond: Integrin Alphal I Domains With High Affinity and Antagonist Activity In Vivo.* Proc Natl Acad Sci U S A, 2001. 98(11): P. 6009-14.
51. Takagi, J. and T.A. Springer, *Integrin Activation and Structural Rearrangement.* Immunol Rev, 2002. 186: P. 141-63.
52. Lu, C., M. Shimaoka, M. Ferzly, C. Oxvig, J. Takagi, and T.A. Springer, *An Isolated, Surface-Expressed I Domain of the Integrin Alphalbeta2 is Sufficient for Strong Adhesive Function When Locked in the Open Conformation with a Disulfide Bond.* Proc Natl Acad Sci U S A, 2001. 98(5): P. 2387-92.
53. Zhang, F., W.D. Marcus, N.H. Goyal, P. Selvaraj, T.A. Springer, and C. Zhu, *Two-Dimensional Kinetics Regulation of Alphalbeta2-ICAM-1 Interaction by Conformational Changes of the AlphaL-Inserted Domain.* J Biol Chem, 2005. 280(51): P. 42207-18.
54. Jin, M., G. Song, C.V. Carman, Y.S. Kim, N.S. Astrof, M. Shimaoka, D.K. Wittrup, and T.A. Springer, *Directed Evolution to Probe Protein Allostery and Integrin I Domains of 200,000-Fold Higher Affinity.* Proc Natl Acad Sci U S A, 2006. 103(15): P. 5758-63.
55. Salas, A., M. Shimaoka, S. Chen, C.V. Carman, and T. Springer, *Transition From Rolling to Firm Adhesion is Regulated by the Conformation of the I Domain of the Integrin Lymphocyte Function-Associated Antigen-1*. J Biol Chem, 2002. 277(52): P. 50255-62.
56. Astrof, N.S., A. Salas, M. Shimaoka, J. Chen, and T.A. Springer, *Importance of Force Linkage in Mechanochemistry of Adhesion Receptors.* Biochemistry, 2006. 45(50): P. 15020-8.

57. Du, X., M. Gu, J.W. Weisel, C. Nagaswami, J.S. Bennett, R. Bowditch, and M.H. Ginsberg, *Long Range Propagation of Conformational Changes in Integrin Alpha IIb Beta 3.* J Biol Chem, 1993. 268(31): P. 23087-92.
58. Takagi, J., H.P. Erickson, and T.A. Springer, *C-Terminal Opening Mimics 'Inside-Out' Activation of Integrin Alpha5beta1.* Nat Struct Biol, 2001. 8(5): P. 412-6.
59. Xiong, J.P., T. Stehle, B. Diefenbach, R. Zhang, R. Dunker, D.L. Scott, A. Joachimiak, S.L. Goodman, and M.A. Arnaout, *Crystal Structure of the Extracellular Segment of Integrin AlphaVbeta3.* Science, 2001. 294(5541): P. 339-45.
60. Nishida, N., C. Xie, M. Shimaoka, Y. Cheng, T. Walz, and T.A. Springer, *Activation of Leukocyte Beta2 Integrins by Conversion from Bent to Extended Conformations.* Immunity, 2006. 25(4): P. 583-94.
61. Beglova, N., S.C. Blacklow, J. Takagi, and T.A. Springer, *Cysteine-Rich Module Structure Reveals a Fulcrum for Integrin Rearrangement upon Activation.* Nat Struct Biol, 2002. 9(4): P. 282-7.
62. Lu, C., J. Takagi, and T.A. Springer, *Association of the Membrane Proximal Regions of the Alpha and Beta Subunit Cytoplasmic Domains Constrains An Integrin in the Inactive State.* J Biol Chem, 2001. 276(18): P. 14642-8.
63. Alonso, J.L., M. Essafi, J.P. Xiong, T. Stehle, and M.A. Arnaout, *Does the Integrin AlphaA Domain Act as a Ligand for Its BetaA Domain?* Curr Biol, 2002. 12(10): P. R340-2.
64. Yang, W., M. Shimaoka, A. Salas, J. Takagi, and T.A. Springer, *Intersubunit Signal Transmission in Integrins by a Receptor-Like Interaction with a Pull Spring.* Proc Natl Acad Sci U S A, 2004. 101(9): P. 2906-11.
65. Shimaoka, M., A. Salas, W. Yang, G. Weitz-Schmidt, and T.A. Springer, *Small Molecule Integrin Antagonists that Bind to the Beta2 Subunit I-Like Domain and Activate Signals in One Direction and Block Them in the Other.* Immunity, 2003. 19(3): P. 391-402.
66. Carman, C.V. and T.A. Springer, *Integrin Avidity Regulation: Are Changes in Affinity and Conformation Underemphasized?* Curr Opin Cell Biol, 2003. 15(5): P. 547-56.
67. Chesla, S.E., P. Selvaraj, and C. Zhu, *Measuring Two-Dimensional Receptor-Ligand Binding Kinetics by Micropipette.* Biophys J, 1998. 75(3): P. 1553-72.
68. Gomes, P. and D. Andreu, *Direct Kinetic Assay of Interactions Between Small Peptides and Immobilized Antibodies Using a Surface Plasmon Resonance Biosensor.* J Immunol Methods, 2002. 259(1-2): P. 217-30.
69. Dustin, M.L., L.M. Ferguson, P.Y. Chan, T.A. Springer, and D.E. Golan, *Visualization of CD2 Interaction with LFA-3 and Determination of the Two-Dimensional Dissociation Constant for Adhesion Receptors in a Contact Area.* J Cell Biol, 1996. 132(3): P. 465-74.
70. Evans, E., D. Berk, and A. Leung, *Detachment of Agglutinin-Bonded Red Blood Cells. I. Forces to Rupture Molecular-Point Attachments.* Biophys J, 1991. 59(4): P. 838-48.

71. Evans, E., K. Ritchie, and R. Merkel, *Sensitive Force Technique to Probe Molecular Adhesion and Structural Linkages at Biological Interfaces.* Biophys J, 1995. 68(6): P. 2580-7.
72. Huang, J., J. Chen, S.E. Chesla, T. Yago, P. Mehta, R.P. McEver, C. Zhu, and M. Long, *Quantifying the Effects of Molecular Orientation and Length on Two-Dimensional Receptor-Ligand Binding Kinetics.* J Biol Chem, 2004. 279(43): P. 44915-23.
73. Dumaswala, U.J., M.J. Wilson, T. Jose, and D.L. Daleke, *Glutamine- and Phosphate-Containing Hypotonic Storage Media Better Maintain Erythrocyte Membrane Physical Properties.* Blood, 1996. 88(2): P. 697-704.
74. Carpen, O., P. Pallai, D.E. Staunton, and T.A. Springer, *Association of Intercellular Adhesion Molecule-1 (ICAM-1) with Actin-Containing Cytoskeleton and Alpha-Actinin.* J Cell Biol, 1992. 118(5): P. 1223-34.
75. Petruzzelli, L., L. Maduzia, and T.A. Springer, *Activation of Lymphocyte Function-Associated Molecule-1 (CD11a/CD18) and Mac-1 (CD11b/CD18) Mimicked by an Antibody Directed Against CD18.* J Immunol, 1995. 155(2): P. 854-66.
76. Robinson, M.K., D. Andrew, H. Rosen, D. Brown, S. Ortlepp, P. Stephens, and E.C. Butcher, *Antibody Against the Leu-CAM Beta-Chain (CD18) Promotes Both LFA-1- and CR3-Dependent Adhesion Events.* J Immunol, 1992. 148(4): P. 1080-5.
77. Williams, T.E., P. Selvaraj, and C. Zhu, *Concurrent Binding to Multiple Ligands: Kinetic Rates of CD16b for Membrane-Bound IgG1 And IgG2.* Biophys J, 2000. 79(4): P. 1858-66.
78. Labadia, M.E., D.D. Jeanfavre, G.O. Caviness, and M.M. Morelock, *Molecular Regulation of the Interaction between Leukocyte Function-Associated Antigen-1 And Soluble ICAM-1 by Divalent Metal Cations.* J Immunol, 1998. 161(2): P. 836-42.
79. Dustin, M.L., S.K. Bromley, M.M. Davis, and C. Zhu, *Identification of Self Through Two-Dimensional Chemistry and Synapses.* Annu Rev Cell Dev Biol, 2001. 17: P. 133-57.
80. Williams, T.E., S. Nagarajan, P. Selvaraj, and C. Zhu, *Concurrent and Independent Binding of Fcgamma Receptors IIa And IIIb to Surface-Bound IgG.* Biophys J, 2000. 79(4): P. 1867-75.
81. Huang, J., J. Chen, S.E. Chesla, T. Yago, P. Mehta, R.P. Mcever, C. Zhu, and M. Long, *Quantifying the Effects of Molecular Orientation and Length on Two-Dimensional Receptor-Ligand Binding Kinetics.* J Biol Chem, 2004.
82. Staunton, D.E., M.L. Dustin, H.P. Erickson, and T.A. Springer, *The Arrangement of the Immunoglobulin-Like Domains of ICAM-1 and the Binding Sites for LFA-1 And Rhinovirus.* Cell, 1990. 61(2): P. 243-54.
83. Smith, J.W., R.S. Piotrowicz, and D. Mathis, *A Mechanism for Divalent Cation Regulation of Beta 3-Integrins.* J Biol Chem, 1994. 269(2): P. 960-7.
84. Williams, T.E., S. Nagarajan, P. Selvaraj, and C. Zhu, *Quantifying the Impact of Membrane Microtopology on Effective Two-Dimensional Affinity.* J Biol Chem, 2001. 276(16): P. 13283-8.

85. Nicholson, M.W., A.N. Barclay, M.S. Singer, S.D. Rosen, and P.A. Van Der Merwe, *Affinity and Kinetic Analysis of L-Selectin (CD62l) Binding to Glycosylation-Dependent Cell-Adhesion Molecule-1.* J Biol Chem, 1998. 273(2): P. 763-70.
86. Mehta, P., R.D. Cummings, and R.P. McEver, *Affinity and Kinetic Analysis of P-Selectin Binding to P-Selectin Glycoprotein Ligand-1.* J Biol Chem, 1998. 273(49): P. 32506-13.
87. Wild, M.K., M.C. Huang, U. Schulze-Horsel, P.A. Van Der Merwe, and D. Vestweber, *Affinity, Kinetics, and Thermodynamics of E-Selectin Binding to E-Selectin Ligand-1.* J Biol Chem, 2001. 276(34): P. 31602-12.
88. Long, M., H. Zhao, K.S. Huang, and C. Zhu, *Kinetic Measurements of Cell Surface E-Selectin/Carbohydrate Ligand Interactions.* Ann Biomed Eng, 2001. 29(11): P. 935-46.
89. Chesla, S.E., P. Li, S. Nagarajan, P. Selvaraj, and C. Zhu, *The Membrane Anchor Influences Ligand Binding Two-Dimensional Kinetic Rates and Three-Dimensional Affinity of Fcgammariii (CD16).* J Biol Chem, 2000. 275(14): P. 10235-46.
90. Thoumine, O., P. Kocian, A. Kottelat, and J.J. Meister, *Short-Term Binding of Fibroblasts to Fibronectin: Optical Tweezers Experiments and Probabilistic Analysis.* Eur Biophys J, 2000. 29(6): P. 398-408.
91. Lomakina, E.B. and R.E. Waugh, *Micromechanical Tests of Adhesion Dynamics Between Neutrophils and Immobilized ICAM-1.* Biophys J, 2004. 86(2): P. 1223-33.
92. Schuck, P., *Use of Surface Plasmon Resonance to Probe the Equilibrium and Dynamic Aspects of Interactions Between Biological Macromolecules.* Annu Rev Biophys Biomol Struct, 1997. 26: P. 541-66.
93. Miller, J., R. Knorr, M. Ferrone, R. Houdei, C.P. Carron, and M.L. Dustin, *Intercellular Adhesion Molecule-1 Dimerization and Its Consequences for Adhesion Mediated by Lymphocyte Function Associated-1.* J Exp Med, 1995. 182(5): P. 1231-41.
94. Reilly, P.L., J.R. Woska, Jr., D.D. Jeanfavre, E. Mcnally, R. Rothlein, and B.J. Bormann, *The Native Structure of Intercellular Adhesion Molecule-1 (ICAM-1) is a Dimer. Correlation with Binding to LFA-1.* J Immunol, 1995. 155(2): P. 529-32.
95. Jun, C.D., M. Shimaoka, C.V. Carman, J. Takagi, and T.A. Springer, *Dimerization and the Effectiveness of ICAM-1 in Mediating LFA-1-Dependent Adhesion.* Proc Natl Acad Sci U S A, 2001. 98(12): P. 6830-5.
96. Vitte, J., A.M. Benoliel, P. Eymeric, P. Bongrand, and A. Pierres, *Beta-1 Integrin-Mediated Adhesion may be Initiated by Multiple Incomplete Bonds, Thus Accounting for the Functional Importance of Receptor Clustering.* Biophys J, 2004. 86(6): P. 4059-74.
97. Zhang, X., E. Wojcikiewicz, and V.T. Moy, *Force Spectroscopy of the Leukocyte Function-Associated Antigen-1/Intercellular Adhesion Molecule-1 Interaction.* Biophys J, 2002. 83(4): P. 2270-9.
98. Miura, S., C.Q. Li, Z. Cao, H. Wang, M.R. Wardell, and J.E. Sadler, *Interaction of Von Willebrand Factor Domain A1 with Platelet Glycoprotein Ibalpha-(1-289).*

Slow Intrinsic Binding Kinetics Mediate Rapid Platelet Adhesion. J Biol Chem, 2000. 275(11): P. 7539-46.
99. Doggett, T.A., G. Girdhar, A. Lawshe, D.W. Schmidtke, I.J. Laurenzi, S.L. Diamond, and T.G. Diacovo, *Selectin-Like Kinetics and Biomechanics Promote Rapid Platelet Adhesion in Flow: The Gpib(Alpha)-Vwf Tether Bond.* Biophys J, 2002. 83(1): P. 194-205.
100. Kumar, R.A., J.F. Dong, J.A. Thaggard, M.A. Cruz, J.A. Lopez, and L.V. Mcintire, *Kinetics of GpIbalpha-VWF-A1 Tether Bond Under Flow: Effect of Gpibalpha Mutations on the Association and Dissociation Rates.* Biophys J, 2003. 85(6): P. 4099-109.
101. Merkel, R., P. Nassoy, A. Leung, K. Ritchie, and E. Evans, *Energy Landscapes of Receptor-Ligand Bonds Explored with Dynamic Force Spectroscopy.* Nature, 1999. 397(6714): P. 50-3.
102. Chilkoti, A. and P.S. Stayton, *Molecular Origins of the Slow Streptavidin-Biotin Dissociation Kinetics.* J Am Chem Soc, 1995. 117: P. 10622-10628.
103. Ludwig, F. and E. Evans, *How Strong is Molecular Anchoring in Biomembranes?* Bif Futura, 2000. 15: P. 96-103.
104. Silvius, J.R. and M.J. Zuckermann, *Interbilayer Transfer of Phospholipid-Anchored Macromolecules Via Monomer Diffusion.* Biochemistry, 1993. 32(12): P. 3153-61.
105. Evans, E., *Probing The Relation Between Force--Lifetime--and Chemistry in Single Molecular Bonds.* Annu Rev Biophys Biomol Struct, 2001. 30: P. 105-28.
106. Luo, B.H., K. Strokovich, T. Walz, T.A. Springer, and J. Takagi, *Allosteric Beta1 Integrin Antibodies that Stabilize the Low Affinity State by Preventing the Swing-Out of the Hybrid Domain.* J Biol Chem, 2004. 279(26): P. 27466-71.
107. Chen, J., J. Takagi, C. Xie, T. Xiao, B.H. Luo, and T.A. Springer, *The Relative Influence of Metal Ion Binding Sites in the I-Like Domain and the Interface with the Hybrid Domain on Rolling and Firm Adhesion by Integrin Alpha4beta7.* J Biol Chem, 2004. 279(53): P. 55556-61.
108. Lu, C., M. Shimaoka, Q. Zang, J. Takagi, and T.A. Springer, *Locking in Alternate Conformations of the Integrin AlphLlbeta2 I Domain with Disulfide Bonds Reveals Functional Relationships Among Integrin Domains.* Proc Natl Acad Sci U S A, 2001. 98(5): P. 2393-8.
109. Yang, W., M. Shimaoka, J. Chen, and T.A. Springer, *Activation of Integrin Beta-Subunit I-Like Domains by One-Turn C-Terminal Alpha-Helix Deletions.* Proc Natl Acad Sci U S A, 2004. 101(8): P. 2333-8.
110. Lu, C., M. Shimaoka, A. Salas, and T.A. Springer, *The Binding Sites for Competitive Antagonistic, Allosteric Antagonistic, and Agonistic Antibodies to the I Domain Of Integrin LFA-1.* J Immunol, 2004. 173(6): P. 3972-8.
111. Shimaoka, M. and T.A. Springer, *Therapeutic Antagonists and Conformational Regulation of Integrin Function.* Nat Rev Drug Discov, 2003. 2(9): P. 703-16.
112. Salas, A., M. Shimaoka, A.N. Kogan, C. Harwood, U.H. Von Andrian, and T.A. Springer, *Rolling Adhesion through an Extended Conformation of Integrin Alphalbeta2 and Relation to Alpha I and Beta I-Like Domain Interaction.* Immunity, 2004. 20(4): P. 393-406.
113. Ludwig, F. and E. Evans, Bif Futura, 2000. 15: P. 96-103.

114. Lu, C.F. and T.A. Springer, *The Alpha Subunit Cytoplasmic Domain Regulates the Assembly and Adhesiveness of Integrin Lymphocyte Function-Associated Antigen-1*. J Immunol, 1997. 159(1): P. 268-78.
115. Wong, J.Y., T.L. Kuhl, J.N. Israelachvili, N. Mullah, and S. Zalipsky, *Direct Measurement of a Tethered Ligand-Receptor Interaction Potential.* Science, 1997. 275(5301): P. 820-2.
116. Leitinger, B., A. Mcdowall, P. Stanley, and N. Hogg, *The Regulation of Integrin Function By Ca(2+).* Biochim Biophys Acta, 2000. 1498(2-3): P. 91-8.
117. Chen, J., A. Salas, and T.A. Springer, *Bistable Regulation of Integrin Adhesiveness by a Bipolar Metal Ion Cluster*. Nat Struct Biol, 2003. 10(12): P. 995-1001.
118. Griggs, D.W., C.M. Schmidt, and C.P. Carron, *Characteristics of Cation Binding to the I Domains of LFA-1 And Mac-1. The LFA-1 I Domain Contains a Ca2+-Binding Site.* J Biol Chem, 1998. 273(34): P. 22113-9.
119. Ajroud, K., T. Sugimori, W.H. Goldmann, D.M. Fathallah, J.P. Xiong, and M.A. Arnaout, *Binding Affinity of Metal Ions to the CD11b A-Domain is Regulated by Integrin Activation and Ligands.* J Biol Chem, 2004. 279(24): P. 25483-8.
120. Rivas, G.A. and J. Gonzalez-Rodriguez, *Calcium Binding to Human Platelet Integrin Gpiib/Iiia and to Its Constituent Glycoproteins. Effects of Lipids and Temperature.* Biochem J, 1991. 276 (Pt 1): P. 35-40.
121. Huth, J.R., E.T. Olejniczak, R. Mendoza, H. Liang, E.A. Harris, M.L. Lupher, Jr., A.E. Wilson, S.W. Fesik, and D.E. Staunton, *NMR And Mutagenesis Evidence for an I Domain Allosteric Site that Regulates Lymphocyte Function-Associated Antigen 1 Ligand Binding.* Proc Natl Acad Sci U S A, 2000. 97(10): P. 5231-6.
122. Renner, M., M.A. Danielson, and J.J. Falke, *Kinetic Control of Ca(II) Signaling: Tuning the Ion Dissociation Rates of Ef-Hand Ca(II) Binding Sites.* Proc Natl Acad Sci U S A, 1993. 90(14): P. 6493-7.
123. Hou, T.T., J.D. Johnson, and J.A. Rall, *Parvalbumin Content and Ca2+ and Mg2+ Dissociation Rates Correlated with Changes in Relaxation Rate of Frog Muscle Fibres.* J Physiol, 1991. 441: P. 285-304.
124. Bennett, A.J. and C.R. Bagshaw, *The Kinetics of Bivalent Metal Ion Dissociation From Myosin Subfragments.* Biochem J, 1986. 233(1): P. 173-7.
125. Busenlehner, L.S. and D.P. Giedroc, *Kinetics of Metal Binding by the Toxic Metal-Sensing Transcriptional Repressor Staphylococcus Aureus Pi258 Cadc.* J Inorg Biochem, 2006. 100(5-6): P. 1024-34.
126. Butcher, E.C., *Leukocyte-Endothelial Cell Recognition: Three (Or More) Steps to Specificity and Diversity.* Cell, 1991. 67(6): P. 1033-6.
127. Lawrence, M.B. and T.A. Springer, *Leukocytes Roll on a Selectin at Physiologic Flow Rates: Distinction from and Prerequisite for Adhesion Through Integrins.* Cell, 1991. 65(5): P. 859-73.
128. Kansas, G.S., *Selectins and Their Ligands: Current Concepts and Controversies.* Blood, 1996. 88(9): P. 3259-87.
129. Varki, A., *Selectin Ligands: Will The Real Ones Please Stand Up?* J Clin Invest, 1997. 99(2): P. 158-62.

130. Campbell, J.J., J. Hedrick, A. Zlotnik, M.A. Siani, D.A. Thompson, and E.C. Butcher, *Chemokines and the Arrest of Lymphocytes Rolling Under Flow Conditions.* Science, 1998. 279(5349): P. 381-4.
131. Divietro, J.A., M.J. Smith, B.R. Smith, L. Petruzzelli, R.S. Larson, and M.B. Lawrence, *Immobilized IL-8 Triggers Progressive Activation of Neutrophils Rolling in vitro on P-Selectin and Intercellular Adhesion Molecule-1.* J Immunol, 2001. 167(7): P. 4017-25.
132. Simon, S.I., Y. Hu, D. Vestweber, and C.W. Smith, *Neutrophil Tethering on E-Selectin Activates Beta 2 Integrin Binding to ICAM-1 through a Mitogen-Activated Protein Kinase Signal Transduction Pathway.* J Immunol, 2000. 164(8): P. 4348-58.
133. Mcdonough, D.B., F.A. Mcintosh, C. Spanos, S. Neelamegham, H.L. Goldsmith, and S.I. Simon, *Cooperativity between Selectins and Beta2-Integrins Define Neutrophil Capture and Stable Adhesion in Shear Flow.* Ann Biomed Eng, 2004. 32(9): P. 1179-92.
134. Hentzen, E., D. Mcdonough, L. Mcintire, C.W. Smith, H.L. Goldsmith, and S.I. Simon, *Hydrodynamic Shear and Tethering through E-Selectin Signals Phosphorylation of P38 Map Kinase and Adhesion of Human Neutrophils.* Ann Biomed Eng, 2002. 30(8): P. 987-1001.
135. Beals, C.R., A.C. Edwards, R.J. Gottschalk, T.W. Kuijpers, and D.E. Staunton, *CD18 Activation Epitopes Induced by Leukocyte Activation.* J Immunol, 2001. 167(11): P. 6113-22.
136. Simon, S.I., A.R. Burns, A.D. Taylor, P.K. Gopalan, E.B. Lynam, L.A. Sklar, and C.W. Smith, *L-Selectin (CD62l) Cross-Linking Signals Neutrophil Adhesive Functions via the Mac-1 (CD11b/CD18) Beta 2-Integrin.* J Immunol, 1995. 155(3): P. 1502-14.
137. Tsang, Y.T., S. Neelamegham, Y. Hu, E.L. Berg, A.R. Burns, C.W. Smith, and S.I. Simon, *Synergy Between L-Selectin Signaling and Chemotactic Activation During Neutrophil Adhesion and Transmigration.* J Immunol, 1997. 159(9): P. 4566-77.
138. Waddell, T.K., L. Fialkow, C.K. Chan, T.K. Kishimoto, and G.P. Downey, *Signaling Functions of L-Selectin. Enhancement of Tyrosine Phosphorylation and Activation of Map Kinase.* J Biol Chem, 1995. 270(25): P. 15403-11.
139. Zarbock, A., C.A. Lowell, and K. Ley, *Spleen Tyrosine Kinase Syk is Necessary for E-Selectin-Induced Alpha(L)Beta(2) Integrin-Mediated Rolling On Intercellular Adhesion Molecule-1.* Immunity, 2007.
140. Constantin, G., M. Majeed, C. Giagulli, L. Piccio, J.Y. Kim, E.C. Butcher, and C. Laudanna, *Chemokines Trigger Immediate Beta2 Integrin Affinity and Mobility Changes: Differential Regulation and Roles in Lymphocyte Arrest Under Flow.* Immunity, 2000. 13(6): P. 759-69.
141. Ma, Y.Q., E.F. Plow, and J.G. Geng, *P-Selectin Binding to P-Selectin Glycoprotein Ligand-1 Induces an Intermediate State of Alphambeta2 Activation and Acts Cooperatively with Extracellular Stimuli to Support Maximal Adhesion of Human Neutrophils.* Blood, 2004. 104(8): P. 2549-56.
142. Evangelista, V., S. Manarini, S. Rotondo, N. Martelli, R. Polischuk, J.L. Mcgregor, G. De Gaetano, and C. Cerletti, *Platelet/Polymorphonuclear Leukocyte*

Interaction in Dynamic Conditions: Evidence of Adhesion Cascade and Cross Talk Between P-Selectin and the Beta 2 Integrin CD11b/CD18. Blood, 1996. 88(11): P. 4183-94.

143. Kuijpers, T.W., B.C. Hakkert, M. Hoogerwerf, J.F. Leeuwenberg, and D. Roos, *Role of Endothelial Leukocyte Adhesion Molecule-1 and Platelet-Activating Factor in Neutrophil Adherence to IL-1-Prestimulated Endothelial Cells. Endothelial Leukocyte Adhesion Molecule-1-Mediated Cd18 Activation.* J Immunol, 1991. 147(4): P. 1369-76.
144. Repo, H., Y.P. Rochon, B.R. Schwartz, S.R. Sharar, R.K. Winn, and J.M. Harlan, *Binding of Human Peripheral Blood Polymorphonuclear Leukocytes to E-Selectin (CD62E) does not Promote Their Activation.* J Immunol, 1997. 159(2): P. 943-51.
145. Mcever, R.P. and R.D. Cummings, *Role of PSGL-1 Binding to Selectins in Leukocyte Recruitment.* J Clin Invest, 1997. 100(11 Suppl): P. S97-103.
146. Puri, K.D., E.B. Finger, and T.A. Springer, *The Faster Kinetics of L-Selectin than of E-Selectin and P-Selectin Rolling at Comparable Binding Strength.* J Immunol, 1997. 158(1): P. 405-13.
147. Blanks, J.E., T. Moll, R. Eytner, and D. Vestweber, *Stimulation of P-Selectin Glycoprotein Ligand-1 on Mouse Neutrophils Activates Beta 2-Integrin Mediated Cell Attachment to ICAM-1.* Eur J Immunol, 1998. 28(2): P. 433-43.
148. Lorant, D.E., K.D. Patel, T.M. Mcintyre, R.P. McEver, S.M. Prescott, and G.A. Zimmerman, *Coexpression of GMP-140 and PAF by Endothelium Stimulated by Histamine or Thrombin: a Juxtacrine System for Adhesion and Activation of Neutrophils.* J Cell Biol, 1991. 115(1): P. 223-34.
149. Lorant, D.E., M.K. Topham, R.E. Whatley, R.P. McEver, T.M. McIntyre, S.M. Prescott, and G.A. Zimmerman, *Inflammatory Roles of P-Selectin.* J Clin Invest, 1993. 92(2): P. 559-70.
150. Evangelista, V., S. Manarini, R. Sideri, S. Rotondo, N. Martelli, A. Piccoli, L. Totani, P. Piccardoni, D. Vestweber, G. De Gaetano, and C. Cerletti, *Platelet/Polymorphonuclear Leukocyte Interaction: P-Selectin Triggers Protein-Tyrosine Phosphorylation-Dependent CD11b/CD18 Adhesion: Role of PSGL-1 as a Signaling Molecule.* Blood, 1999. 93(3): P. 876-85.